FZR-431

Wissenschaftlich-Technische Berichte
FZR-431 August 2005 ISSN 1437-322X

T. Höhne, S. Kliem, T. Toppila, J. Elter,
J. Remis, J. Klepac, I. Farkas, T. Farkas,
I. Boros, A. Aszodi

The European project FLOMIX-R: Description of the experimental and numerical studies of flow distribution in the reactor primary circuit Final report on WP 3

Editor: T. Toppila

Forschungszentrum
Rossendorf

Wissenschaftlich-Technische Berichte
FZR-431
August 2005

T. Höhne, S. Kliem, T. Toppila, J. Elter,
J. Remis, J. Klepac, I. Farkas, T. Farkas,
I. Boros, A. Aszodi

The European project FLOMIX-R: Description of the experimental and numerical studies of flow distribution in the reactor primary circuit Final report on WP 3

Editor: T. Toppila

Forschungszentrum
Rossendorf

EUROPEAN COMMISSION
5th EURATOM FRAMEWORK PROGRAMME 1998-2002
KEY ACTION : NUCLEAR FISSION

FLOMIX-R

FIKS-CT-2001-00197

Deliverable D10

Description of the experimental and numerical studies of flow distribution in the reactor primary circuit (Final report on WP 3)

Contributors:

Forschungszentrum Rossendorf
Fortum Nuclear Services
KFKI Atomic Energy Research Institute
Paks Nuclear Power Plant
TU Budapest
VUJE Trnava

Dissemination level :

Pu: Public

Authors

FORSCHUNGSZENTRUM ROSSENDORF (FZR):
T Höhne (Chapter B.3.1), S Kliem (Chapter B.1)

FORTUM NUCLEAR SERVICES (Fortum):
T Toppila (Chapter B.4.2)

PAKS NUCLEAR POWER PLANT (Paks):
J Elter (Chapter B.2.1, Appendix 1)

VUJE Trnava (VUJE):
J Remis, J Klepac (Chapters B.3.2, B.4.1) with contributions of I Farkas, T Farkas (Chapters B.3.3, B.4.1), I Boros and A Aszodi (Chapter B.4.1)

Manuscript prepared by:
T Toppila

Table of contents

A Objectives and scope

Flow distribution in the primary circuit of the pressurized water reactor (PWR) is an important issue connected to many operational problems. The temperature profile at the core outlet, relevant for the determination of the reactor power and thus for economical plant operation, is directly influenced by the flow distribution at the core inlet. Also the quasi-steady flow with macroscopic oscillating swirls inside the reactor vessel can cause temperature fluctuations and therefore is of importance to long-term thermal fatigue.

The flow distribution at the core inlet is influenced by the flow field in the pressure vessel and the flow distribution between the loops. The flow distribution between the loops is a particularly important factor during the asymmetric loop flow or temperature conditions. The asymmetric loop flow distribution is possible for example due to the pump operation uncertainties during power operation or due to the total pump failure during accident scenarios. The asymmetric temperature conditions are especially important in case of a steam line break. During a steam line break the overcooling of one or more primary circuit loops occurs. The mixing of the loop flows before the core inlet must be properly modelled in order to correctly predict the reactivity margin or the power excursion of the core.

The main objectives of the work package 3 were first to study the primary circuit flow distribution using experimental data from steady state experiments carried out with the ROCOM (Rossendorf Coolant Mixing Model) test facility and from the thermal mixing phenomena experiments at the VVER type reactor at Paks NPP. Here the main emphasis was on the

- influence of the flow pattern entering the downcomer,
- swirl behaviour in the downcomer and the lower plenum and
- efficiency of the mixing of the loop flows before the core inlet.

The experimental data both from the test facility and the real NPP experiments were further used for the validation and testing the Computational Fluid Dynamics (CFD) methods for the simulation of the primary circuit flow field. In recent years the rapid development on computers technology has made the CFD simulation a real alternative for many nuclear power applications.

Typically in case of the primary circuit flow scenarios presented above at least some of the main coolant pumps are operating or a fully developed natural circulation is established. Therefore, a turbulent quasi steady-state flow field and a momentum controlled mixing are expected to be the relevant flow and mixing mechanisms. It is in principle possible to model this kind of forced flow with current commercial CFD codes. However this requires validation and testing for example of the effect of different geometrical simplifications and the modelling of the turbulence. Commercial CFD codes CFX-4, CFX-5 and FLUENT were used for the simulation of the experiments by the FLOMIX-R partners.

B Work performed and results

Work made by the FLOMIX-R partners related to the primary circuit flow field is presented in this chapter.

The steady state mixing experiments carried out with a 4-loop 1/5-scale ROCOM (Rossendorf Coolant Mixing Model) mock-up by FZR are presented in chapter B.1. A series of nine experiments were accomplished to find out the influence of the total flow rate, the number of operating loops, the relative location of operating loops and the asymmetry of loop flow rates to the flow field in the downcomer and the core inlet. The steady state mixing experiment data was also added to the data base of FLOMIX-R for use for the Computational Fluid Dynamics (CFD) code validation.

The experimental investigation of thermal mixing phenomena in a six loop VVER type reactor at Paks NPP is presented in chapter B.2 and in the appendix 1. An experimental method is used with an operational reactor for the measurement of temperature field at the core entrance and based on these measurements the mixing factors at the core entrance are determined for the flow from each one of the six cold legs.

The CFD simulations of the steady state experiments at the ROCOM test facility are presented in chapter B.3. The selected test cases are simulated by FZR, VUJE and AEKI to validate the CFD codes CFX-4, CFX-5 and FLUENT for primary circuit flow simulations. The conclusions are made concerning the applicability of CFD methods to the primary circuit flow simulations as well as the recommendations for the CFD modelling are summed up. A fully detailed presentation of all computation grids, turbulence model and discretization method tests are presented in the final report of work package 4 while the main emphasis here is on the primary circuit simulation related aspects.

The VVER related CFD simulations are summarized in chapter B.4. A selected Paks VVER-440 mixing experiment with symmetric loop flow rates in all six loops but reduced water temperature in one loop was simulated by AEKI, VUJE and TU Budapest and the simulated concentration field at the core inlet was compared to the experimental data. In addition some VVER-440 specific geometry modelling aspects were studied, such as how to model the perforated elliptic bottom plate to get the best results and what is the effect of the cold leg bends to the flow field entering to the downcomer. The results are presented in chapter B.4.1.

The VVER-440 flow field was also simulated by Fortum. With simulations having symmetric or slightly asymmetric loop flow rates the effect of asymmetry of flow rates, the cold leg bends and the geometric details like the ECC water guides and the core basket alignment drifts to the downcomer flow field was studied. Simulation results were also qualitatively compared to the real plant measurements of Loviisa VVER-440 NPP. CFD simulations with model descriptions, results and conclusions are presented in chapter B.4.2.

B.1 Steady state mixing experiments at the ROCOM test facility

B.1.1 Introduction

ROCOM (Rossendorf Coolant Mixing Model) is a test facility for the investigation of coolant mixing operated with water at room temperature. The facility models a KONVOI type reactor with all important details for the coolant mixing in a linear scale of 1:5. ROCOM is a four-loop test facility with a RPV mock up made of acrylic glass (Fig. 1-1). Individually controllable pumps in each loop give the possibility to perform tests in a wide range of flow conditions, from natural circulation to nominal flow rate including flow ramps (pump start up). The transparent material for the pressure vessel allows the measurement of velocity profiles in the downcomer by laser Doppler anemometry.

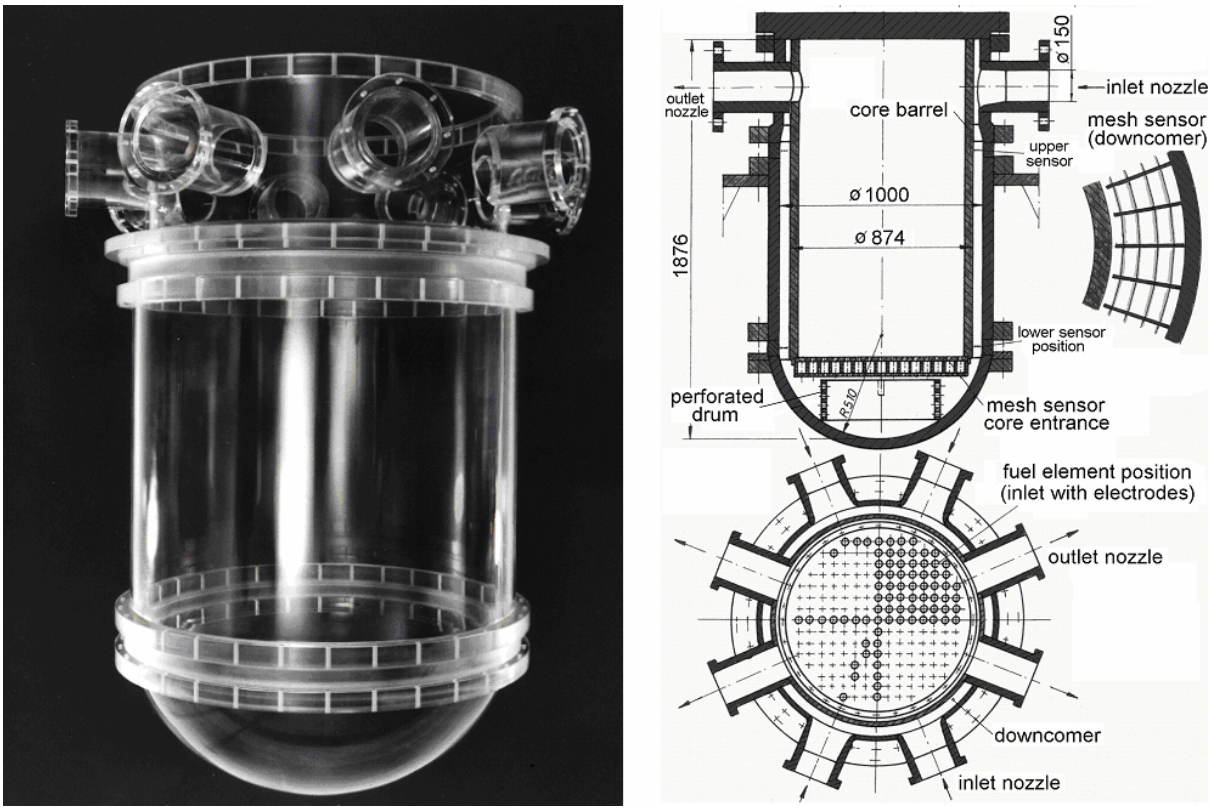

Fig. 1-1 Pressure vessel of the ROCOM facility (left) and positions of the wire mesh sensors

Both boron concentration and temperature fields are modelled by the concentration field of a tracer solution. The disturbance is created by computer controlled injection of salted water into the cold leg of one of the loops, while the test facility is operated with de-mineralised water. The test facility is equipped with wire-mesh sensors for the electrical conductivity measurement, which allow a high resolution determination of the transient tracer concentration in space and time. Four such sensors are installed in the reactor pressure vessel model with altogether about 1000 single measurement positions and a measuring frequency of up to 200 Hz. The location of the sensors in the model is shown on Fig. 1-1.

The measured conductivity values are transformed into a mixing scalar $\Theta_{x,y,z}(t)$. It is calculated by relating the local instantaneous conductivity $\sigma_{x,y,z}(t)$ to the amplitude of the conductivity change in the inlet nozzle of the disturbed loop.

$$\Theta_{x,y,z}(t) = \frac{\sigma_{x,y,z}(t) - \sigma_0}{\sigma_1 - \sigma_0} \qquad \text{(Equ. 1-1)}$$

Θ represents the contribution of the coolant from the disturbed loop to the mixture at the given position x,y,z. The determination of the upper reference value σ_1 in (Equ. 1-1) depends on the kind of the experiments carried out. For the steady state experiments described here, the value is calculated by averaging the quasi-stationary concentration plateau at the sensor in the cold leg. An example is shown on Fig. 1-2. The lower reference value σ_0 is the initial conductivity of the water in the test facility before the tracer is injected and is determined before the tracer reaches the first sensor cross section.

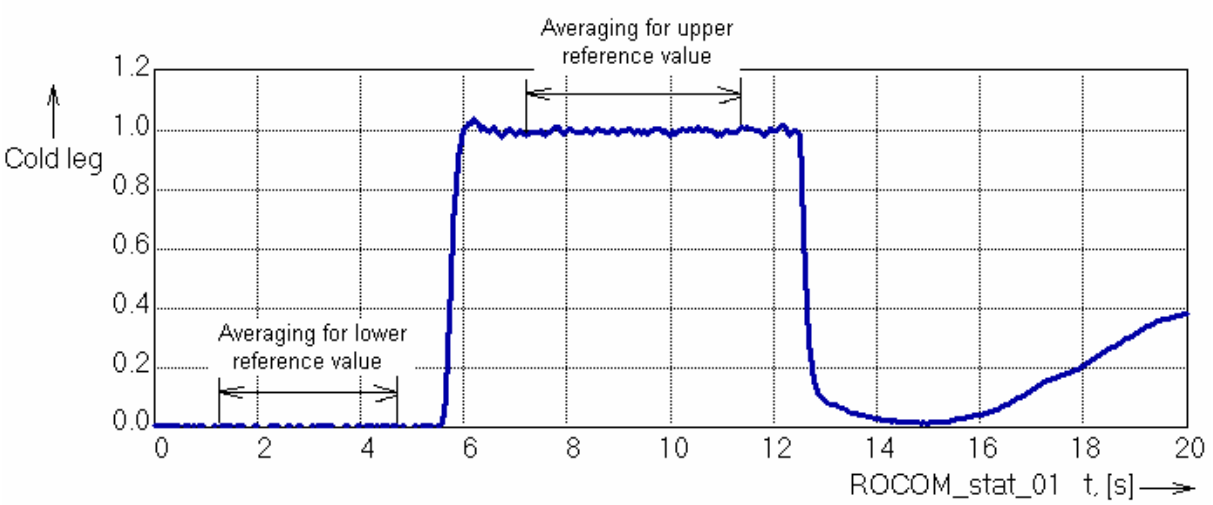

Fig. 1-2 Determination of the reference values for the mixing scalar

All details about the ROCOM test facility, the measurement and the auxiliary systems can be found in [Roh04].

B.1.2 Matrix of the experiments

The test matrix of the ROCOM steady state experiments was based on the requirements, elaborated in the frame of the determination of the key phenomena [Roh02]. The experiments in the matrix were selected in such a way, that conclusions can be drawn concerning the influence of the following aspects:

- Total flow rate
- Number of operating loops
- Relative location of operating loops
- Asymmetry of loop flow rates

Tab. 1-1 Test matrix on ROCOM steady state mixing experiments

Run	**Volume flow rate [m^3/h]**				**Single realisa-tions**	**Velocity measure-ments**
	Loop 1	Loop 2	Loop 3	Loop 4		
ROCOM-STAT-01	185.0	185.0	185.0	185.0	5	x
ROCOM-STAT-01a	185.0	185.0	185.0	185.0	5	
ROCOM-STAT-02	46.3	46.3	46.3	46.3	5	-
ROCOM-STAT-03	185.0	backflow	backflow	backflow	5	x
ROCOM-STAT-03a	185.0	backflow	backflow	backflow	5	
ROCOM-STAT-04	185.0	185.0	185.0	backflow	5	x
ROCOM-STAT-05	185.0	backflow	185.0	backflow	5	x
ROCOM-STAT-06	185.0	185.0	backflow	backflow	5	x
ROCOM-STAT-07	185.0	backflow	backflow	185.0	5	x
ROCOM-STAT-08	203.5	166.5	185.0	185.0	5	x
ROCOM-STAT-09	222.0	148.0	185.0	185.0	5	x

The flow field is observed by measuring tracer concentration distribution in all experiments. For all experiments except ROCOM-STAT-01a, ROCOM-STAT-03 and ROCOM-STAT-03a stationary mixing matrices for each measurement position at the core inlet were determined. These mixing matrices describe the share of the initial perturbation at the current position. For that purpose, tracer injection was performed over a time interval to be long enough to reach quasi-stationary concentration level at the core inlet. The asymptotic mixing matrix for the experiment ROCOM-STAT-03 (one-loop operation) would be unity. Therefore, only the time dependent concentration field is determined. Together with the experiments ROCOM-STAT-01a and ROCOM-STAT-03a, where the tracer injection was shortened, these data were added to the data base to contribute to the CFD-code validation.

For most of the experiments as shown in Tab. 1-1, velocity measurements by means of a laser Doppler anemometer were performed.

All experimental data of the carried out matrix (Tab. 1-1) are documented in [Kli03]. That documentation contains the boundary conditions and the experimental results in graphical and digital form.

B.1.3 Experimental results on concentration measurements

B.1.3.1 Experiment ROCOM-STAT-01

The general conduction of an experiment is here described on behalf of the experiment ROCOM-STAT-01. In this experiment, the flow rates in all four loops correspond to the nominal values. The pump frequency values necessary for the selected flow regime were determined in preceding hydraulic experiments. These values are input to all four pumps, and the facility is operated over a certain time interval until the flow regime reached stable conditions. Tracer injection is performed by means of a set of computer controlled pneumatic and magnetic valves. The activation of the tracer injection is made inside the measurement program of the wire mesh sensors. Details about valves, the mixing device at the injection positions and the wire mesh sensors including the measurement procedure can be found in

[Roh04]. Usually five seconds after starting the measurement program, the tracer injection valves are opened starting a continuous injection of salted water into the flow of loop N° 1. The time point for closing the valves is selected in such a way, that the tracer distribution reaches a saturation level at the core inlet. On the other hand, the injection should be finished, before the slug of the tracer has travelled through the whole facility and reaches the measurement positions for a second time. In the experiment ROCOM-STAT-01 the injection time was 7.0 s. Each experiment was repeated five times, the corresponding time curves at each measurement position are averaged, the upper reference value in Equ. 1-1 is determined from the averaged time curve. All measured values at the quasi-stationary concentration plateau are used for the determination of the mixing coefficients.

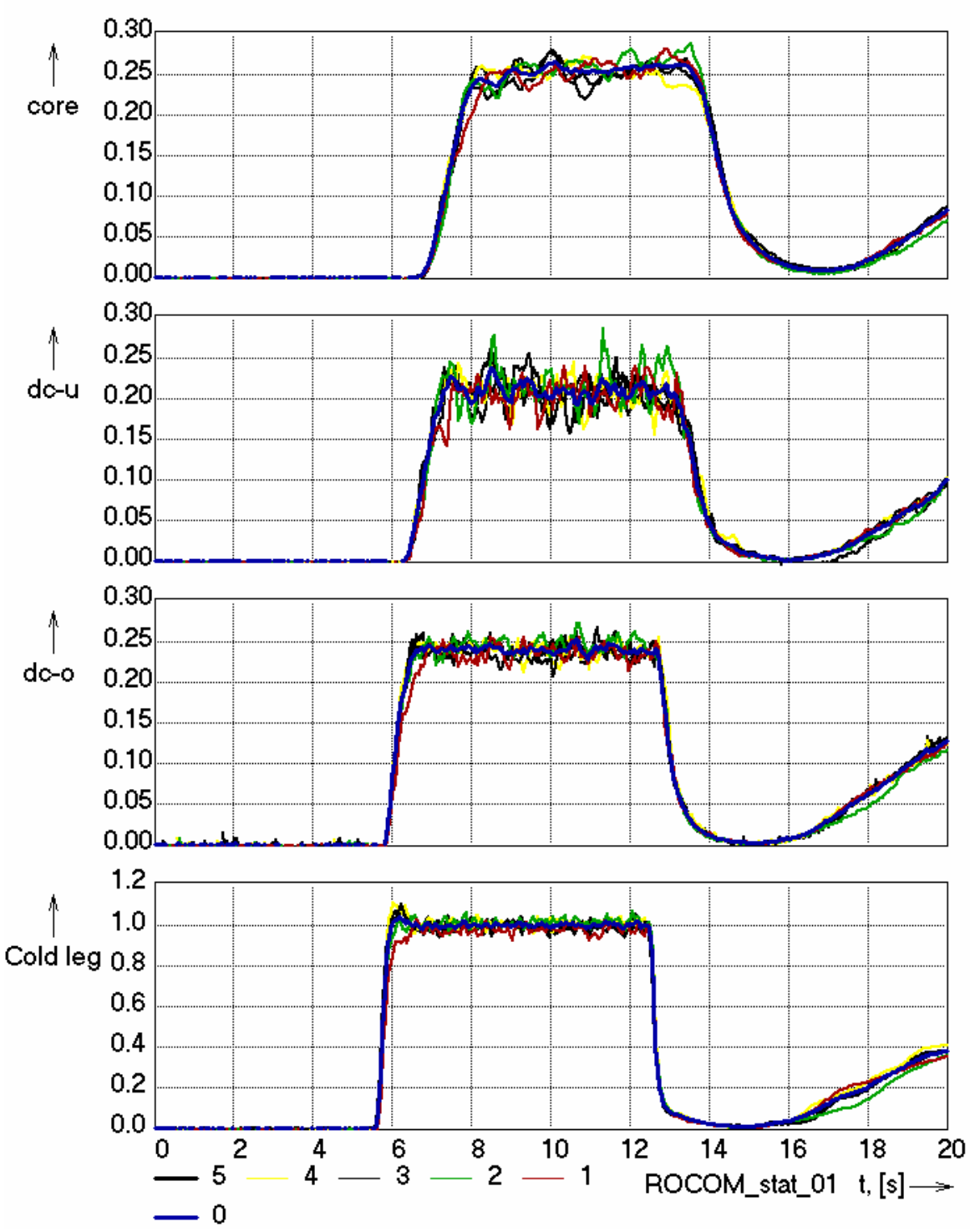

Fig. 1-3 Time evolution of the average mixing scalar at all sensor in the single realizations of experiment ROCOM-STAT-01

Fig. 1-3 shows the time evolution of the average mixing scalar at all sensors in the test facility. The figure demonstrates the reproducibility of the boundary conditions for the experiments. The turbulent fluctuations of the single realizations are damped by averaging. Further, it is to be seen at all sensors, that the injection was finished, before the tracer returns after one circulation to the measurement position. The left part of Fig. 1-4 shows the time

evolution of the mixing scalar at both sensors in the downcomer (shown in an unwrapped view). Already at the upper sensor, the redistribution of the flow is finished. The sector with the tracer shifted from the inlet position (22.5°) to the sector corresponding to the share of the total flow (middle position now is 45°). The sector covered by the tracer is 90°, what confirms the quality of the boundary conditions (equal flow rates in all loops).

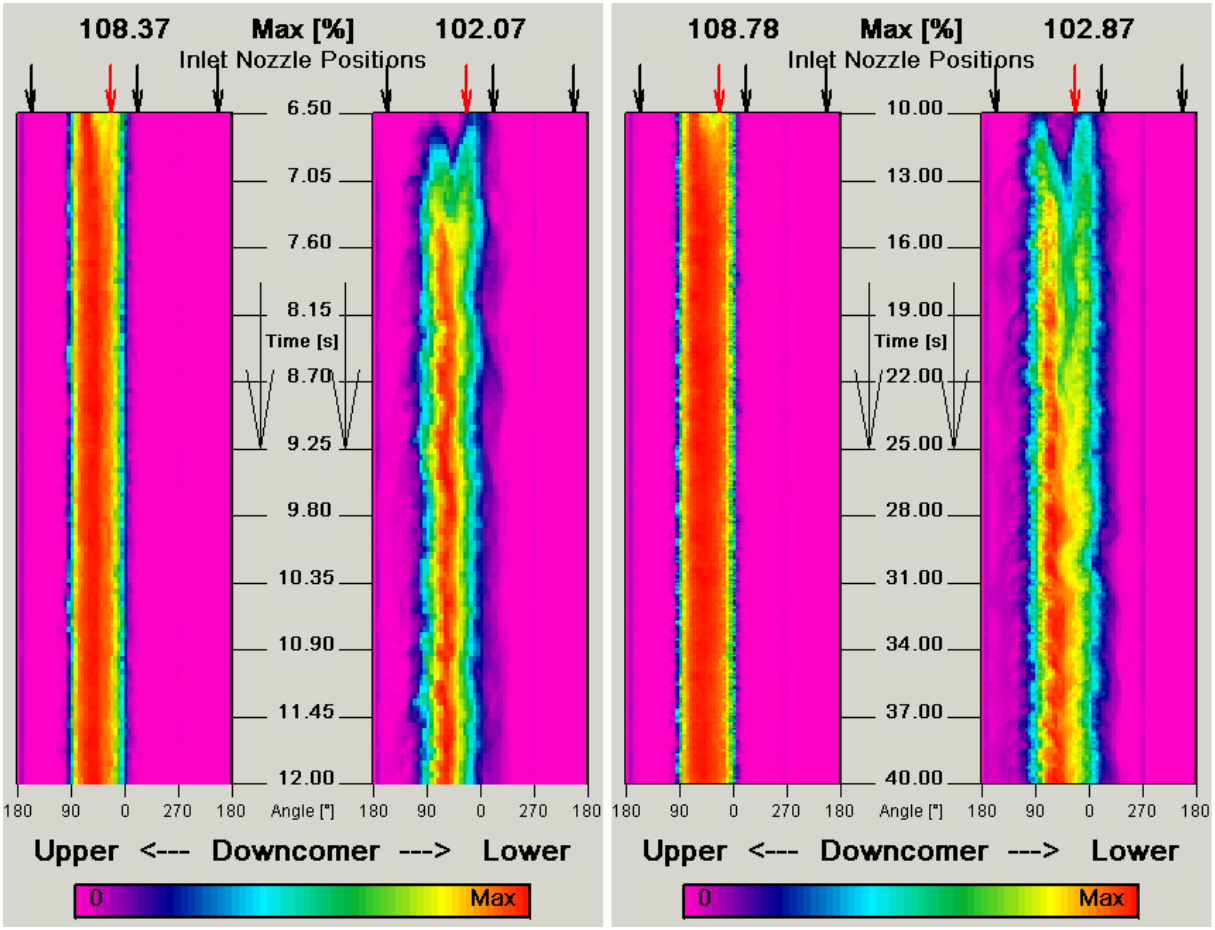

ROCOM_STAT_01 ROCOM_STAT_02

Fig. 1-4 Time evolution of the mixing scalar at the sensors in the downcomer (the red arrow indicates the azimuthal position of the loop with tracer injection)

At the lower sensor, the tracer remains in the indicated sector, but fluctuations of the whole flow field are observed. They were confirmed by the velocity measurements (see chapter 1.4). Mixing with the ambient coolant takes places at the outer edges of the sector.

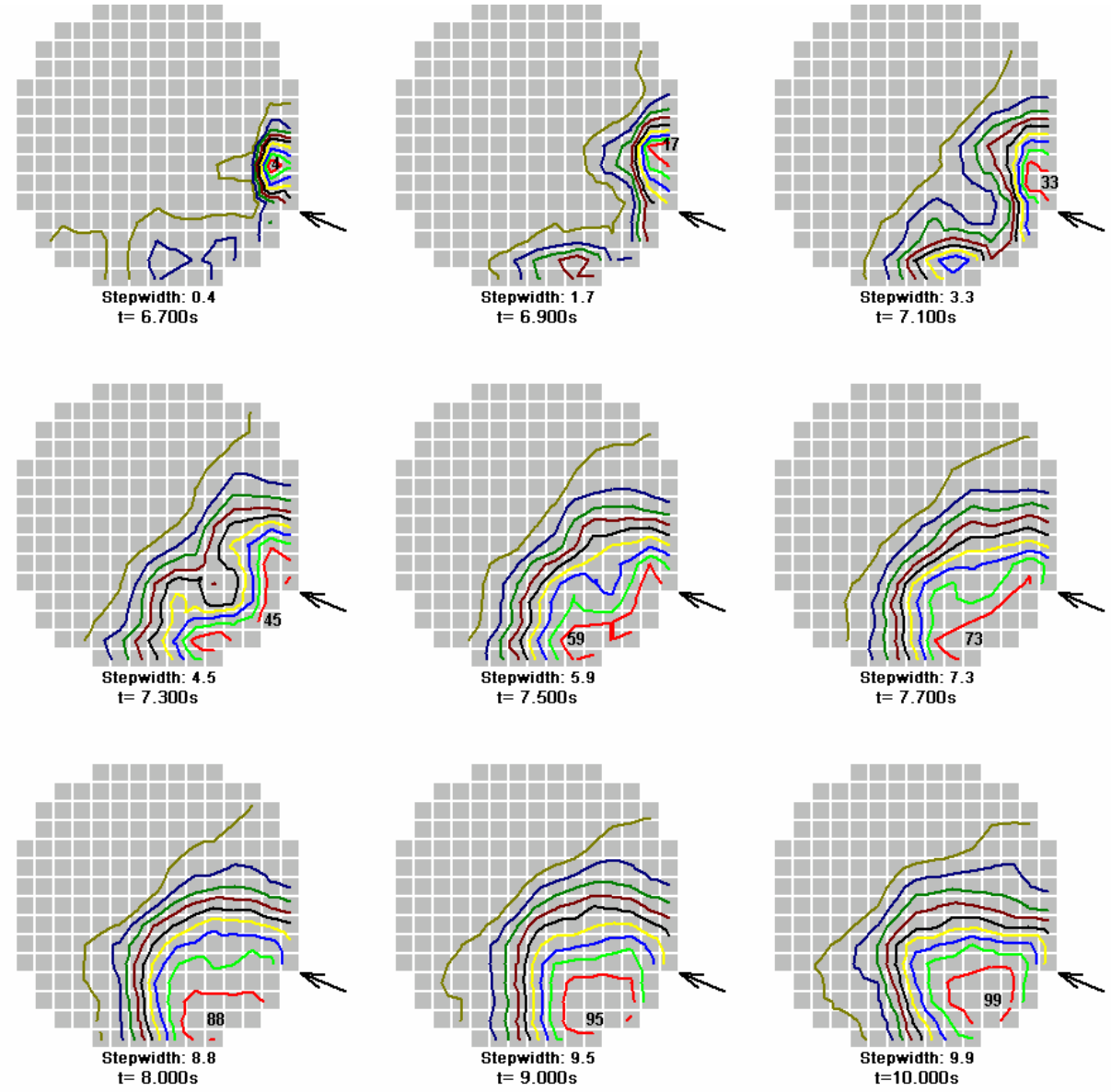

Fig. 1-5 Time sequences of the mixing scalar at the core inlet plane in the experiment ROCOM-STAT-01

At the core inlet, the tracer arrives at two positions at the border of the sector belonging to the corresponding loop at the same time. Only with growing time, the part in the middle of the sector is filled with tracer. After several seconds, the quasi-stationary concentration level establishes with a maximum in the middle of the sector.

B.1.3.2 Determination of stationary mixing matrices

As already mentioned, the mixing coefficients representing the share of the initial perturbation in the cold leg at the corresponding measurement position are determined by averaging all values at the quasi-stationary concentration field in the core inlet plane. The time interval used for the experiment ROCOM-STAT-01 is shown on Fig. 1-6.

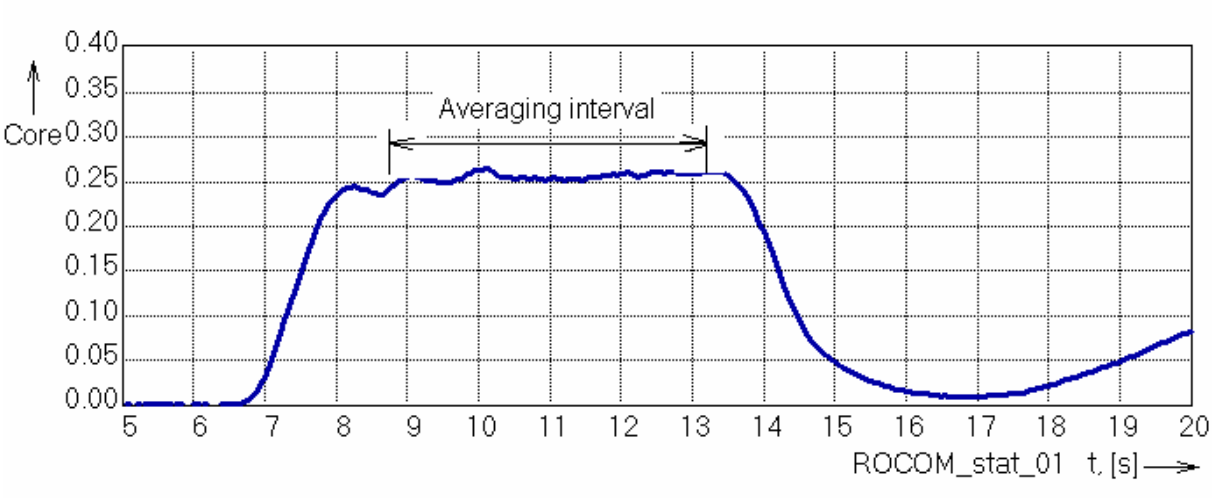

Fig. 1-6 Time interval for determination of the mixing coefficients at the core inlet in the experiment ROCOM-STAT-01

The time interval (as shown in Fig. 1-6) is identical for all measurement positions of the core inlet sensor. Fig. 1-7 shows the time evolution of the average mixing scalar and the mixing scalar at the inlet into fuel assembly 25 (position 02:07). All values in the indicated time interval are used for the determination of the mixing coefficient. These are 475 single values. They are all included in Fig. 1-8, which demonstrates the evolution of the mixing coefficient with growing number of considered values. The single values were used to calculate the standard deviation and the different confidence intervals according to the following formulas:

$$FS_{\min,\Theta}(x,y,z) = \sum_{k=1}^{n} (\theta_{ROCOM,k}(x,y,z) - \overline{\theta}_{ROCOM}(x,y,z))^2 \qquad \text{(Equ. 1-2),}$$

where FS_{min} is the minimum error amount and n the number of single values used for the determination of the mixing coefficient.
The standard deviation is calculated according to

$$s_{\Theta}(x,y,z) = \sqrt{\frac{FS_{\min,\Theta}(x,y,z)}{n-1}} \qquad \text{(Equ. 1-3).}$$

In the last step, the confidence intervals can be calculated using equ. (Equ. 1-4).

$$u_{z,\Theta}(x,y,z) = \pm t_P . \frac{s_{\Theta}(x,y,z)}{\sqrt{n}} \qquad \text{(Equ. 1-4)}$$

The calculated values for the standard deviation and the confidence intervals of 68.3 % and 95.4 % are stored on the CDROM with the experimental data [Kli03]. In the corresponding description, the time intervals for averaging are indicated for all experiments. Figures of the core inlet plane with the values of the mixing coefficients are given there, too.

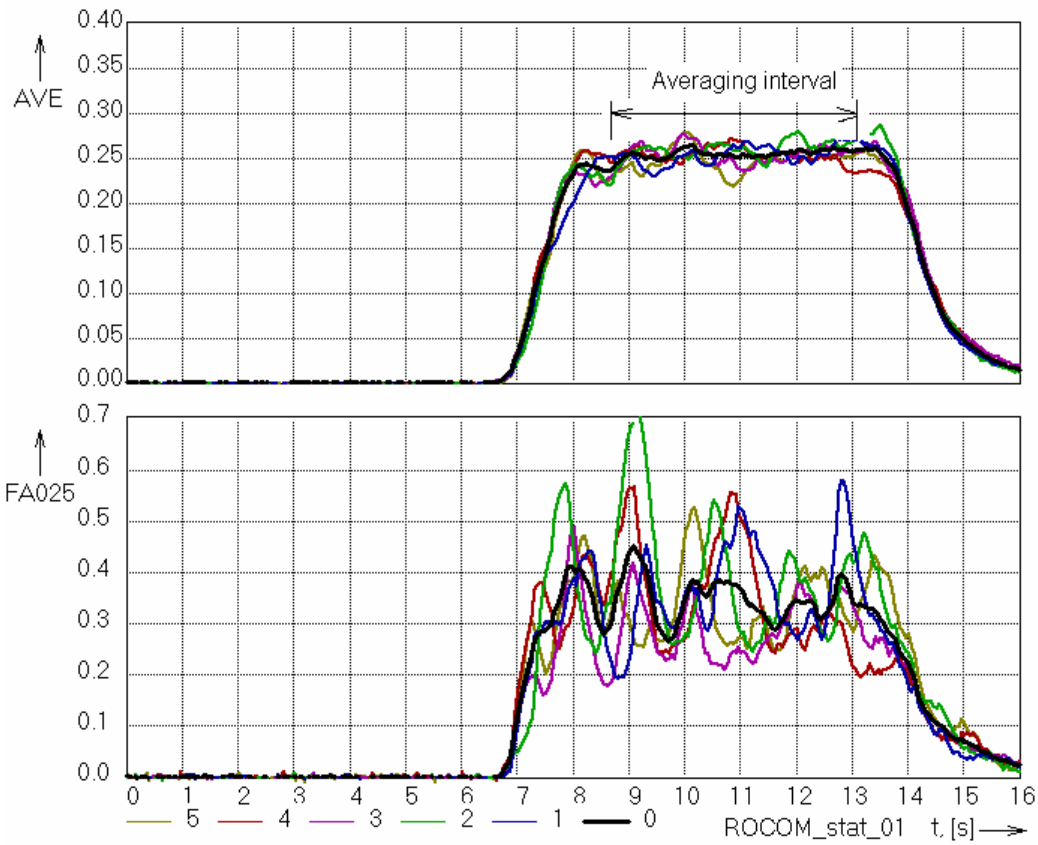

Fig. 1-7 Time evolution of the average mixing scalar (upper part) and at one certain position (lower part) in the single realizations of the experiment ROCOM-STAT-01

Mixing coefficients were determined for the two sensors in the downcomer of the ROCOM test facility in a similar way. They are stored on the CDROM with the experimental data [Kli03].

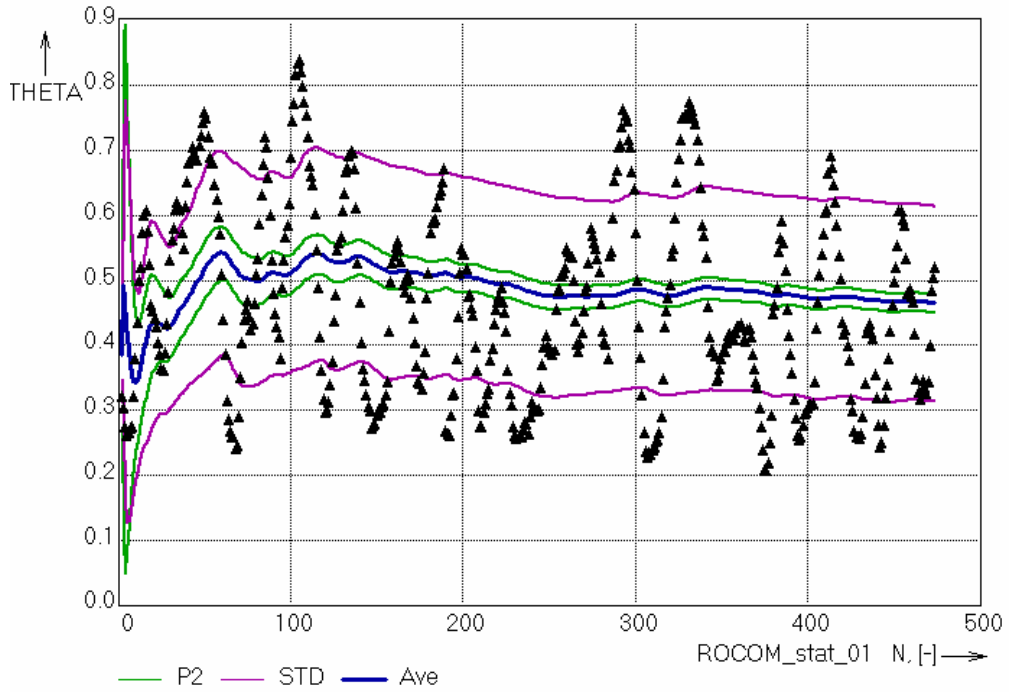

Fig. 1-8 Single values of the mixing scalar at measurement position 25 and evolution of the standard deviation and the confidence interval with growing number of values

B.1.3.3 Influence of the total flow rate

In the experiment ROCOM-STAT-02, the volume flow rate in all loops was reduced to 25 %. The right part of Fig. 1-4 shows the time evolution of the mixing scalar at the two sensors in the downcomer in the experiment ROCOM-STAT-02. The behaviour at the upper sensor is identical to the experiment ROCOM-STAT-01. The azimuthal redistribution takes place in a similar way, the covered by tracer sector ranges from 0° to 90°. At the lower sensor, the sector covered by tracer has a greater azimuthal extension. It seems, that during the transport through the downcomer, the mixing with the ambient water is more intensive than in the experiment ROCOM-STAT-01. In Fig. 1-9, the mixing coefficients at the core inlet are shown for both experiments. It is clearly to be seen, that in the case of reduced flow rates, the sector covered by the tracer is greater, the maximum value is lower (2 percentage points). That confirms the observation made in the lower part of the downcomer. Further, it is clearly to be seen, that the shape of the distribution differs. In the experiment with 100 % flow rate, the maximum is in the second row of measurement positions (fuel assemblies), the isolines of constant mixing scalars are closed. In the experiment with reduced flow rates, the maximum is shifted to the border of the core inlet plane, the shape of the isolines has been changed.

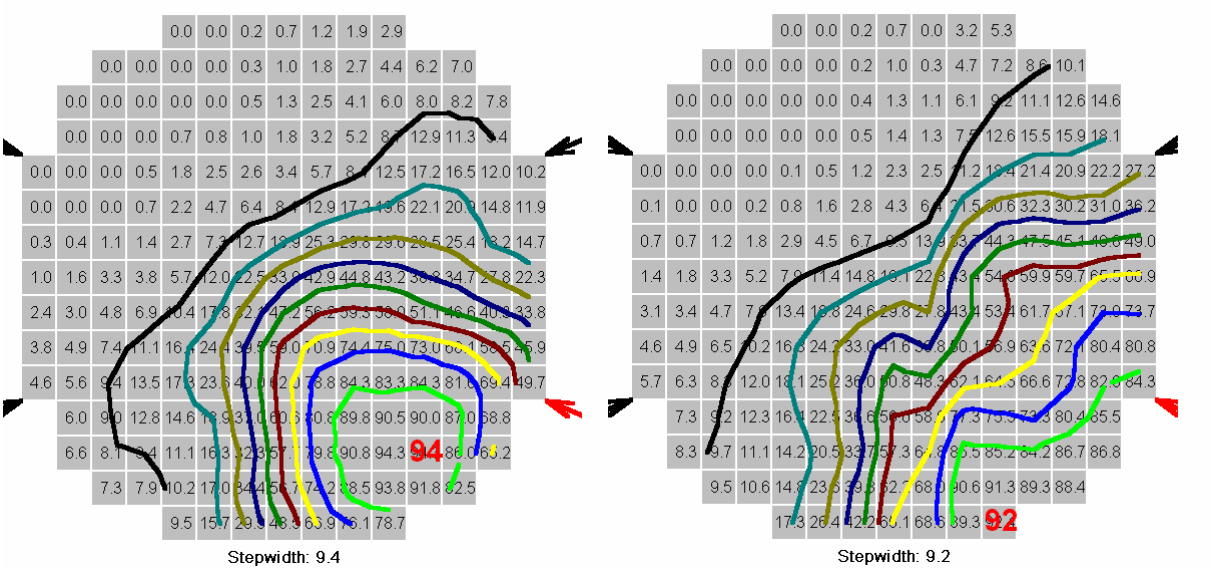

Fig. 1-9 Distribution of the mixing coefficients at the core inlet (perturbation in loop 1(red arrow); maximum: bold red number)

B.1.3.4 Influence of the position of operating loops

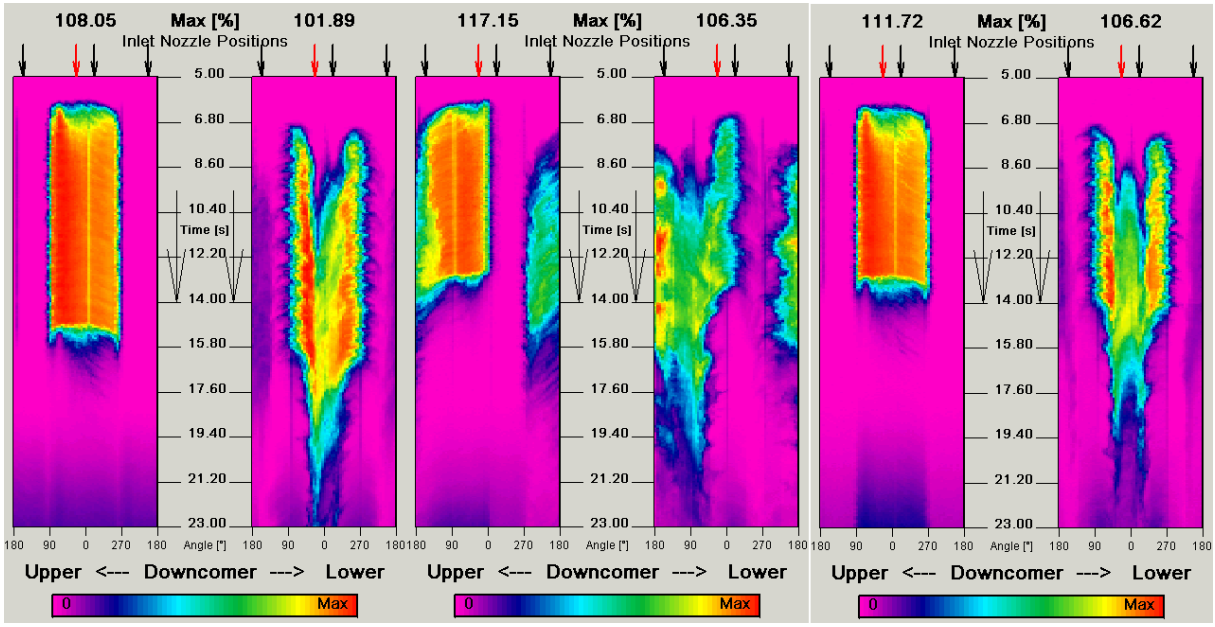

a) ROCOM-STAT-05 (Loop 1;3)

b) ROCOM-STAT-06 (Loop 1;2)

c) ROCOM-STAT-07 (Loop 1;4)

Fig. 1-10 Time evolution of the mixing scalar at the two sensors in the downcomer in the different experiments with changing of operating loop position

In the experiments ROCOM-STAT-05, ROCOM-STAT-06 and ROCOM-STAT-07, two loops were operating, tracer injection was always performed into operating loop 1, and the second operating loop was changed. Fig. 1-10 illustrates the time evolution of the mixing scalar in the downcomer in dependence on the position of the second operating loop. When the operating loops are in a greater distance (Fig. 1-10 a and c), then the distribution of the mixing scalar at the upper sensor is comparable to the situation with four loop operation. An azimuthal redistribution takes place and the tracer covers the corresponding sector due to the share of the flow rate, in this case 50 %. In both cases, the distribution covers the same area, independent on the fact which loop is the second operating one. The redistribution leads to the same final result. The distribution at the lower sensor confirms the findings stated above. The clearly expressed spreading of the tracer in the beginning can be explained by the velocity field, which is discussed in chapter 1.4. In case of operating loop 1 and 2, which are in an angular distance of only 45°, the redistribution leads to a different shape of the mixing scalar. The sector covered by the tracer is greater than 50 %, what can be explained by additional mixing during the redistribution process. At the lower sensor, the tracer covers a greater sector, too.

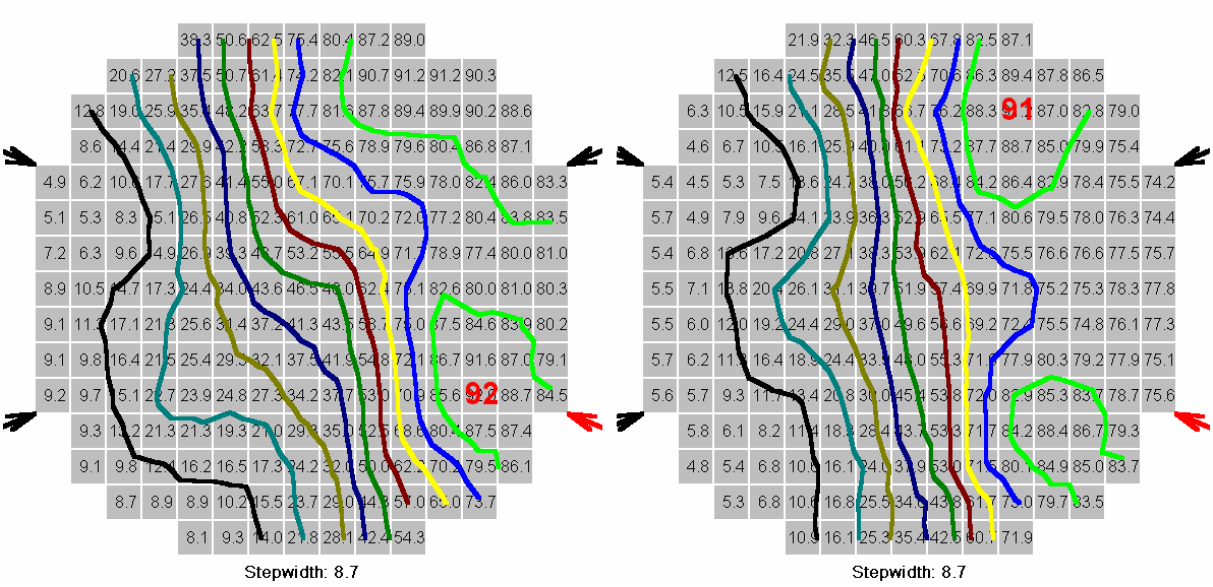

a) ROCOM-STAT-05 (Loop 1;3)

b) ROCOM-STAT-07 (Loop 1;4)

Fig. 1-11 Distribution of the mixing coefficients at the core inlet in the experiments ROCOM-STAT-05 and ROCOM-STAT_07 (perturbation in loop 1(red arrow); maximum: bold red number)

Fig. 1-11 compares the mixing coefficients at the core inlet in the experiments with operating loop 1 and 3 (a) and loop 1 and 4 (b). The distributions are nearly similar, the observed identical redistribution is the downcomer is also responsible for the identical shape at the core inlet. The reached maximum value itself differs only by less than 1 percentage point. The distribution in the experiment ROCOM-STAT-06 (operating loops 1 and 2) has a different shape, further the maximum value is about 10 percentage points lower than in the two other experiments with two loop operation (Fig. 1-12).

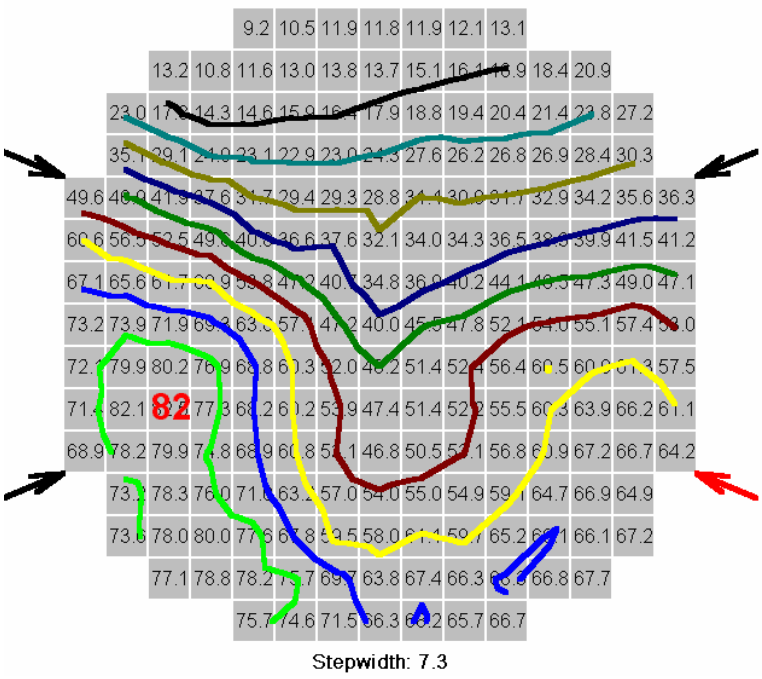

Fig. 1-12 Distribution of the mixing coefficients at the core inlet in the experiment ROCOM-STAT-06 (perturbation in loop 1(red arrow); maximum: bold red number)

B.1.3.5 Asymmetry in loop flow rates

Two cases with an asymmetry of 10 % and 20 % in the flow rates between two loops are considered being of interest from the viewpoint of NPP operation, where loop flow rate differences can occur (ROCOM-STAT-08, -STAT-09). The asymmetry was introduced in such a way that the total flow rate (sum of all four loops) remains identical, only the flow rate in loop 1 is increased by 10 % or 20 %, and the flow rate in loop 2 is reduced by the same value. Tracer injection was performed in the same time interval as in the experiment ROCOM-STAT-01, being the reference for the two asymmetric cases. Fig. 1-13 shows the time evolution at the two downcomer sensors in the three considered experiments (growing asymmetry from left to right). At both sensors, the left border (between loop 1 and 4) of the tracered sector remains at the same position, the right one moves according to the increase/decrease of the flow rates in loop 1 and 2. The fine colour scaling in the figure reveals the profile of the tracer concentration inside the tracered sector, especially at the lower downcomer sensor. In the reference experiment, the highest concentration is in the center of the sector. The maximum stays at the same position in the experiments with loop asymmetry. The widening of the sector leads to a reducing of the tracer concentration only at the side of azimuthal position of loop 2. The small line of tracer at the upper sensor in both experiments with loop asymmetry, separated from the tracer bulk by a sector of undisturbed coolant is not an error of the measurement device. This small amount of tracer is located in the middle between the azimuthal positions of loop 3 and 4. Here is the outer side of one of the swirls found in the downcomer during the velocity measurements, creating a recirculation area. In such a way, a small part of the tracer is transported back from the bulk to the measurement plane. The unequal velocity distribution in the downcomer is also responsible for the splitting of the first part of the tracer front in the lower part of the downcomer.

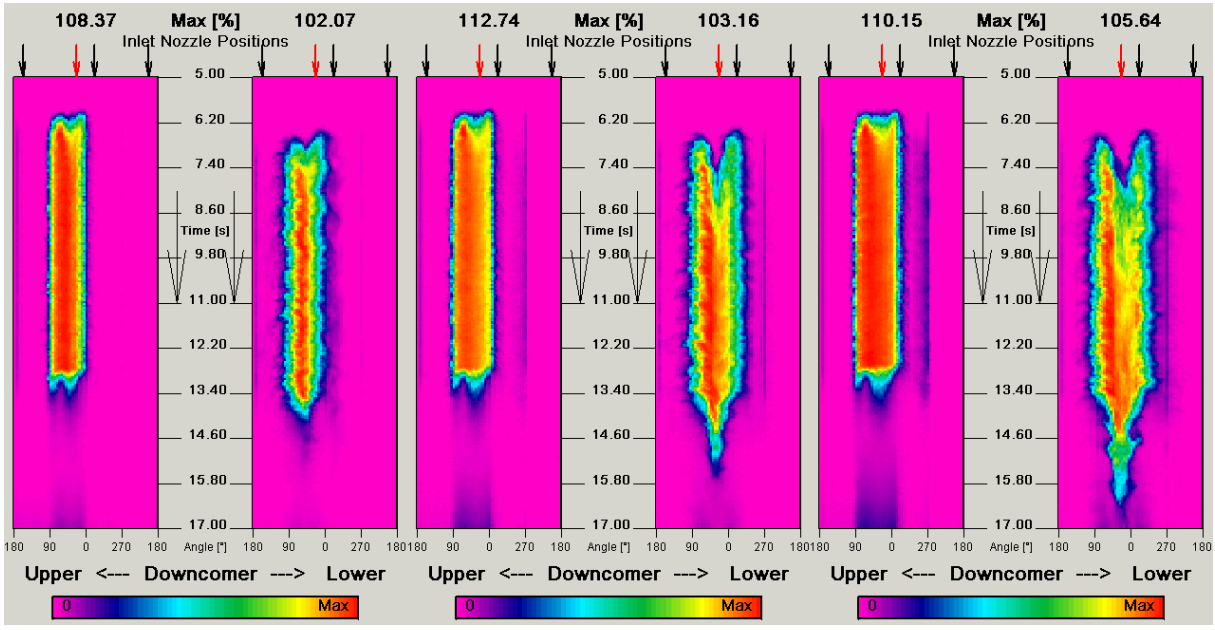

a) ROCOM-STAT-01 (0 %)

b) ROCOM-STAT-08 (10 %)

c) ROCOM-STAT-09 (20 %)

Fig. 1-13 Time evolution of the mixing scalar at the two sensors in the downcomer in the different experiments with asymmetry of the loop flow rates

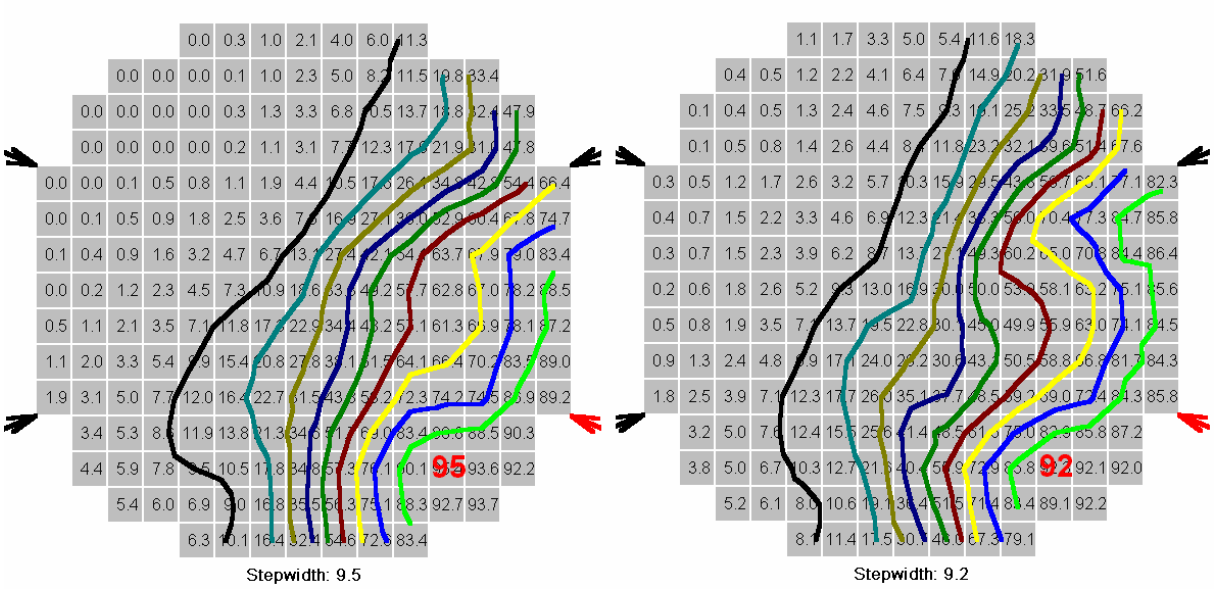

a) ROCOM-STAT-08
(10 %)

b) ROCOM-STAT-09
(20 %)

Fig. 1-14 Distribution of the mixing coefficients at the core inlet in the experiments ROCOM-STAT-08 and ROCOM-STAT_09 (perturbation in loop 1(red arrow); maximum: bold red number)

With growing asymmetry, a second maximum appears in the distribution at the core inlet (Fig. 1-14). The splitting of the tracer already starts in the lower part of the downcomer (Fig. 1-13). Due to the asymmetry in the flow rates, the distribution of the tracer is comparable with an experiment with tracer injection into two loops. As already mentioned, the velocity field in the downcomer is responsible for this splitting.

B.1.3.6 Transient slugs in a stationary velocity field

Two additional experiments were carried out, where tracer was injected over a short time into the stationary flow field. In all cases described above, the concentration level was at saturation. The additional experiments described now were conducted to extent the data base for CFD code validation. These experiments open the possibility to carry out transient calculation in a stationary flow field. This approach is an intermediate step between the stationary calculations to obtain the stationary mixing coefficients and the post test calculations for the slug mixing experiments during pump start-up, described in [Roh04]. The additional experiments were carried out for four-loop operation at nominal flow rate and for one-loop operation at nominal flow rate, too. The latter corresponds to the final state of the basic slug mixing experiments, when the first main coolant pump is started.

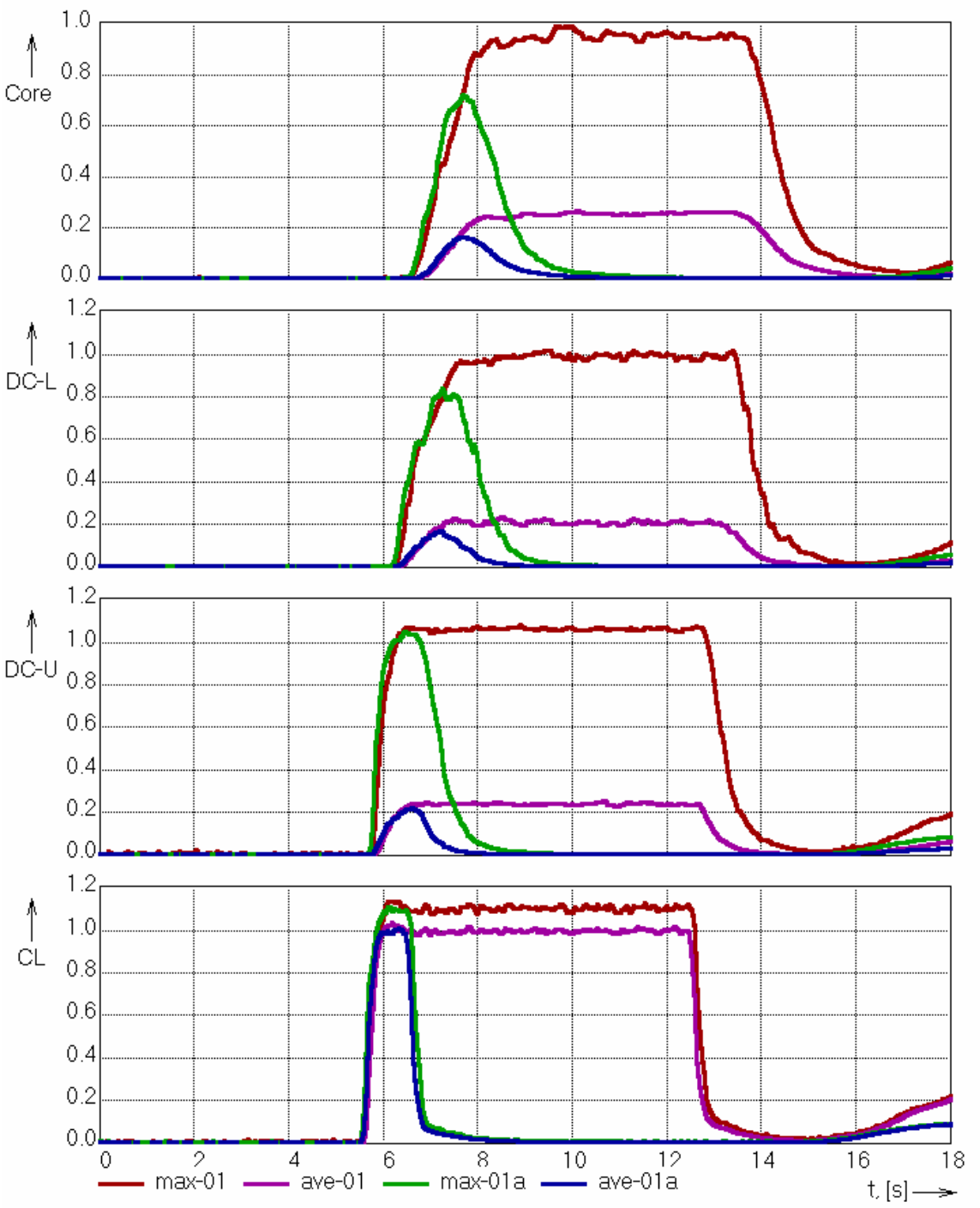

Fig. 1-15 Time evolution of the maximum and the average mixing scalar at all sensor in the experiments ROCOM-STAT-01 and ROCOM-STAT-01a.

Fig. 1-15 shows the time behaviour of the mixing scalar at all four sensors in the experiments ROCOM-STAT-01 and 01a. The shorter slug in the second experiment reaches the cross section of the corresponding wire mesh sensor at the same time as in the basic experiment, confirming the reproducibility of the hydraulic boundary conditions at the ROCOM test facility. At the first two sensors (cold leg and upper downcomer), the reached maximum value in the short injection experiment is identical to the basic experiment with long term injection. In the lower part of the downcomer and in the core inlet plane, the maximum value does not reach the saturation level.

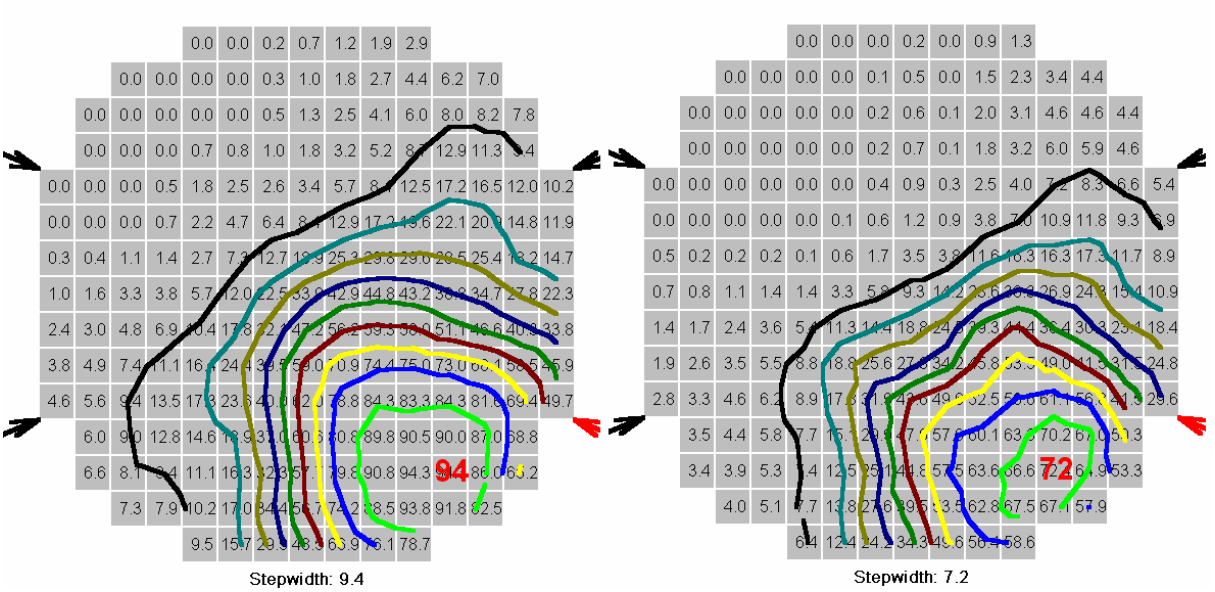

a) ROCOM-STAT-01
(plateau averaged values)

b) ROCOM-STAT-01a
(time of maximum)

Fig. 1-16 Distribution of the mixing scalar at the core inlet in the experiments ROCOM-STAT-01 and ROCOM-STAT_01a (perturbation in loop 1(red arrow); maximum: bold red number)

The snapshot of the distribution at the time point of maximum in the experiment ROCOM-STAT-01a (Fig. 1-16) shows an identical shape as the plateau averaged values in the basic experiment, the values at the corresponding positions are lower.

The same quality was achieved in the short term injection experiment with one-loop operation, as can be seen from Fig. 1-17. The distribution at the core inlet plane is in both cases the snapshot at the time point of maximum deboration. As already mentioned, mixing coefficients were not determined during one-loop operation. For the one-loop operation, the time dependent mixing data for two transient slugs of different size in the stationary flow field are available.

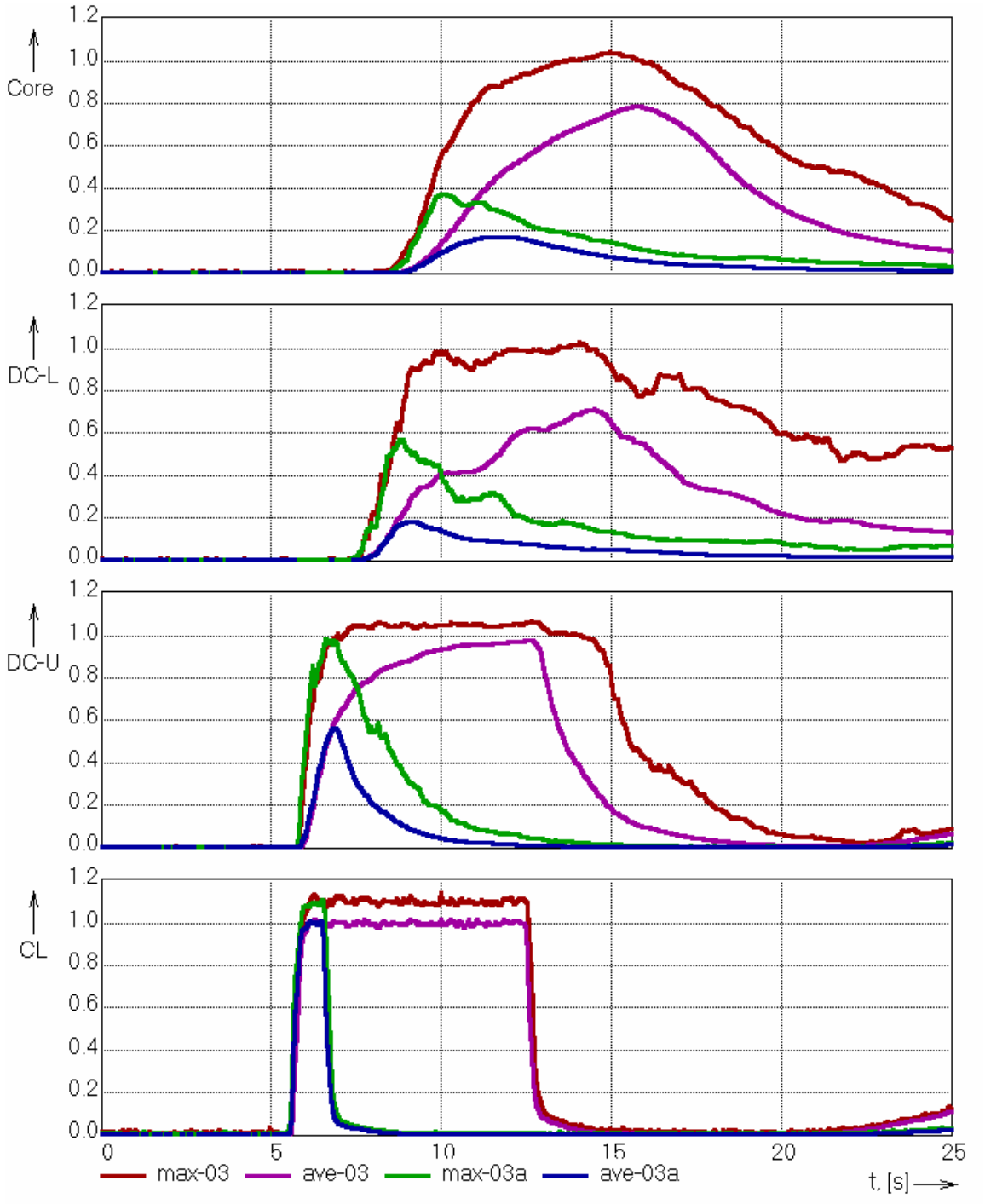

Fig. 1-17 Time evolution of the maximum and the average mixing scalar at all sensor in the experiments ROCOM-STAT-03 and ROCOM-STAT-03a

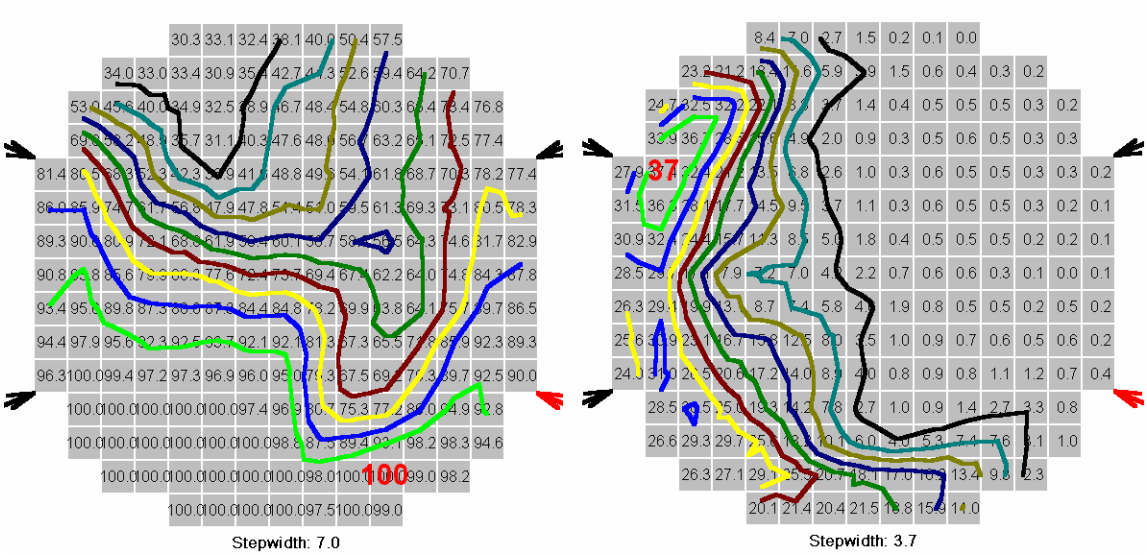

a) ROCOM-STAT-03
(time of maximum)

b) ROCOM-STAT-03a
(time of maximum)

Fig. 1-18 Distribution of the mixing scalar at the core inlet in the experiments ROCOM-STAT-03 and ROCOM-STAT_03a (perturbation in loop 1(red arrow); maximum: bold red number)

Most of the tracer, especially in the short term injection experiment is found on the side opposite to the azimuthal position of the loop with injection (Fig. 1-18). This is due to the typical one-loop operation velocity field in the downcomer with a maximum on the opposite side (see next chapter).

B.1.4 Experimental results on velocity measurements

B.1.4.1 Measurement system and positions

The measurements of the velocity were carried out by means of a laser Doppler anemometer. The velocity was measured at the outlet of the downcomer in a plane 1045 mm below the middle of the nozzle region. Measurements of the vertical and the horizontal velocity components were made at 32 positions equally distributed around the circumference of the downcomer. In radial direction, the measurement position was in the middle of the downcomer. Data of the measurements are stored in clockwise direction. For all cases, measurement was continued until 1000 bursts were registered in the counting device of the laser system. The data were averaged over the 1000 single values, standard deviation was calculated, showing the fluctuation of the velocity at a certain position in the stationary flow field.

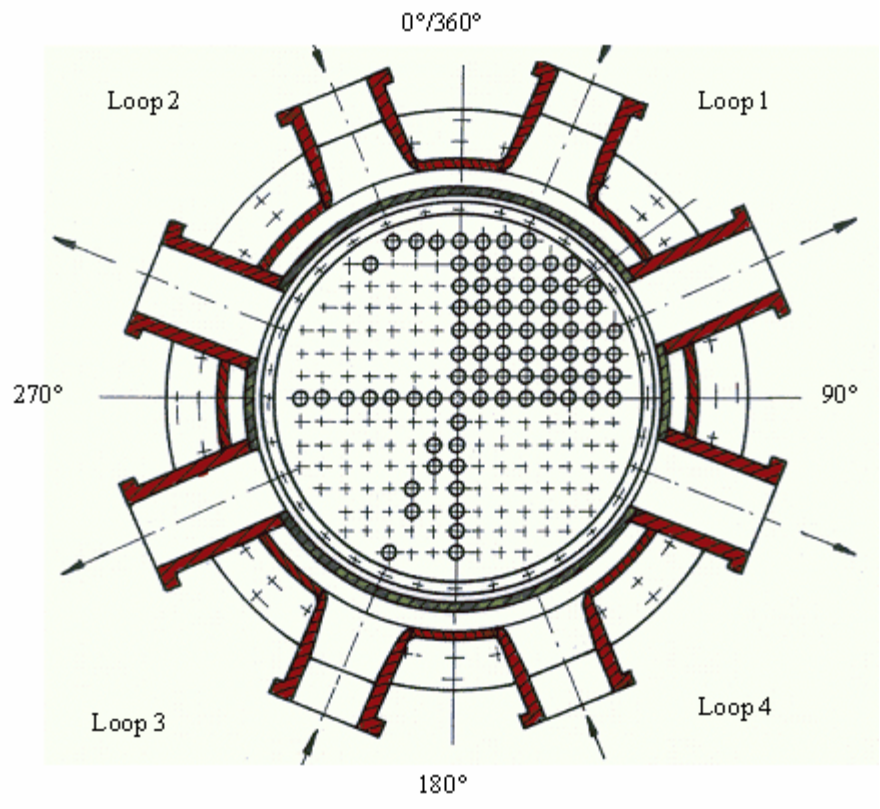

Fig. 1-19 Arrangement of the loops at ROCOM and the corresponding angle positions

B.1.4.2 Experiment ROCOM-STAT-01

In the experiment ROCOM-STAT-01, the pumps in all loops were working at nominal conditions. Fig. 1-20 shows the measured vertical component of the velocity in the experiment ROCOM-STAT-01 together with the confidence interval of 68.3 % (In all figures with velocity, negative values mean downwards directed flow!). It is clearly to be seen, that the velocity heavily depends on the measurement position on the circumference. At the positions 0 °, 90 °, 180 ° and 270 °, that means in the middle between two neighbouring inlet or outlet nozzles, a maximum of the velocity is observed. Minima of the velocity are measured at the positions between the above mentioned angle positions (45 °, 135 °, 225 ° and 315 °). The non-uniformity of the velocity field at the outlet of the downcomer is caused by a group of eight recirculating swirls, forming up below the inlet nozzle region.

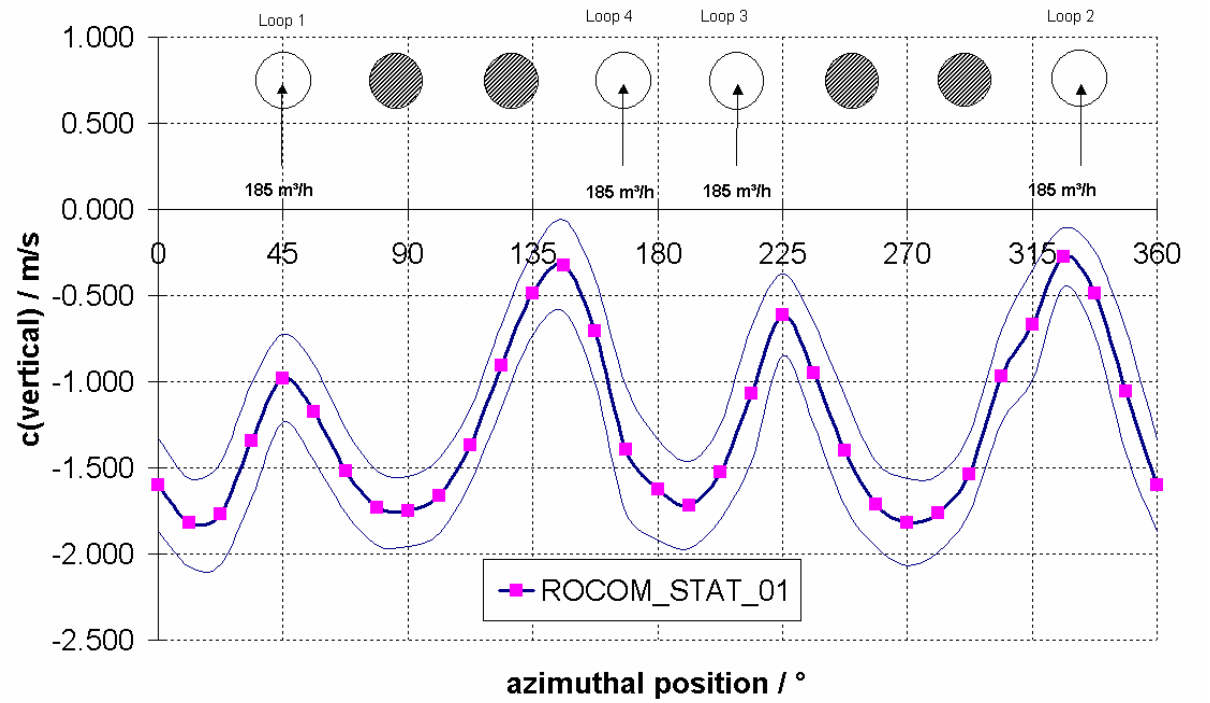

Fig. 1-20 Profile of the velocity in circumferential direction at the outlet of the downcomer in the experiment ROCOM-STAT-01

B.1.4.3 Experiment ROCOM-STAT-03

The experiment ROCOM-STAT-03 is characterized by one-loop operation at nominal flow rate. This regime corresponds to the final state of the slug mixing experiments (see [Roh04]). After entering the downcomer, the flow from the only working loop 1 hits the core barrel and splits into two parts, flowing right and left around the barrel to the opposite side. Here, they meet together and create a downwards directed flow to the outlet of the downcomer. The maximum of the velocity is measured between the position of the inlet nozzles 3 and 4 (Fig. 1-21). A recirculation area exists below the inlet nozzle with the working loop. This velocity distribution is the explanation for the distribution of the mixing scalar at the core inlet in the corresponding tracer injection experiments (Fig. 1-18).

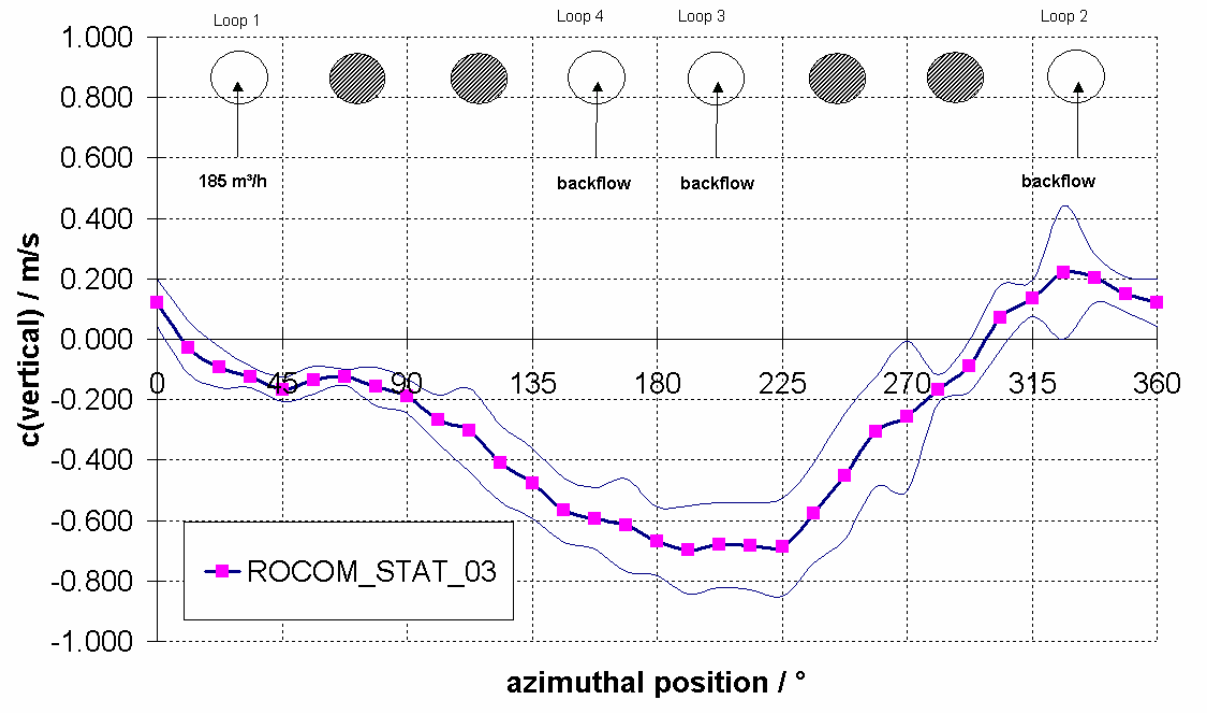

Fig. 1-21 Profile of the velocity in circumferential direction at the outlet of the downcomer in the experiment ROCOM-STAT-03

B.1.4.4 Three-loop operation (ROCOM-STAT-04)

In the experiment ROCOM-STAT-04, the pumps in loops 1 to 3 work at nominal conditions, the pump in loop 4 is switched off. In this loop configuration, only three maxima of the velocity are present. The position of the maxima is shifted in comparison to the four-loop operation measurements. A minimum of the velocity is measured between inlet nozzles 3 and 4. At this position and at the position of the minimum between the nozzles of loop 2, even a small backward flow is measured (Fig. 1-22).

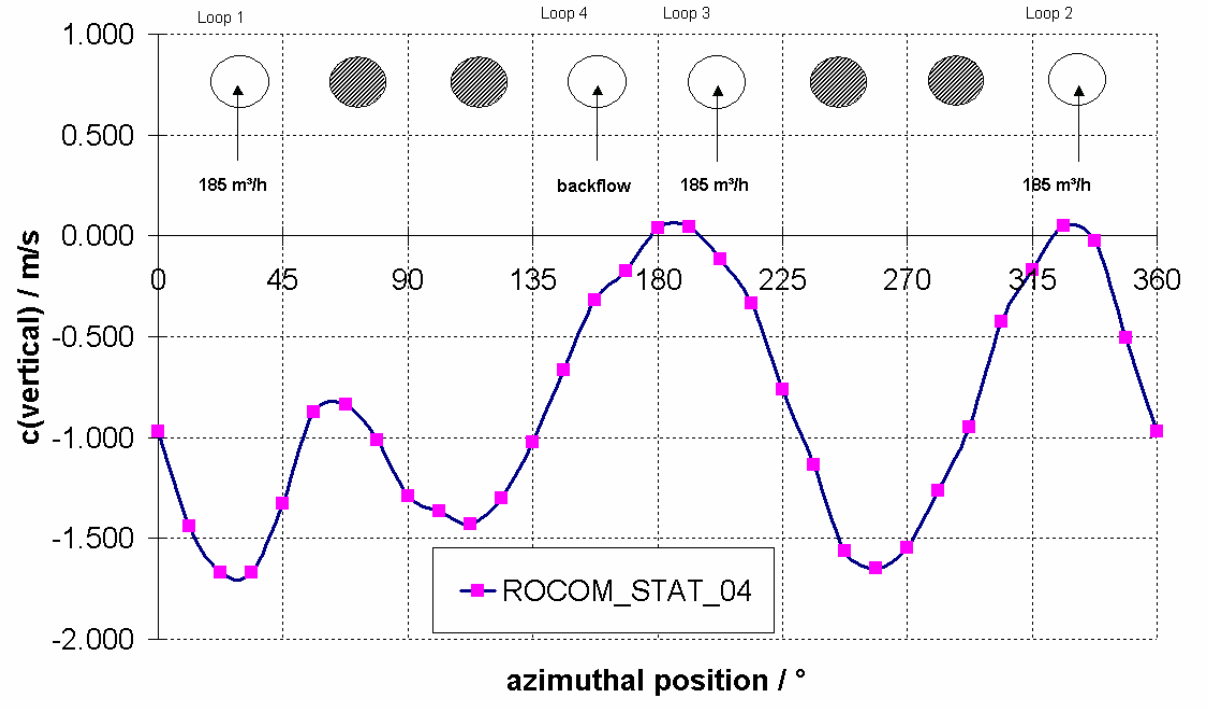

Fig. 1-22 Profile of the velocity in circumferential direction at the outlet of the downcomer in the experiment ROCOM-STAT-04

B.1.4.5 Different combinations of two-loop operation

In the case of two-loop operation with switched off pumps in loop 3 and 4 (ROCOM-STAT-06), only one maximum of the velocity at the outlet of the downcomer is found (Fig. 1-23). It is located below the inlet nozzle of loop 1. Below inlet nozzle of loop 2, a minimum of the velocity is measured revealing a recirculation area. This backward flow is responsible for the tracer distribution in the downcomer in the experiment ROCOM-STAT-06 (Fig. 1-10). The small time delay between the appearance of the tracer below inlet nozzle 1 and 2 indicates, that the tracer in the measurement plane of the downcomer sensors below nozzle 2 is transported with the upwards directed flow, what is fully in accordance with the velocity measurements.

In case of operation of loops 1 and 3 and 1 and 4, the measured velocity fields are quite similar (Fig. 1-24). The redistribution of the flow after entering the downcomer leads to identical final results. The same conclusion was drawn from the concentration measurements (see above). Two maxima are measured between the outlet nozzles 1 and 4 and 2 and 3. Two minima of the velocity with backward flow are found between the inlet nozzles of the same loops.

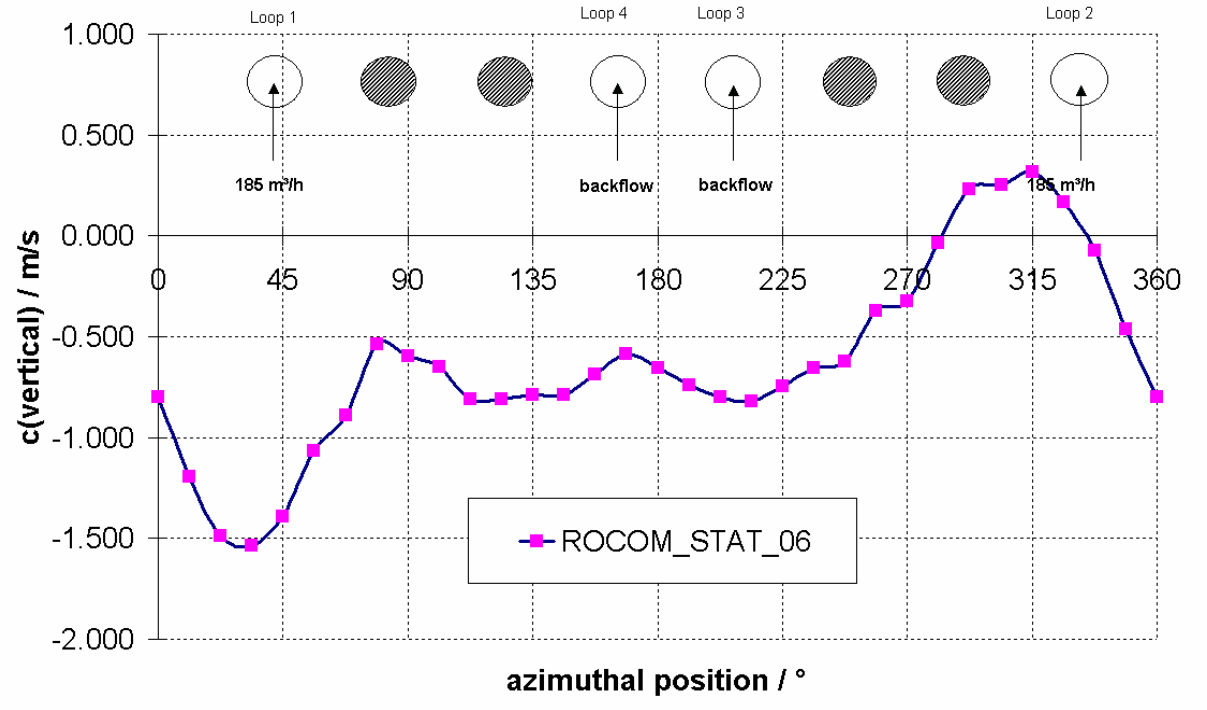

Fig. 1-23 Profile of the velocity in circumferential direction at the outlet of the downcomer in the experiment ROCOM-STAT-06

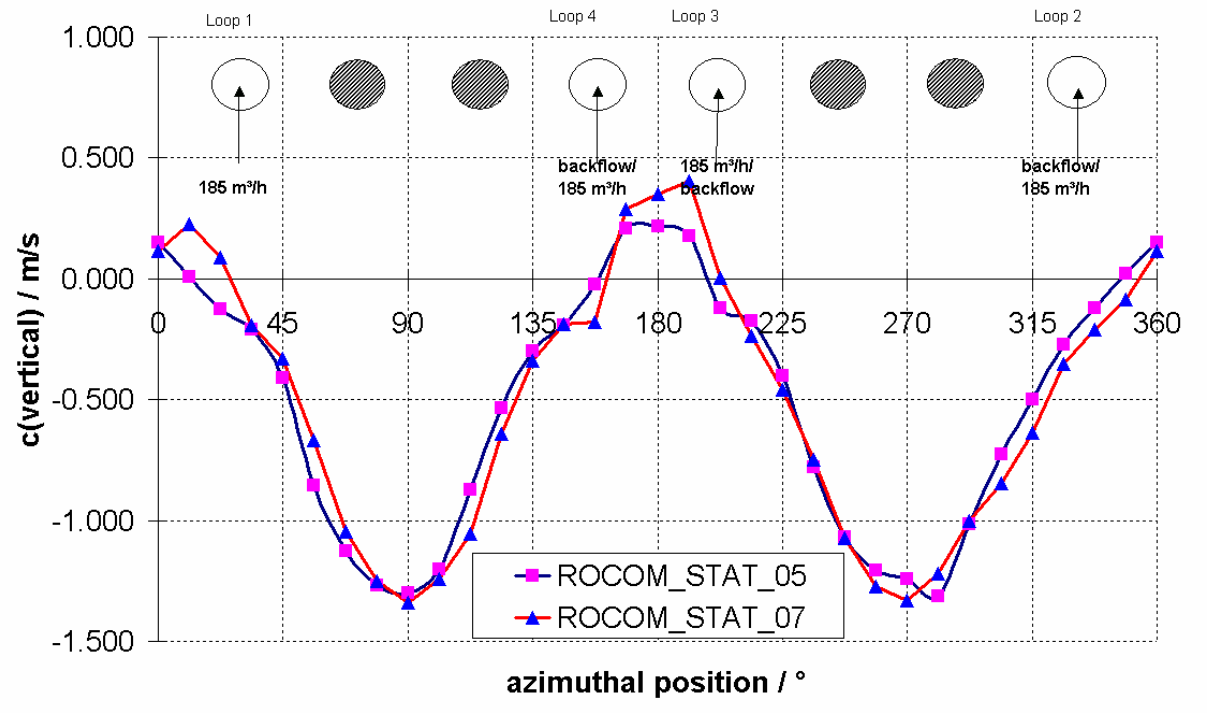

Fig. 1-24 Profile of the velocity in circumferential direction at the outlet of the downcomer in the experiments ROCOM-STAT-05 and ROCOM_STAT_07

B.1.4.6 Variation of loop flow rates at constant total flow rate

The increase of the flow rate in loop 1 and the simultaneous decrease of the flow rate in loop 2 leads to a widening of the area below the nozzle region influenced by loop 1 and a shift of the minimum of the velocity below loop 2, accompanied by a increase of the absolute value of the velocity at that position (Fig. 1-25). The position and values of the maxima below the loops 3 and 4 are not affected by the variation of the flow rates in loop 1 and 2. The change in position of the maximum of the velocity and maximum value itself is greater between 0 and 10 % asymmetry than between 10 and 20 %. The measured velocity profile corresponds to the measured tracer concentration profile (Fig. 1-13) in a very good manner.

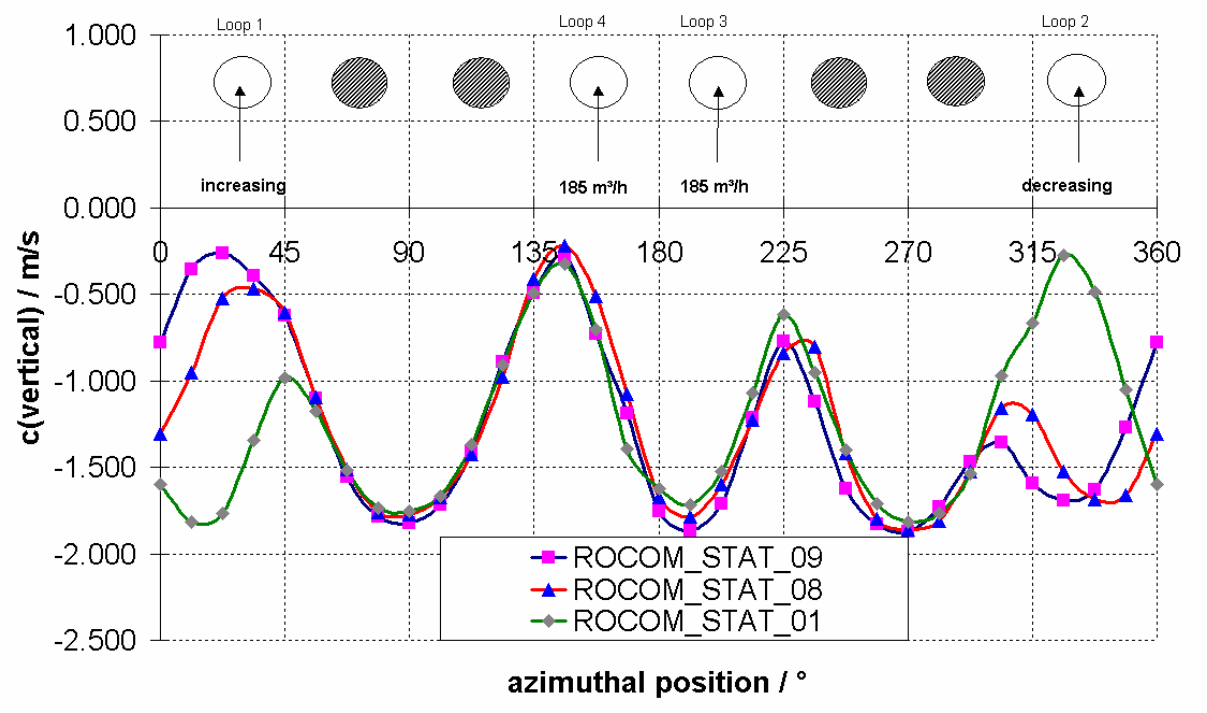

Fig. 1-25 Profile of the velocity in circumferential direction at the outlet of the downcomer in the experiments with growing asymmetry between loops 1 and 2

B.2 Experimental investigation of thermal mixing phenomena in a six loop VVER type reactor

The experiment summary report of investigation of thermal mixing phenomena in the Paks six loop VVER type reactor is attached in its entirety as an appendix 1 to this report. In the following chapter B.2.1 is presented the abstract of this report.

B.2.1 Abstract of the experiment summary report of investigation of thermal mixing phenomena in a six loop VVER type reactor at Paks NPP

Certain conditions in a pressurised water reactor with six coolant loops may cause the flow rate and the temperature from one of the cold legs to differ significantly from those in the other loops.

Thermal mixing tests at the Paks NPP indicated that total mixing did not occur in the downcomer and in the lower plenum, thus temperature distribution at the core inlet becomes non-uniform. The assumption of perfect mixing may lead to an erroneous prediction the inlet temperature field.

The paper (appendix 1) presents a simple experimental method used an operational reactor for the measurement of temperature field at the core entrance and based on these tests the determination of the mixing factors.

In order to create a significant asymmetry between the temperatures of the cooling loops, the measurements were performed on power, undertaking serious problems arising during the test evaluation.

The different steam generator pressure has been used as a source of the asymmetry, which has been reached by successively closing the valves on the steam lines.

With linear regression analyses the mixing factors for the inlet points of those assemblies in the outlet of which the thermometers are located have been determined.

B.3 CFD simulations of ROCOM steady state mixing experiments

A set of the steady state mixing experiments at the ROCOM test facility were simulated by FZR, AEKI and VUJE. In chapter B.3.1 is summed up the post-test calculations of FZR made using CFD codes CFX-4 and CFX-5. Two steady-state tests simulated by VUJE are presented in chapter B.3.2 and two forced flow ROCOM tests simulated by AEKI are presented in chapter B.3.3. The code used by VUJE and AEKI was FLUENT.

The main objective of the CFD simulations was the CFD code validation. The detailed results and comparisons to the experimental results are presented in the final report of work package 4. The computation results presented here are "the best results" used to determine the primary circuit flow field characteristics. However some observations and conclusions concerning the CFD modelling of the primary circuit flow are also presented here.

B.3.1 Post-Test calculations of ROCOM steady state mixing experiments with CFX-4 and CFX-5 by FZR

B.3.1.1 Computational modelling

The used CFD-Codes for mixing studies at the Forschungszentrum Rossendorf (FZR) are CFX-4 and CFX-5 [CFX4, CFX5].

CFX-4 is a finite volume program that offers the following options, which can be used in the mixing studies:

- Block structured discretization grids
- Solution of the Navier-Stokes-Equations for steady and unsteady flows for compressible and incompressible fluids
- Applicability for laminar and turbulent flows (different turbulence models)
- Porous media model, implementation of body forces added to the momentum equation, user defined scalar equations
- A wide range of physical models and User Fortran.

In addition CFX-5 offers:

- Advanced coupled multigrid linear solver technology
- Unmatched meshing flexibility
- Superb parallel efficiency
- Excellent pre- and post-processing capabilities and a lot more.

First CFX-4 calculations were performed using the porous body approach. CFX-5 calculations with a very detailed mesh were used to confirm the CFX-4 results without additional physical models.

B.3.1.1.1 Turbulence modelling

The modelling of the turbulence is important both for the flow field and the concentration field. At the same time turbulence modelling is one of the biggest problems in the field of the CFD. In the boron-diluted slug mixing calculations made so far the mostly used turbulence model is the standard K-ε model and it's variations like RNG K-ε model. Some occasional tests are made also with Reynolds Stress Model (RSM) and even using Large Eddy

Simulation (LES) [Be96]. However in spite of the well-known limitations the most common and the most robust models like k-ε seems to be most often used. In the calculated cases the turbulence was modelled using the standard (k, ε) approximation.

B.3.1.1.2 Numerical diffusion, nodalization and time step size

Numerical error is a combination of many aspects; the grid density, discretization method, time step size and convergence error have all their own effect. When a validation of the computational model is made using a certain experiment, the separation of different numerical effects is difficult; for example, the numerical diffusion, which acts like an artificial extra diffusion, can affect to the result in the same direction like too large turbulent viscosity used in some turbulence models.

The numerical diffusion can be minimized using denser grids, higher order discretization methods and suitable time step size. Often the computation time puts some limits for these, but anyhow in all CFD computations results should be ensured to be grid and time-step independent, and if not possible, the uncertainties should be quantified. The ERCOFTAC Best Practice Guidelines [BPG], which have been specified for nuclear reactor safety calculations within the ECORA project [ECO], have been used when making sensitivity tests for:

- Computational mesh
- Numerical schemes
- Convergence criteria
- Time step
- Boundary positions
- Boundary conditions
- Internal geometry modelling
- Turbulence models.

Based on these tests the production mesh was created and the final CFD calculations were performed.

B.3.1.1.3 Geometrical Simplifications, Local Details

The geometric details of the construction internals have a strong influence on the flow field and therefore on the mixing. Therefore, an exact representation of the inlet region, extension of the downcomer below the inlet region and the obstruction of the flow by the outlet nozzles cut through the downcomer is necessary (Figures 3.1-2 and 3.1-3).

In the CAD-File for the CFX-5 solver, generated with CFX-Build, all geometrical details are modelled accurately, like: inlet nozzles incl. the diffuser part, orifices of the outlet nozzles, downcomer extension, lower plenum, core support plate, perforated drum, core simulator, upper plenum and the outlet nozzles (see also Fig. 3.1-3). No additional physical models (Porous media, Body Forces) are necessary.

In CFX-4 geometrical simplifications were made for the perforated drum and the core support plate. The core simulator, the upper plenum and the outlet nozzles were not modelled. The CFX-4 Preprocessor Meshbuild was used.

The core support plate and the perforated drum were modelled as porous regions. The porosity value γ for perforated plates is determined by relating the area of orifices to the total

area of the sieve. Body forces B are added to the momentum equation (Equ. 3.1-1), to take into account distributed friction losses in the sieve plate. Using the Cartesian coordinate system, the momentum equation is written:

(j=1,2,3)

$$\rho\left(\frac{\partial U_j}{\partial t} + U_i \frac{\partial U_j}{\partial x_i}\right) = B_j - \frac{\partial}{\partial x_i}\tau_{ij} \qquad \text{(Equ. 3.1-1)}$$

$$B = B_F - \left(R_C + R_F|\overline{u}|\right)\overline{u} \qquad \text{(Equ. 3.1-2)}$$

In the equation (Equ. 3.1-1) U_j are the components of velocity and τ is the shear stress, B_F, R_C and R_F are the coefficients of the body force dependence on the velocity. In the model, only the second order contribution of the body forces according to relation (Equ. 3.1-2) is used being typical for turbulent flow. The corresponding coefficient is obtained from calculated values for the flow resistance coefficient.

B.3.1.1.3.1 The Core Support Plate

The plate (Fig. 3.1-2) contains 193 orifices with a diameter of d=20 mm each. This plane was modelled in detail in CFX-5, in CFX-4 the porosity of the plane was modelled (β=0.229) and Body Forces used to model the measured pressure loss through the plate.

B.3.1.1.3.2 The Perforated Drum

The perforated drum (Fig. 3.1-1) contains 410 orifices of 15 mm diameter. In CFX-4 it was modelled as a porous body, with additional body forces. The drum has a porosity of β=0.208. In CFX-5 the drum was modelled in detail (see Fig. 3.1-1)

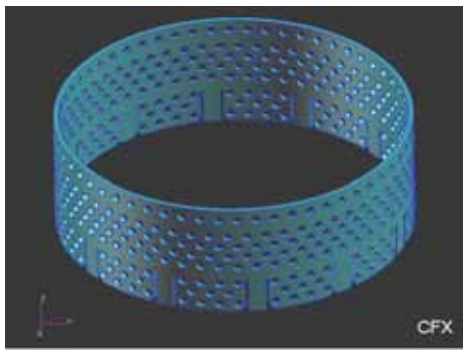

Fig. 3.1-1 Perforated drum (CFX-5)

B.3.1.1.3.3 The Core

The core contains 193 fuel element dummies. The fluid flows through the hydraulic core simulator inside the tubes. In CFX-4 the core was modelled as a free flow field as it will probably not significantly effect the mixing in the lower plenum. However a detailed modelling was used in CFX-5 (Fig. 3.1-3).

B.3.1.1.4 Grid Generation

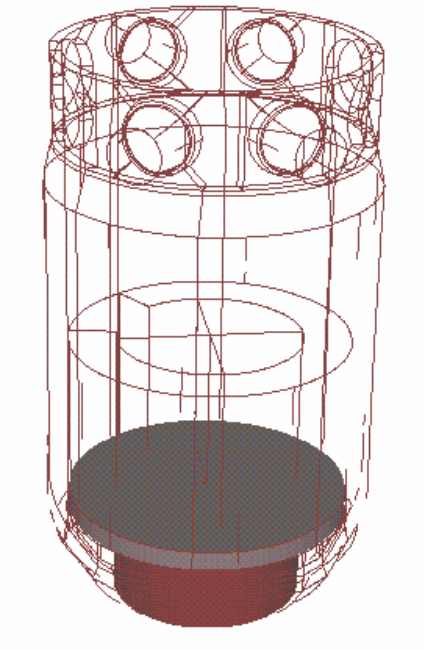

Fig. 3.1-2 Computational grid CFX-4, block structured

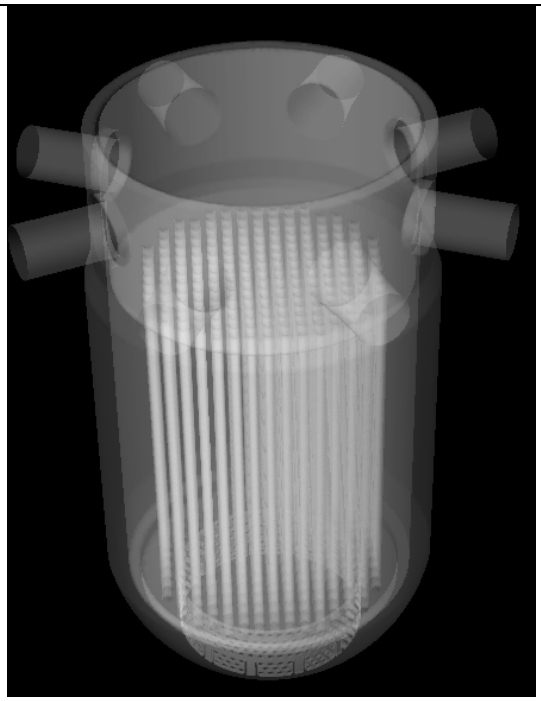

Fig. 3.1-3 Computational grid CFX-5, unstructured

In CFX-4 the generated block structured grid contained ca. 450000 hexahedral elements (Fig. 3.1-2). A finer mesh was created in the area of the inlet nozzle plane, in the area of the downcomer extension, around the perforated drum and at the core support plane. In CFX-5 the mesh contained 5 Mio. tetrahedral elements (Fig. 3.1-3). Mesh refining was used in the area of the perforated drum and in the lower support plate.

B.3.1.1.5 Boundary Conditions

The inlet boundary conditions (velocity, mixing scalar etc.) were set at the inlet nozzles. No specific velocity profile is given. As an initial guess of the turbulent kinetic energy and the dissipation rate the code standard is used. The outlet boundary conditions were pressure controlled. Passive scalar fields were used to describe the boron dilution processes.

Steady state calculations with at least 1000 iterations last a few hours, parallel transient calculations one or two weeks on a 64 processor MSC LINUX cluster (dual CPU compute nodes, each containing 2GB RAM).

In the calculated cases the time step of 0.05 s was taken according to the BPG studies and in agreement with the time solution of the measured data.

B.3.1.2 Results of steady state flow and mixing at ROCOM

To simulate the mixing of the coolant under MSLB scenarios with operating main coolant pumps, generic experiments at the ROCOM test facility and CFD-calculations were made at nominal conditions, i.e. all main coolant pumps were operating.

In the Figures 3.1-4 and 3.1-5 the flow condition is demonstrated with the help of streamlines in one quarter of the RPV. The other 3 quarters look similar. The velocity field, determined in

the CFX-4 and CFX-5 calculations, show a qualitatively good agreement with experimental results (air operated model of Ulrych and Weber [Ul83] and LDA measurements at ROCOM [Pr03]). The calculations especially confirm location of minimum flow velocities below the inlet nozzles found in earlier experiments [Ul83]. A maximum velocity exists at azimuthal positions between the two inlet resp. the two outlet nozzles (Fig. 3.1-6). In the investigated flow rate turbulent flow is fully developed.

Mixing test experiments were carried out under steady state flow field conditions at different mass flow conditions. To have a comparison between the CFD calculations with measurements, an experiment at 185 m^3/h per loop with steady flow conditions was chosen and a large slug of salted water was injected.

At the inlet nozzle (Fig. 3.1-7a) the same conditions as in the experiments (mixing scalar per time step at 0.05 s in one loop, velocities in all loops) were set as inlet boundary conditions for the CFD calculations (CFX-4 and CFX-5).

In Fig. 3.1-6b the instantaneous maximum of the mixing scalar at the core inlet independently of the actual fuel element position is plotted against the time. The maximum mixing scalar at the core inlet rapidly increases to the maximum. There is a good agreement between the measurement and the CFD calculations, especially in the averaged global mixing scalar at the core inlet (Fig. 3.1-7c).

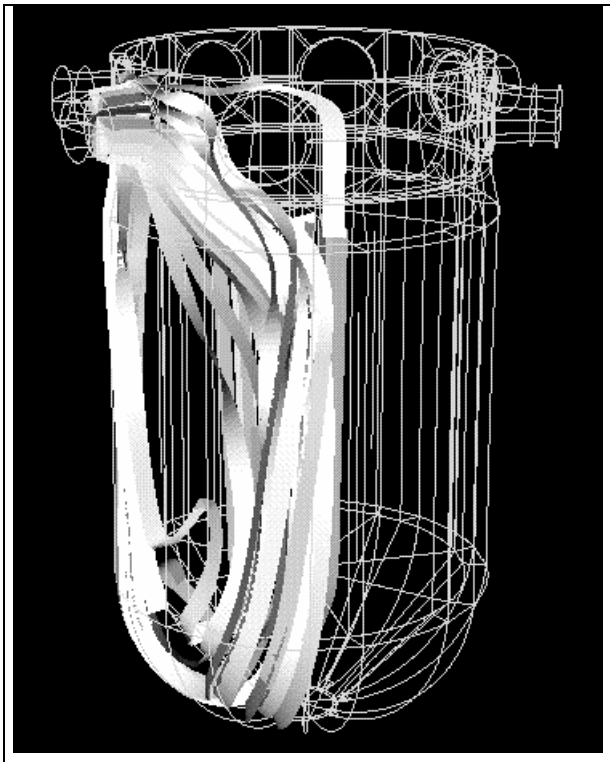

Fig. 3.1-4 Streamlines representing the flow in the downcomer (CFX-4)

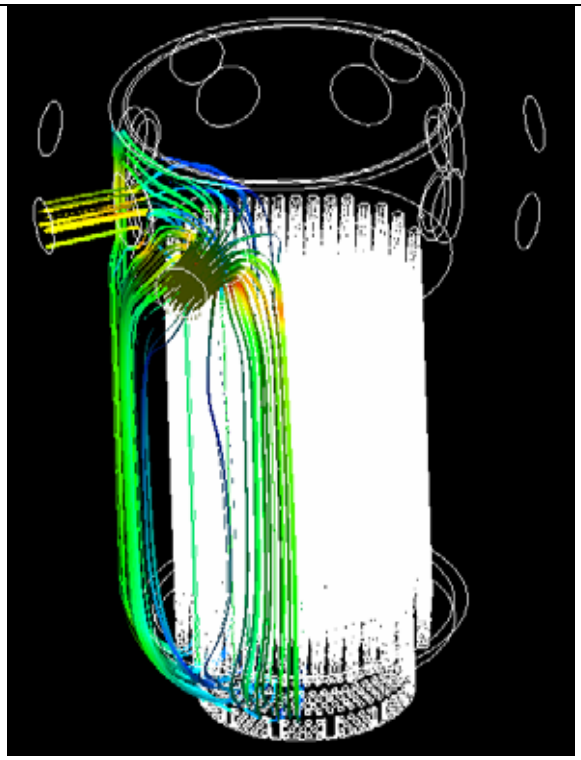

Fig. 3.1-5 Streamlines (CFX-5)

At the local position of the maximum mixing scalar the time course of the measurement and the calculations are also in good agreement (Fig. 3.1-7d). The coolant from the disturbed inlet nozzle almost completely arrives in the corresponding sector of the core inlet (Figures 3.1-7e,f). On the other hand, areas of the core inlet were not affected at all.

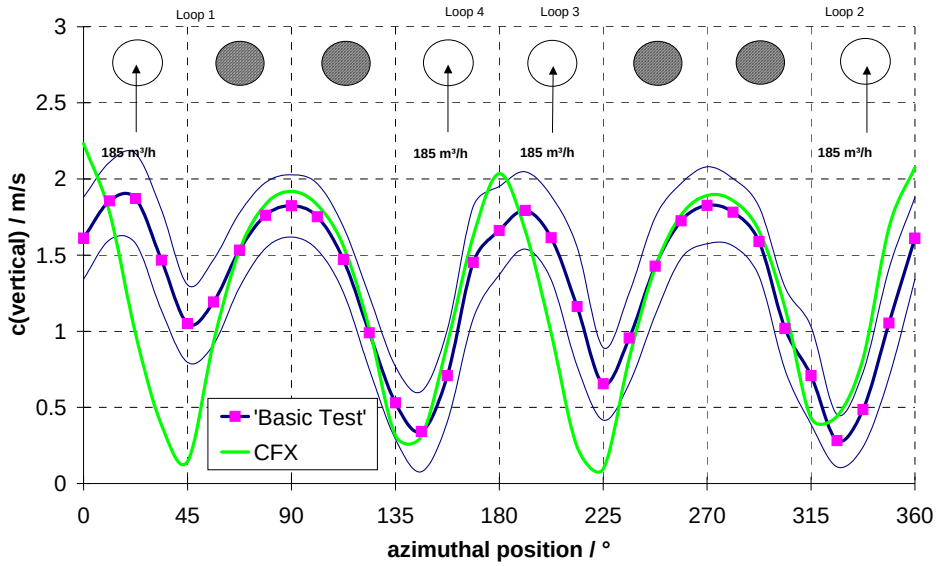

Fig. 3.1-6 Velocity measurements vs. CFX-5 results at the end of the downcomer

Despite of the flow deflection in the lower plenum and the partial penetration of the perforated barrel, the maximum disturbance observed at the core inlet is 91 % (CFX-4), 94% (CFX-5) and 95% (measurement) in comparison to a 100 % concentration change at the inlet nozzle. These results can only be obtained, if a sufficiently large slug of tracer has been injected to create a tracer plateau shown in Figure 3.1-7c, on which all data were time averaged. If smaller slugs are injected, steady state conditions at the core inlet are not achieved.

There are some local differences between the results of the CFX-4 and CFX-5 calculations seen at the sector of the maximum mixing scalar (Figures 3.1-7e and 3.1-7f). Nevertheless, the comparison shows, that the use of the porous body approach with additional body forces gives reasonable results. However, there are local differences of both calculations to the experimental values, which are probably a result of unknown unsteady inlet boundary conditions (changing velocity profiles, turbulent fluctuations etc.).

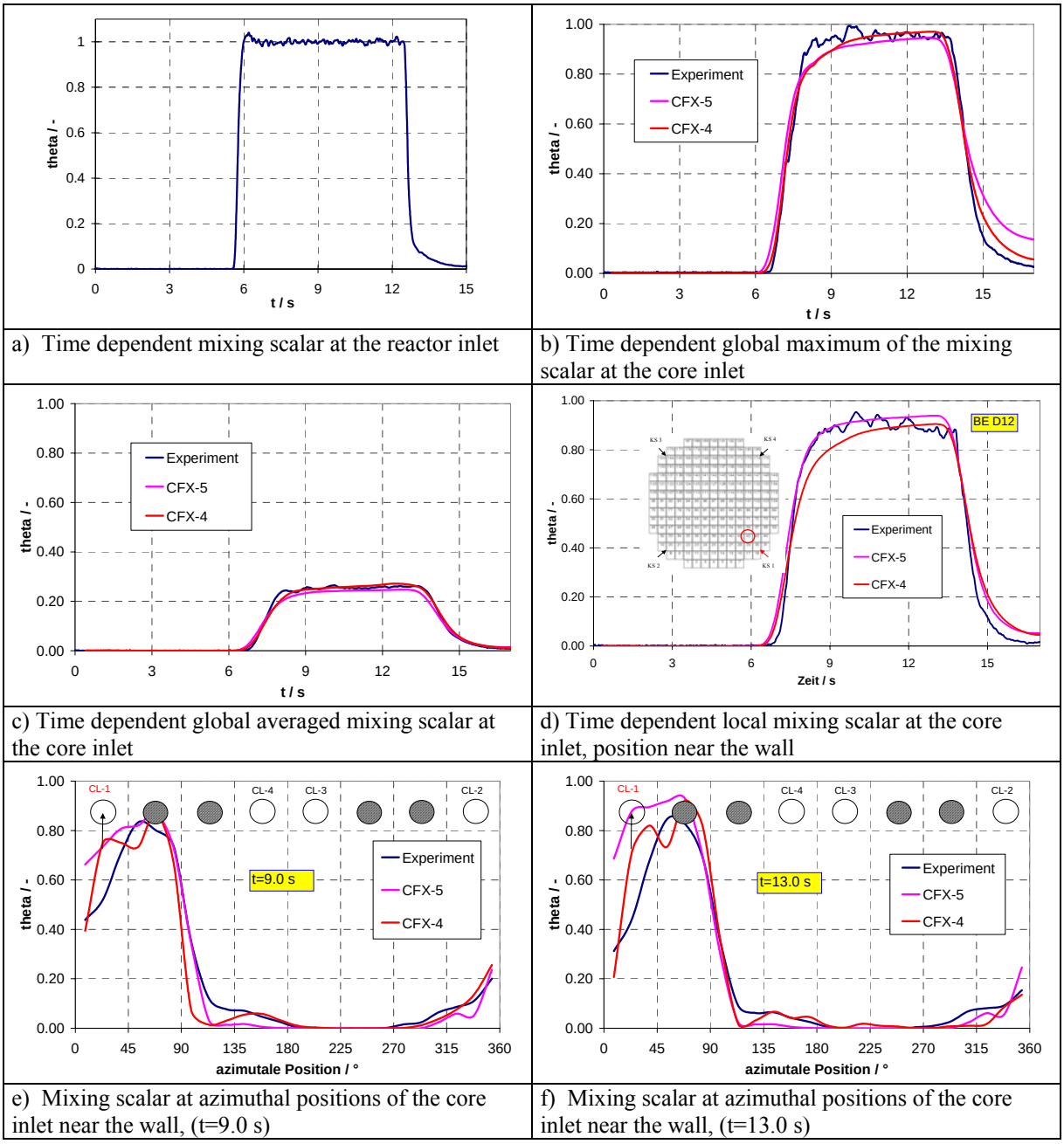

a) Time dependent mixing scalar at the reactor inlet

b) Time dependent global maximum of the mixing scalar at the core inlet

c) Time dependent global averaged mixing scalar at the core inlet

d) Time dependent local mixing scalar at the core inlet, position near the wall

e) Mixing scalar at azimuthal positions of the core inlet near the wall, (t=9.0 s)

f) Mixing scalar at azimuthal positions of the core inlet near the wall, (t=13.0 s)

Fig. 3.1-7 Comparison of the measured and calculated mixing scalar (steady state flow field, 185 m³/h)

Figure 3.1-8 shows the plateau averaged mixing scalar distribution at the core inlet of the experiments and two CFX-5 calculations. One calculation was done with the steady state flow field and the transient slug behaviour was modelled (see also Fig. 3.1-7). The other calculation was done in a steady state mode. For the transient calculated case the maximum value (94%) and the shape of distribution of the mixing scalar is in good accordance with the experimental value. The sector formation of the mixing scalar below the injection loop is clearly to be seen in all pictures.

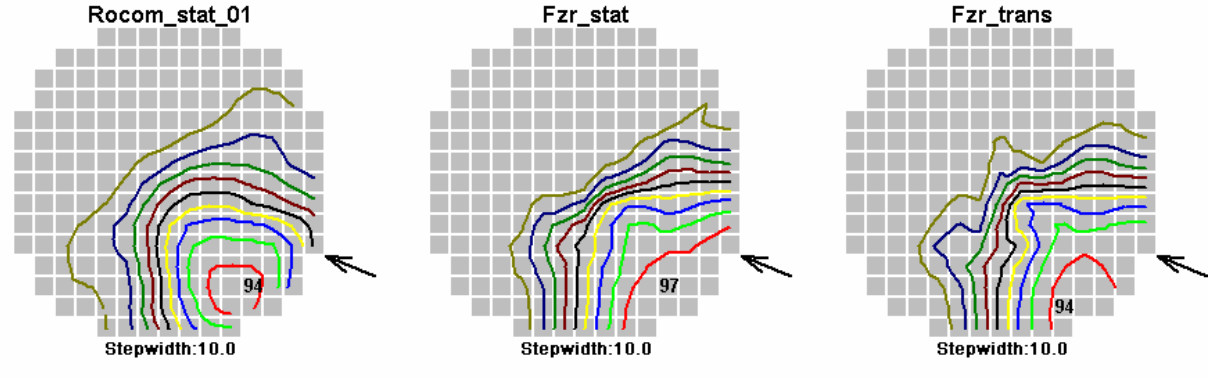

Fig. 3.1-8 Comparison of the measured and calculated mixing scalar at the core inlet with the help of isolines (steady state flow field, 185 m³/h)

B.3.1.3 Summary and Conclusions

The work was aimed at the numerical simulation of coolant mixing in the downcomer and the lower plenum of the Rossendorf test facility ROCOM. The CFD calculations were carried out with the CFD-codes CFX-4 and CFX-5. In the case of stationary mixing, the maximum value of the averaged mixing scalar at the core inlet was found in the sector below the inlet nozzle, where the tracer was injected. The comparison of a very detailed mesh (CFX-5) and a mesh with simplifications and additional physical models (CFX-4) showed, that in the referred case the use of these models are allowed. For turbulent flows CFX-4 and CFX-5 were validated in accordance with the Best Practice Guidelines and can be used in the reactor safety analysis. A better description of the mixing processes inside the RPV is the basis of a more realistic safety assessment.

B.3.2 Calculations of ROCOM steady state mixing experiments with FLUENT by VUJE

VUJE contribution to the project goals consisted of CFD code analyses for the code validation. For this purpose two ROCOM experiments were used. The first was steady-state experiment STAT_01, the second, steady-state experiment STAT_04 performed at ROCOM test facility.

Test ROCOM STAT_01 consisted of symmetric coolant injection into all 4 inlet nozzles, while in the nozzle loop No.1 the specific concentration of salt (NaCl) was dissolved in the coolant. After passing the downcomer and the core, coolant is flowing out of reactor vessel through outlet nozzles in the upper part of the reactor vessel. The experiment was designed with the aim to investigate coolant mixing in symmetric operation of all loops by measuring coolant velocities in the LDA position and concentration of salt in measurement sensors in the coolant flow path (see Fig. 3.2-1).

The experiment ROCOM STAT_04 was designed with the aim to investigate coolant mixing in asymmetric operation of loops by measuring coolant velocities in the LDA position and concentration of salt in measurement sensors in the coolant flow path (see Fig. 3.2-1). The test consisted of asymmetric coolant injection into inlet nozzles: coolant with the same specified flow rate was injected into inlet nozzles of loops 1, 2 and 3, while the loop No. 4 was let as additional outlet from the reactor vessel. Specific concentration of salt was dissolved in the nozzle No. 1. After passing the downcomer and the core, coolant is flowing out of reactor vessel through outlet nozzles in the upper part of the reactor vessel.

B.3.2.1 Computational modelling

CFD code FLUENT version 6.1.18 was used for the calculations described in this section. FLUENT is a finite volume code that offers the following options, which can be used in the mixing studies:

- flows in 2D or 3D geometries using unstructured using solution-adaptive triangular/tetrahedral, quadrilateral/hexahedral or hybrid grids;
- incompressible or compressible inviscid, laminar and turbulent flows
- steady state or transient analysis;
- convective, coupled conduction/convective or radiation heat transfer;
- inertial or non-inertial reference frame models;
- multiple moving reference frames;
- chemical species mixing and reaction, including combustion submodels and surface deposition reaction models;
- arbitrary volumetric sources of heat, mass, momentum, turbulence and chemical species;
- Lagrangian trajectory calculations for a dispersed phase of particles, including coupling with the continuous phase;
- porous media model, implementation of body forces added to the momentum equation;
- two phase flows including cavitation;
- a wide range of physical models.

B.3.2.2 Turbulence modelling

In presented calculations two turbulence models were used with the aim to find the impact of different turbulence models on results.

Standard k-ε model

The standard k-ε model is a semi-empirical model based on model transport equations for the turbulence kinetic energy (k) and its dissipation rate (ε). The model transport equation for k is derived from the exact equation, while the model transport equation for ε as obtained using physical reasoning and bears little resemblance to its mathematically exact counterpart.
In the derivation of the k-ε model, it was assumed that the flow is fully turbulent, and the effects of molecular viscosity are negligible. The standard k-ε model is therefore valid only for fully turbulent flows.

RNG k-ε model

The RNG k-ε model was derived using a rigorous statistical technique (called renormalization group theory). It is similar in form to the standard k-ε model, but includes the following refinements:

- The RNG model has an additional term in its ε equation that significantly improves the accuracy for rapidly strained flows.
- The effect of swirl on turbulence is included in the RNG model, enhancing accuracy for swirling flows.

- The RNG theory provides an analytical formula for turbulent Prandtl numbers, while the standard *k*-ε model uses user-specified, constant values.
- While the standard *k*-ε model is a high-Reynolds-number model, the RNG theory provides an analytically-derived differential formula for effective viscosity that accounts for low-Reynolds-number effects. Effective use of this feature does, however, depend on an appropriate treatment of the near-wall region.

These features make the RNG *k*-ε model more accurate and reliable for a wider class of flows than the standard *k*-ε model.

B.3.2.3 Numerical diffusion, nodalization and time step size

Discretisation schemes
FLUENT uses a control-volume-based technique to convert the governing equations to algebraic equations that can be solved numerically. This control volume technique consists of integrating the governing equations about each control volume, yielding discrete equations that conserve each quantity on a control-volume basis.

When first-order accuracy is desired, quantities at cell faces are determined by assuming that the cell-centre values of any field variable represent a cell-average value and hold throughout the entire cell; the face quantities are identical to the cell quantities.

When second-order accuracy is desired, quantities at cell faces are computed using a multidimensional linear reconstruction approach. In this approach, higher-order accuracy is achieved at cell faces through a Taylor series expansion of the cell-centred solution about the cell centroid.

In calculations presented in this section both, first order and second order upwind schemes were applied to assess their influence on results. In terms of discretisation scheme the following combinations of optional models were selected:

	1st option	2nd option
Momentum:	1st order upwind	2nd order upwind
Pressure:	PRESTO	PRESTO
k:	1st order upwind	2nd order upwind
ε:	1st order upwind	2nd order upwind
Pressure-velocity coupling:	SIMPLE	SIMPLE

During the calculation of Case 1 and 2 it was shown that 2nd order numerical schemes give significantly different results, i.e. for both Grid 1 and Grid 2. This indicates that the solutions are not completely grid independent.

Relaxation
Following (default) under-relaxation factors were used in calculations:

- Pressure: 0.3
- Density: 1.0
- Body forces: 1.0
- Momentum: 0.7
- Turbulence kinetic energy: 0.8
- Turbulence dissipation rate: 0.8
- Turbulence viscosity: 1.0

Time step
As the ROCOM tests were steady-state tests and were calculated as steady-state problems, no time step was defined in the calculations.

B.3.2.4 Geometrical Simplifications, Local Details

Omitted (i.e. not modelled) geometry:

- Small structures, protrusions and chambers.
- Wire-mesh sensors of the measurement system

Simplified geometry:

- Perforated drum - two models were used: porous media and reduced number of holes.
- The core was modelled as porous media model or omitted at all.

B.3.2.4.1 The Core Support Plate
Two types of grids were used in the lower plenum region, depending on whether the porous body was modelled "realistically" as a solid structure with reduced number of holes or as a perforated drum. In both cases the grids of reactor vessel bottom, perforated drum and core support plate were made of triangles. Walls of the holes in the core support plate were meshed with quadrilaterals. Boundary layer option was not applied in this region

B.3.2.4.2 The Perforated Drum
Cylindrical perforated drum in the lower plenum (Fig. 3.2-1) was modelled variantly either as porous medium with direction-dependent hydraulic resistance (there were used various initial value of the resistance) or as a cylindrical structure with reduced number of holes but with maintained equivalent flow cross-section.

B.3.2.4.3 The Core
The core was modelled using porous media model.

B.3.2.5 Grid generation

CFD analysis of ROCOM STAT_01 and STAT_04 experiments focused on assessment of the influence of the level of grid details (coarse or fine mesh), type and location of outlet condition as well as the extent and ways of modelling of internal geometry. These goals require development of more than one geometry model and computational grids. In the final calculation, adapted hybrid mesh with perforated drum modelled as solid structure with reduced number of holes was used. The mesh consisted of 1.504.881 cells.

Originally developed and adapted grids are presented in Fig. 3.2-1.

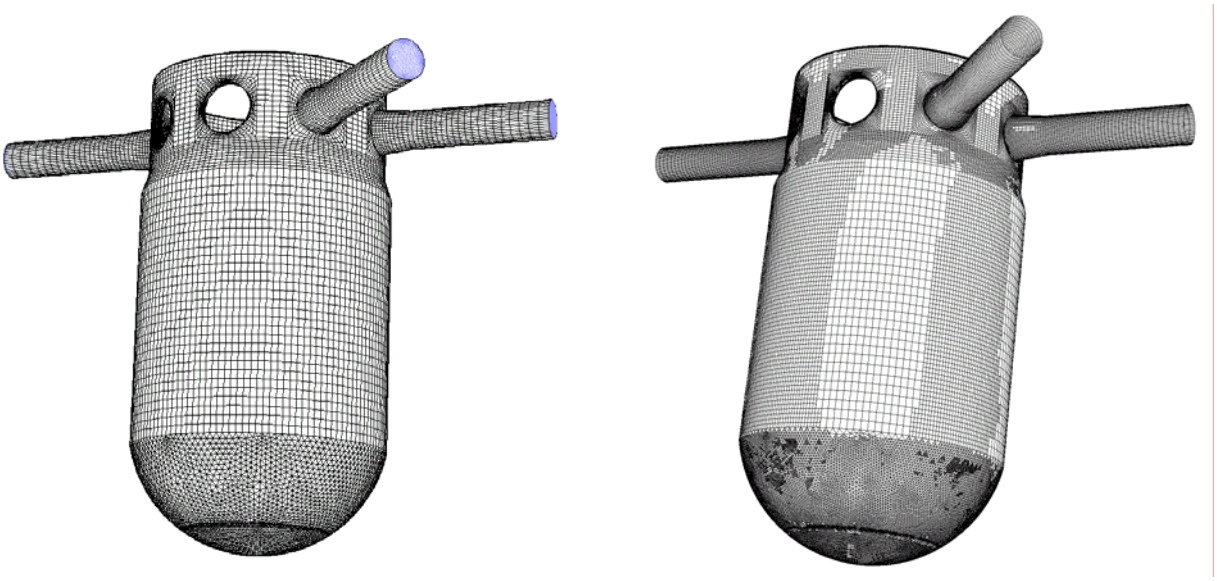

Fig. 3.2-1 Original and refined (adapted) grid used in calculations

B.3.2.6 Boundary Conditions

Inlet boundary positions are located at the inlet nozzles of all 4 loops so that geometry of inlet nozzles, downcomer, reactor lower plenum and structures in the reactor vessel can be taken into account.

Outlet boundary position is located at half of the core.

Boundary conditions for the inlets were:

- inlet velocity (2.91 m/s);
- constant temperature corresponding to the respective concentration in each loop;
- turbulence intensity (3.7 %)
- hydraulic diameter (0.2 m)

Boundary condition for the outlet was:

- pressure outlet

B.3.2.7 Results of steady state flow and mixing at ROCOM

Sensitivity calculations with the ROCOM model were performed in accordance with the Best Practice Guidelines [BPG] and described in final report of Work Package 4. Only the final calculation is presented in this report.

Due to limited computer resources, solving through the viscous sublayer was not possible. Wall functions therefore had to be used. For presented calculation the standard wall function was chosen.

Following options were selected for discretisation scheme:

- Momentum: 2nd order upwind;
- Pressure: 2nd order;
- k: 2nd order upwind;
- ε: 2nd order upwind;
- Pressure-velocity coupling: SIMPLE

Tab. 3.2-1 Overview of conditions applied in final ROCOM STAT_01 test calculation

Grid	Perforated drum	Outlet	Turbulence model	Wall function	Discretisation
Grid 5	Reduced number of holes	Half of the core	Standard k-e	Standard	2nd option

For quantitative assessment of results was used following error specification:

$$ERROR1_i = c_{c,i} - c_{m,i} \quad \text{(calculated value − measured value)} \quad [-]$$
$$ERROR2_{RMS} = \sqrt{(\Sigma\ ERROR1_i^2)} * 100\% \quad [\%]$$
$$ERROR3 = ERROR2_{RMS} / n \quad [\%]$$
$$ERROR4_{ABS} = \Sigma\ |ERROR1_i| \quad [-]$$

where: i = goes through all measurement points and n = total number of measurement points.

Overall agreement with experimental values is assessed by the means of $ERROR4_{ABS}$. This quantitative assessment is summarized for final STAT_01 calculation, which gave the best (lowest) error values.

Total errors are quantified for three locations, where measurement probes were installed – for upper part of the downcomer, lower part of the downcomer and for core inlet.

Tab. 3.2-2 Quantitative assessment of final STAT_01 calculation based on $ERROR4_{ABS}$

Case No.	$ERROR4_{ABS}$		
	Upper downcomer	Lower downcomer	Core inlet
10	7.91	19.31	12.39

In the table the lowest errors are highlighted in blue colour, the largest errors are in red colour. It can be seen that the least errors are indicated for case 10. This result is in agreement with expectations as case 10 has the finest grid from all cases compared and perforated drum modelled in detail. On the other hand, RNG k-ε standard turbulence model and non-equilibrium wall function don't have noticeable beneficiary effect on the results.

Mixing scalars and derived errors for case 10 are graphically expressed in Fig. 3.2-2.

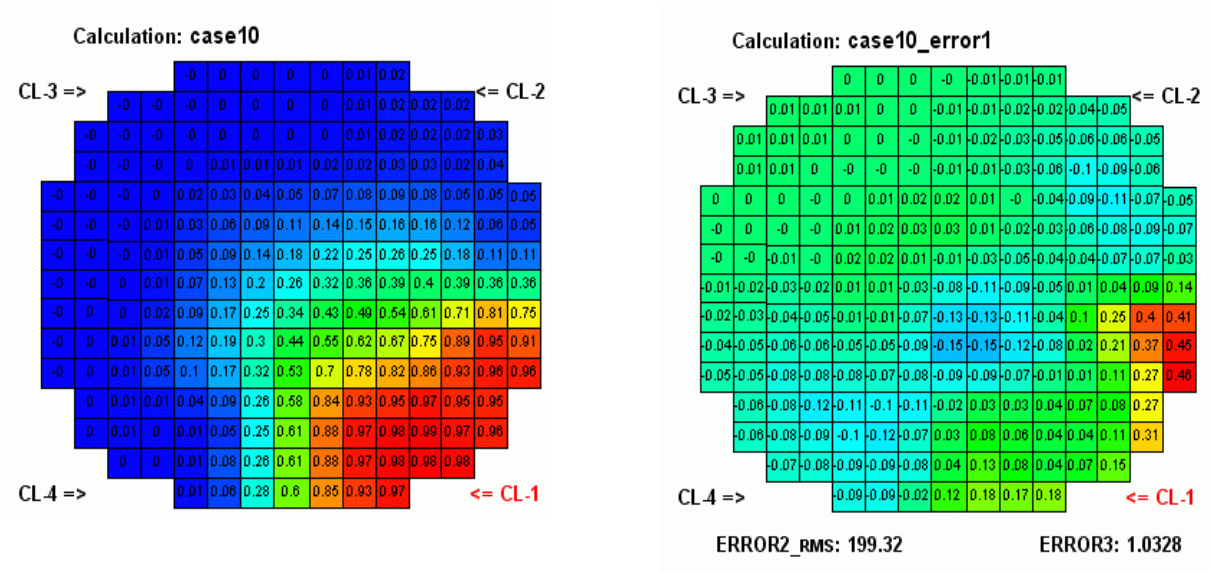

Fig. 3.2-2 Calculated results of ROCOM STAT_01 and errors for final case 10

Vertical velocities in the downcomer were another indicator of how the code can predict flow patterns. Although in general the calculated velocities have the same character, their absolute values differs from measured velocities, especially where maximum and minimum velocities are observed. At the azimuthal position of 45°, under the loop 1 nozzle, no decrease in the "peak" of velocity was calculated, though such a decrease was measured. Measured and calculated vertical velocities around the dowmcomer are depicted in Fig. 3.2-3 below.

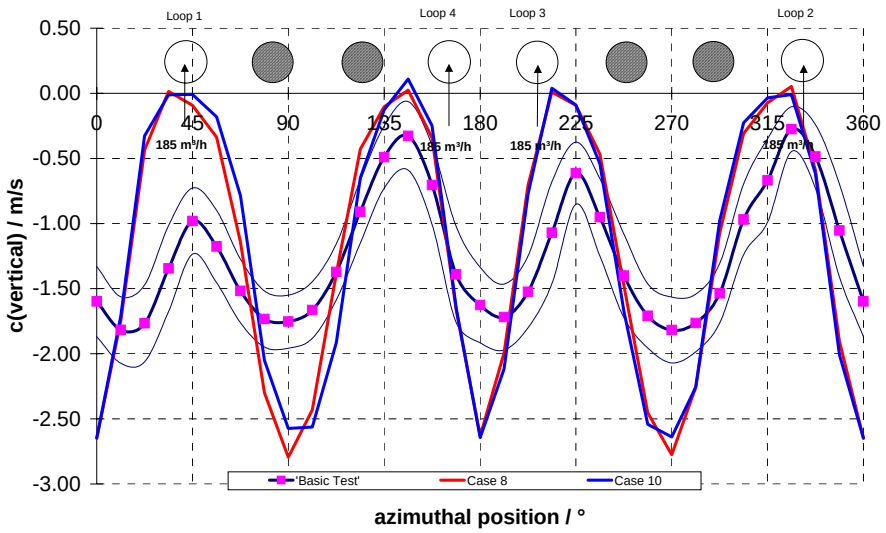

Fig. 3.2-3 Measured and calculated vertical velocities around the downcomer

Conclusions for STAT_01 test:

Finer grids tend to give better results. Also modelling of perforated sheets (such as the drum in the downcomer) as real structure rather than porous medium improves quality of results.

Influence of porous medium as a substitute of a perforated sheet can be, in some extent, controlled by proper definition of direction-dependent resistance of the porous medium.

Other investigated effects (turbulence model, wall function, position of outlet boundary) do not have an unambiguous influence on results.

Test ROCOM STAT_04

Results of test STAT_04 were used for testing the effect of various options available in FLUENT on obtained results. Complete set of results is documented in final report of WP4, here only the results of final calculation (Case 47) are presented.

Tab. 3.2-3 Overview of conditions of final VUJE calculation performed for ROCOM STAT_04 test

Case	Grid	Perforated drum	Outlet *	Turbulence model	Wall function	Discretisation
47	Grid 5	Reduced no. of holes	"long" cold legs – outflow	Standard k-ε	Standard	2nd option

* The main outlet is situated at the half height of the core. There is a backflow in the cold leg No. 4.

The results at the core inlet sensors for the case 47 are presented in Fig. 3.2-4 and ERROR1 for all measurement points is presented in Fig. 3.2-4.

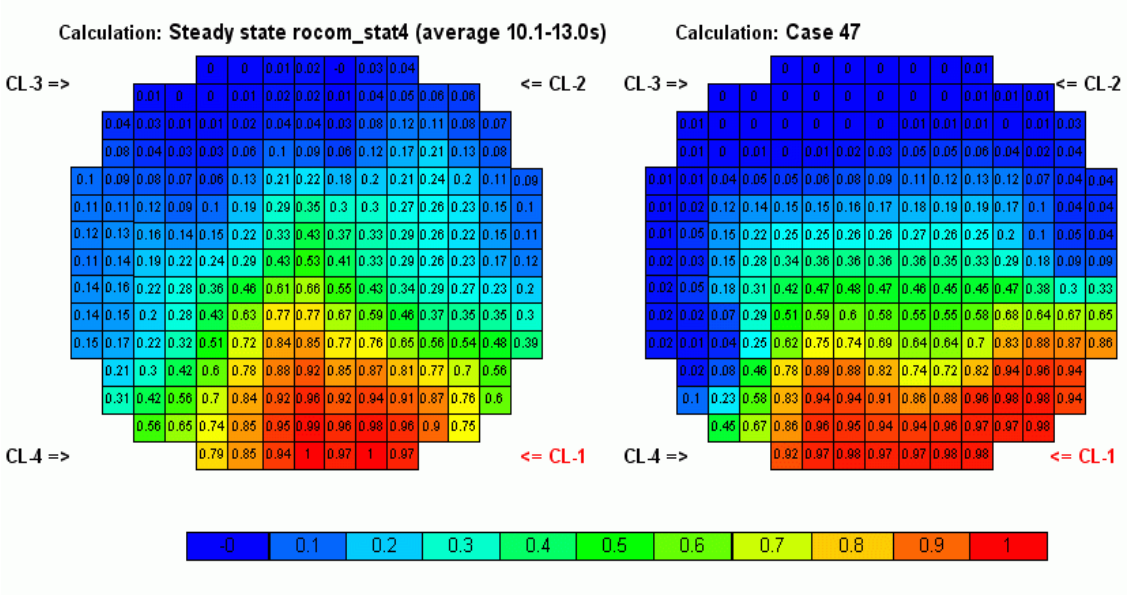

Fig. 3.2-4 Comparison of measured and calculated results of ROCOM STAT_04 for Case 47

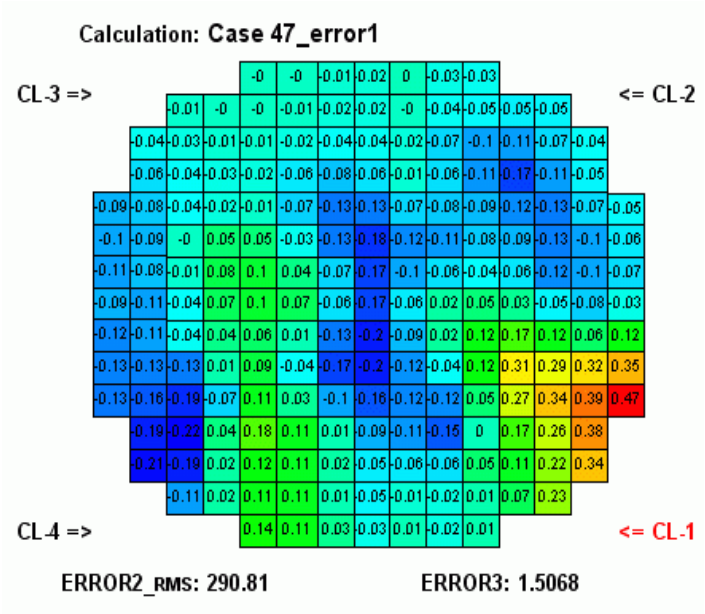

Fig. 3.2-5 Distribution of ERROR1 at the core inlet

It can be seen that calculated values of mixing factor are “smeared” more than in measurement, with mixing factors over-predicted anticlockwise and under-predicted clockwise relative to the measured pattern.

Calculated vertical velocities in the downcomer have, in general, similar character as measured velocities with exception of the region below the nozzle of loop 1. While the measured velocity near the loop 1 nozzle was significantly negative, calculated velocities reached positive values in all calculated variants.

Vertical downcomer velocities (left figure) and their deviations from measured values (right figure) for Case 47 are shown in figure 3.2-6.

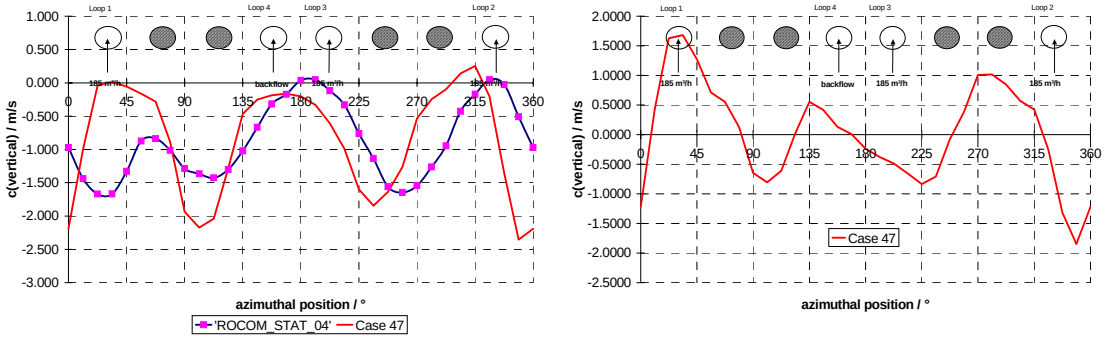

Fig. 3.2-6 Measured and calculated downcomer vertical velocities in STAT_4 test

Mixing scalars (left figure) and their deviations from measured values (right figure) for upper and lower part of the downcomer are shown in figures 3.2-7 and 3.2-8, respectively.

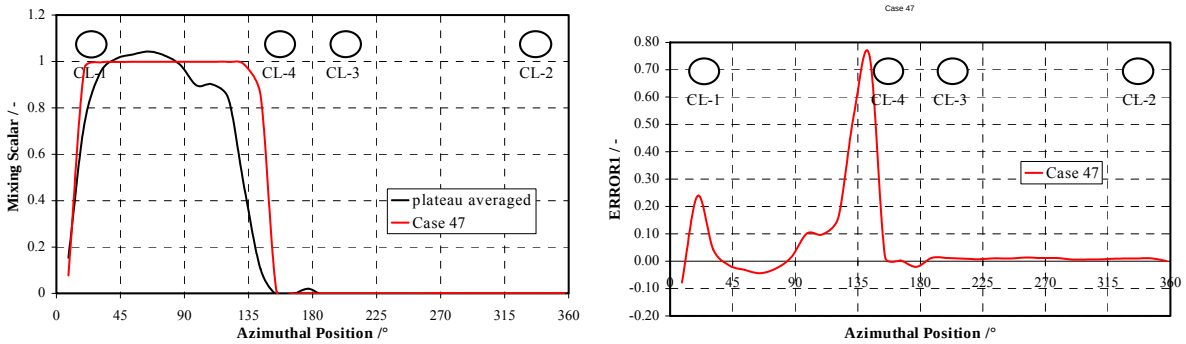

Fig. 3.2-7 Mixing scalar and Error1 of mixing scalar in the upper part of downcomer

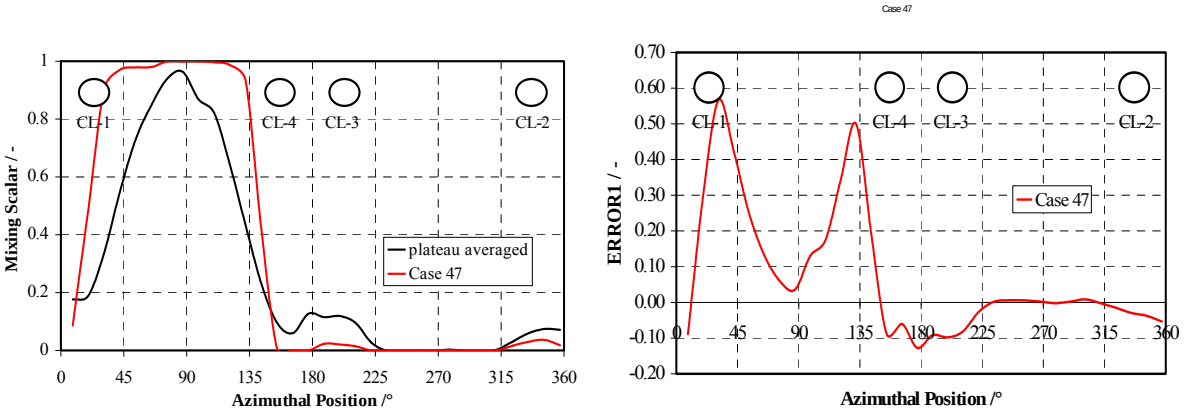

Fig. 3.2-8 Mixing scalar and Error1 of mixing scalar in the lower part of downcomer

Conclusions for STAT_04 test:

Practically, the same conclusions as those derived for ROCOM STAT_01 test are applicable also for STAT_04 test.

B.3.3 Calculations of ROCOM steady state mixing experiments with FLUENT by AEKI

The steady state calculations of test cases ROCOM_stat01 (total flow rate) and ROCOM_stat09 (asymmetry in flow rates) were performed. Calculated vertical velocity in the downcomer, tracer concentration at two levels in the downcomer and at the core inlet were compared with results of tests.

B.3.3.1 Computational modelling

CFD code Fluent version 6.2.22 was used for the calculations running on HP RX2600 workstation (IA64 2GHz processor and 2GB memory, operating system HP UNIX ver.11).

B.3.3.2 Turbulence modelling

From the tested turbulence models the Reynolds Stress Model with standard wall function model gives best agreement with experimental data.

B.3.3.3 Numerics

Solver
Segregated solver was used.

Discretization schemes
Using high order discretisation schemes the turbulent effects were overestimated.

- Momentum: 1st order upwind
- Pressure: Standard
- Turbulence: 1st order upwind
- Species Transport: 1st order upwind

Pressure-velocity coupling
SIMPLE pressure-velocity coupling was used.

B.3.3.4 Geometry

All geometrical details, including core support plate (contains 193 orifices) were modelled accurately. The perforated drum is modelled as porous media (inertial resistance coefficient C_2=8 500 1/m), and the core as free flow field (Fig.3.3-1).

B.3.3.5 Grid

The grid developed by Gambit 1.3 consists 435 810 cells (hexahedral elements 82,63 %, tetrahedral elements 15.69 %, pyramid elements 1.68 %). The maximum aspect ratio is 6.91 and the average skewness of the grid is 0.265. The calculation grid was generated by inlet chamber region adaptation of first grid. The final grid contains 638 866 cells.

Fig. 3.3-1 AEKI model of ROCOM

B.3.3.6 Physical models

Fluid properties
Fluid properties were downloaded from the FLUENT database and set constant.

- Temperature wasn't defined (no energy equation was activated),

- Density = 998.2 kg/m^3,
- Viscosity = 0.001003 kg/m-s,
- Mass diffusivity = $2.88 \cdot 10^{-5}$ m^2/s.

Modelling of mixing
Mixing was modelled by using species transport model with turbulent Schmidt number 0.7.

B.3.3.7 Boundary positions and boundary conditions

The inlet boundary conditions were set at the inlet nozzles:

- ROCOM_stat01 (total flow rate): $v_{Loop1-4}$ =2.91 m/s,
- ROCOM_stat09 (asymmetry in flow rates): v_{Loop1}=3.49 m/s; v_{Loop2}=2.33 m/s; $v_{Loop3,4}$=2.91 m/s,
- Tracer concentration C =1 in the Loop1 only.

The outlet boundary was put above core support plate. A constant static pressure was specified.

B.3.3.8 Results of steady state flow calculations

Sensitivity calculations with the ROCOM model were performed in accordance with the Best Practice Guidelines [BPG] and there are described in the final report of Work Package 4. Only the calculation yielding best results is presented in this report.

Test ROCOM STAT_01

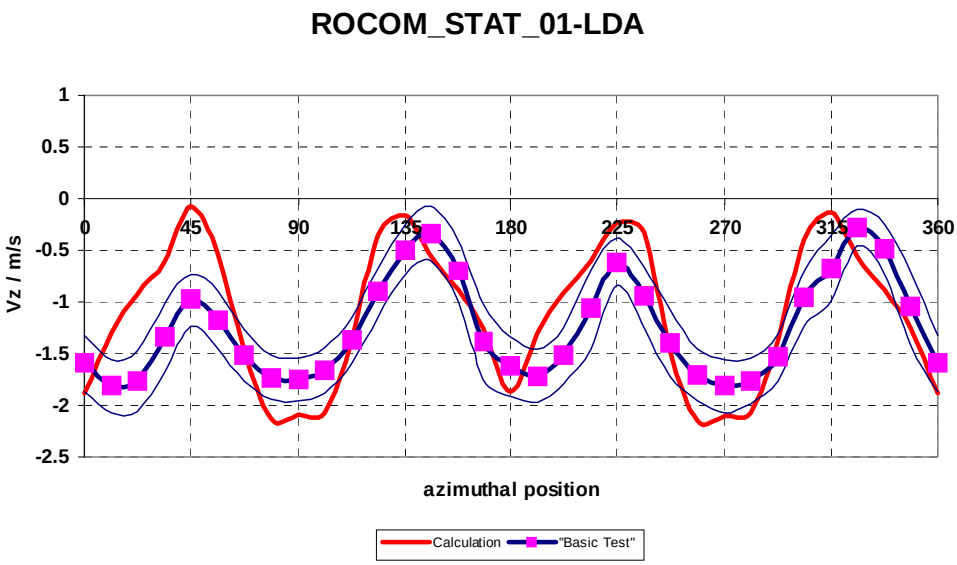

Fig.3.3-2 Velocity distributions in the downcomer (ROCOM_STAT_01)

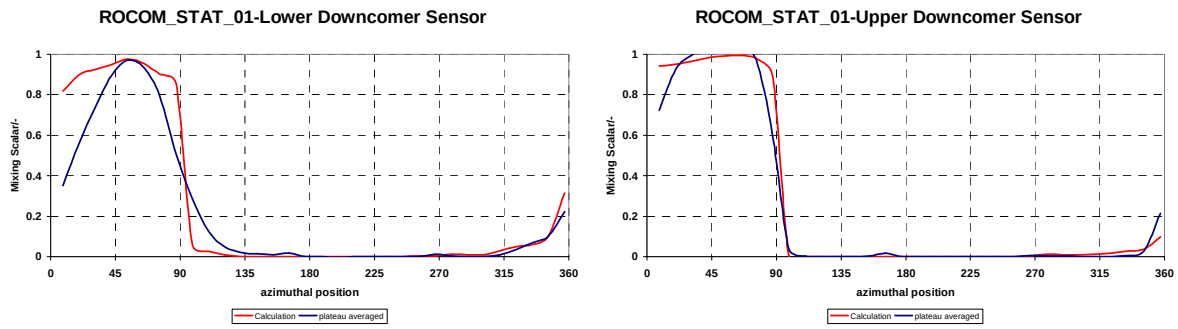

Fig.3.3-3 Concentration distributions in the downcomer (ROCOM_STAT_01)

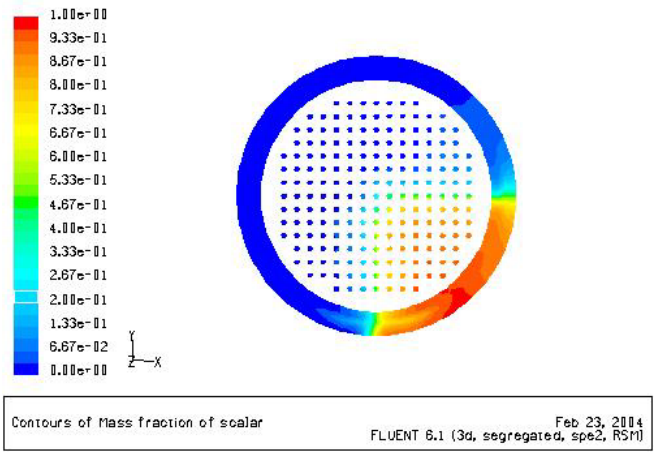

Fig.3.3-4 Concentration distribution at the core inlet plane (ROCOM_STAT_01)

Test ROCOM STAT_09

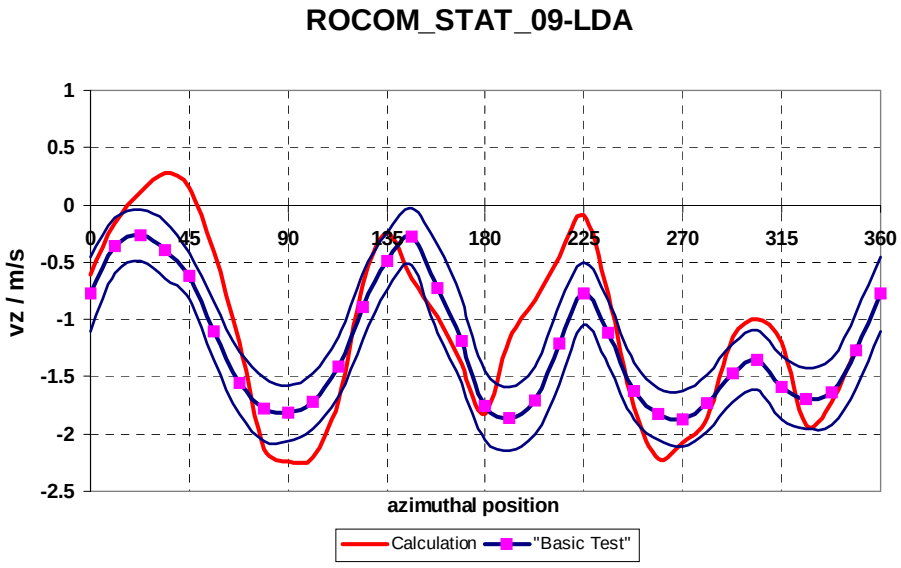

Fig.3.3-5 Velocity distributions in the downcomer (ROCOM_STAT_09)

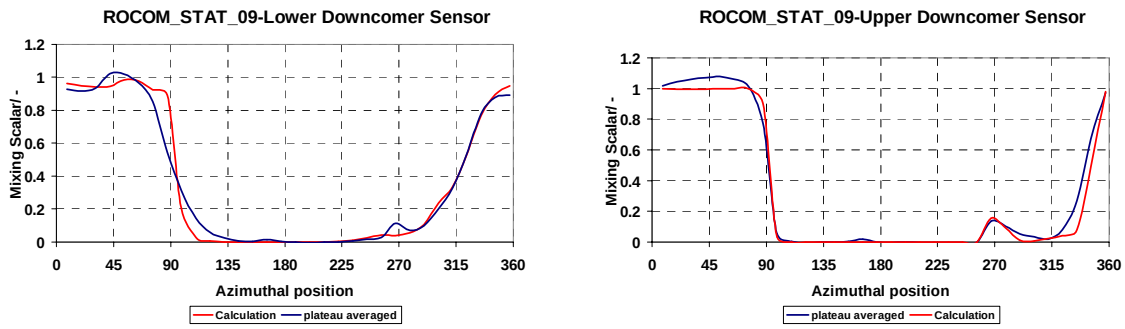

Fig.3.3-6 Concentration distributions in the downcomer (ROCOM_STAT_09)

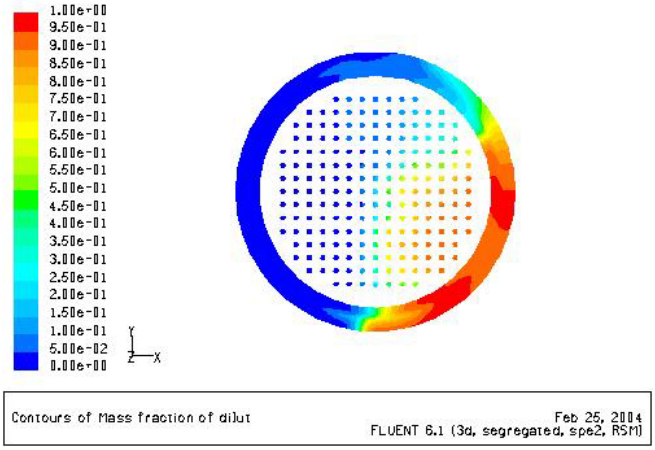

Fig.3.3-7 Concentration distribution at the core inlet plane (ROCOM_STAT_09)

B.4 CFD simulation of VVER primary circuit flow field

The mixing tests at Paks NPP presented in chapter B.2 were used for the CFD code validation by VUJE, AEKI and TU Budapest. Selected tests were simulated with varying modelling setting and the loop mixing factors at the core inlet plane were compared to the real plant measurements This work is presented in chapter B.4.1.

The same VVER-440 geometry with asymmetric loop flow rates was simulated by Fortum. This work is presented in chapter B.4.2. The main goals of the Fortum simulations were to find the effect of different geometric details like the cold leg bend and the ECC water guides to the flow field in the downcomer.

B.4.1 CFD simulation of mixing tests at Paks NPP VVER-440 reactor by VUJE, AEKI and TU Budapest

Additional test data were made available by Paks NPP and AEKI for the project. The data come from the commissioning tests of Paks NPP performed in years 1987-1989. The tests addressed mixing among coolant loop flows in the downcomer and up to the core inlet in forced flow conditions. The goal of the tests was investigation of potential loop temperature asymmetry that might occur and significantly affect power distribution in the core. Detail description of the tests can be found in appendix 1 of this report.

The tests used in the project were performed under the following conditions:

- Reactor power (10-15 %);
- Higher temperature at the reactor inlet from one loop (the gate valve on the loop steam-line closed);
- The cold leg temperature of the investigated steam generator was by 8-9 °C higher than temperature in the others steam generators (the assembly heat-up in such cases is only 3-4 °C);
- The effect of the asymmetry was significantly reflected in the outlet temperatures measured in the assembly heads.

Paks mixing experiments were calculated by AEKI (FLUENT), VUJE (FLUENT) and TU Budapest (CFX5).

B.4.1.1 Paks NPP mixing tests calculated by VUJE

CFD code FLUENT 6.1.18 was used in these analyses by VUJE.

B.4.1.1.1 Computational modelling

Pre-processor GAMBIT 2.0.4 and solver FLUENT 6.1.18 on a PC with Intel Pentium 4 (1.7 GHz, 32 bits, 1 Gb RAM) under operating system Windows 2000 were used in the simulations of Paks mixing tests.

Basic characteristics of FLUENT are presented in Section 3.2.1.1 and fully described in references [Flu, Flu03].

B.4.1.1.2 Turbulence modelling

In presented calculations two turbulence models were used with the aim to find the impact of different turbulence models on results: Standard *k*-ε model and RNG *k*-ε model. The flow is non-buoyant. Therefore, no buoyancy terms in the turbulence models were applied.

Characteristics of these models are presented in Section 3.2.1.

B.4.1.1.3 Numerical diffusion, nodalization and time step size

Discretisation schemes

In calculations presented in this section both, first order and second order upwind schemes were applied to assess their influence on results. In terms of discretisation scheme the following combinations of optional models were selected:

	1st option	2nd option
Momentum:	1st order upwind	2nd order upwind
Pressure:	PRESTO	PRESTO
k:	1st order upwind	2nd order upwind
ε:	1st order upwind	2nd order upwind
Pressure-velocity coupling:	SIMPLE	SIMPLE

Relaxation

Following (default) under-relaxation factors were used in calculations:

- Pressure: 0.3
- Density: 1.0
- Body forces: 1.0
- Momentum: 0.7
- Turbulence kinetic energy: 0.8
- Turbulence dissipation rate: 0.8
- Turbulence viscosity: 1.0

Time step

As the Paks mixing tests were calculated as steady-state problems, no time step was defined in the calculations.

B.4.1.1.4 Geometrical Simplifications, Local Details

Comprehensive computer model of VVER 440 reactor vessel was developed at VUJE (Fig. 4.1-1). The model consisted of 1.610.231 cells. It included inlet nozzles from all 6 loops and three baffles, whose purpose is deflecting the coolant injected to the reactor vessel from the safety injection tanks. Eight support consoles for the core barrel alignment were modelled as well.

Simplified geometry:

- Baffles - simplified geometry.
- Alignment drifts – simplified geometry.
- Elliptical perforated plate – two models were used: porous media and a structure with reduced number of holes but with the same flow cross-section.
- Planar perforated plate – porous media

- Lower guide tubes – simplified geometry of perforation or omitted
- Lower core support plate – porous jump or omitted
- Core – porous media or omitted

Omitted (i.e. not modelled) geometry:

- The inlet nozzles of two ECC pipes and the measuring pipe situated at the level of the RPV inlet nozzles.
- Small structures, protrusions and chamfers (except RPV inlet nozzles).

Reactor internal structures were modelled as follows.

B.4.1.1.4.1 The Elliptical Perforated Plate

The elliptical perforated plate at the bottom part of the reactor vessel was modelled with reduced number of holes - 227 holes with 98 mm in diameter (in reactor are 1362 holes with 40 mm in diameter).

B.4.1.1.4.2 The Core Support Plate

Planar perforated plate between the lower plenum and lower core support plate was modelled as porous medium with equivalent internal resistance of 776 m^{-1} and porosity = 37.3%.

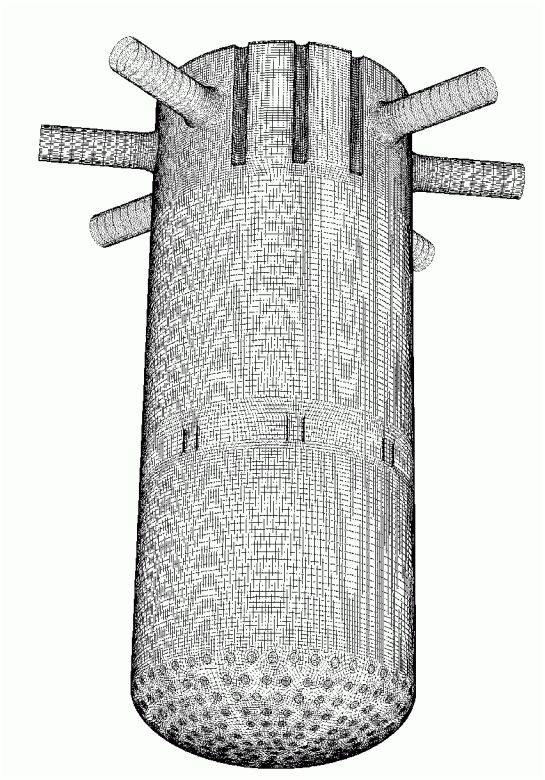

Fig. 4.1-1 Model of VVER 440 V-213 reactor

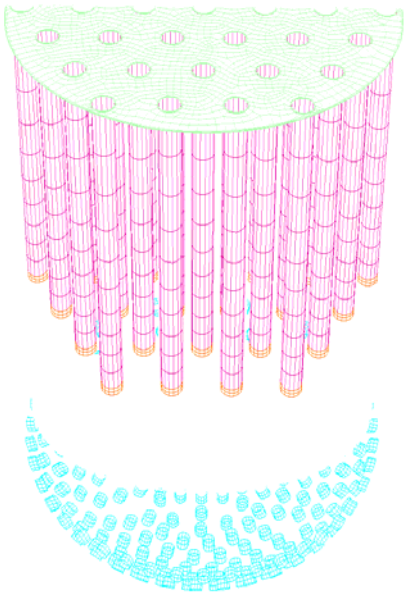

Fig. 4.1-2 Model of reactor internals (as modelled in Grid 3)

B.4.1.1.4.3 The Lower Plenum Guide Tubes

Guide tubes: 37 lower control rod guide tubes. The lower core support plate is modelled as porous jump with internal resistance 10 m^{-1} and the core is modelled as porous medium with internal resistance 52 m^{-1} and porosity 46.4% (Fig.4.1-2).

B.4.1.1.4.4 Extended Reactor Inlet Nozzles

With the aim to include the influence of bends in the cold leg, the model was modified and inlet nozzles were extended (Fig. 4.1-3). The effect of reactor coolant pump was calculated as well, but it turned out that the effect of loop bend was dominant.

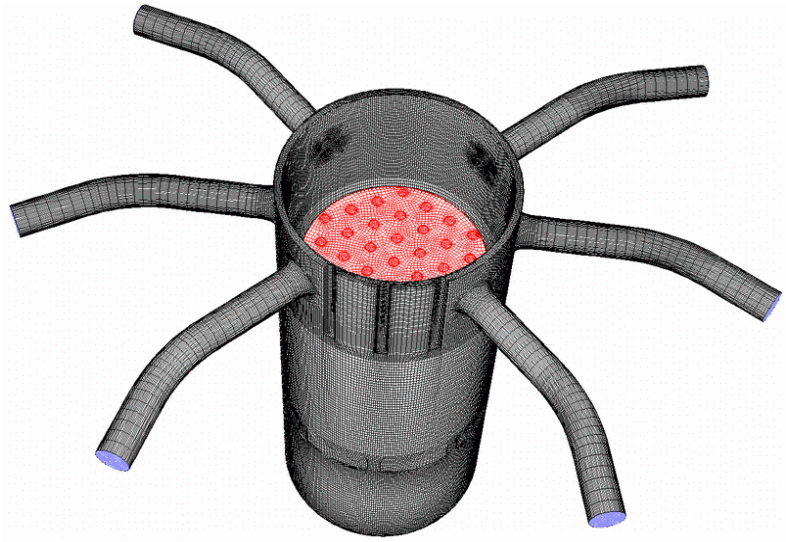

Fig. 4.1-3 Model of reactor vessel with extended cold legs (Grid 4)

B.4.1.1.4.5 The Core

In several cases the core was modelled using porous media model, in others the core was omitted and calculation domain ended at the core inlet.

B.4.1.1.5 Grid generation

The following four grids were used in Paks mixing tests calculated by VUJE:

- **Grid 1**: 1.752.069 cells (structured hexahedral mesh)
- **Grid 2**: 1.609.231 cells (hybrid mesh)
- **Grid 3**: 1.698.319 cells (hybrid mesh)
- **Grid 4**: 1.6431.99 cells (hybrid mesh)

Grid 1 is a finer structured hexahedral mesh including following internal geometry:

- Six inlet nozzles
- Three baffles (cross-flow allowed)
- Eight alignment drifts with vertical holes
- Downcomer extension
- Elliptical perforated plate

- Planar perforated plate
- Lower plenum
- Core

The inlet position is situated approximately 4 diameters from the downcomer inlet. The elliptical perforated plate is modelled as porous medium divided to three vertical layers. Also the planar perforated plate and the core are modelled as porous media.

Grid 2 is a hybrid mesh based on Grid 1, to which models of the lower guide tubes and the core support plate were added. Model of the lower guide tubes includes also a simple model of perforation. Inlet part of each guide tube bears 8 holes ∅20 mm that are represented by a flow path with the same cross-section. The core support plate is modelled as porous jump with internal resistance tuned so that required flow rate is obtained through the lower guide tubes. The elliptical perforated plate was changed to the solid structure with equivalent flow-path area. 1362 holes of 40 mm in diameter were modelled by 227 holes with equivalent diameter of 98 mm. The boundary layer was improved

Grid 3 is a hybrid mesh based on Grid 2. Difference between the grids is only that the model of the inlet pipe including bends was added to reactor inlet nozzles.

Grid 4 is a hybrid mesh based on Grid 3. The model of the core was removed.

Information about details of grids used in Paks mixing test can be found in reference [Kle04].

B.4.1.1.6 Boundary Conditions

Following boundary positions were defined in the test calculations:

- Inlet boundary positions were located at the inlet nozzles of all 6 loops so that geometry of inlet nozzles was included. In sensitivity calculations the inlet legs of all loops were extended beyond the bends in the legs.
- Outlet boundary position was located either at the outlet of the core or in the core inlet.

Boundary conditions for the inlets were:

- Mass flow inlet – the same value (1460 kg/s) in all 6 loops;
- The same constant temperature in 5 loops (270°C), and lower temperature in one loop (265°C);
- Turbulence intensity at the inlet was 5%.

Boundary condition for the outlet was:

- Pressure outlet.

B.4.1.2 Paks NPP mixing tests calculated by AEKI

As detailed information on FLUENT modelling capabilities is presented in Section 3.2.1, only specific options selected in AEKI calculations of Paks mixing tests are presented in this

section. Comprehensive description of FLUENT code capabilities can be found in references [Flu, Flu03].

B.4.1.2.1 Computational modelling
CFD code FLUENT 6.1.22 was used by AEKI, under MS-Windows XP, with Intel Pentium4 3GHz processor and 1GB memory in analyses of Paks mixing tests.

B.4.1.2.2 Turbulence modelling
In presented calculations standard RSM turbulence model with standard wall functions were used.

Mixing was modelled by using species transport model with turbulent Schmidt number 0.7.

B.4.1.2.3 Numerical diffusion, nodalization and time step size

Discretisation schemes
In calculations presented in this section, first order discretization scheme and SIMPLE pressure-velocity coupling was used by AEKI.

Relaxation
Default under-relaxation factors were used in calculations.

Time step
As the Paks mixing tests were calculated as steady-state problems, no time step was defined in the calculations.

B.4.1.2.4 Geometrical Simplifications, Local Details
Computer model of VVER 440 reactor vessel starting from the inlet pipe and ending at the core outlet was developed. The model consisted of 1 172 618 cells. It included inlet nozzles from all 6 loops and three baffles, whose purpose is deflecting the coolant injected to the reactor vessel from the safety injection tanks. Eight support consoles for the core barrel alignment were modelled also (Fig. 4.1-4).

Detailed geometry:

- Six inlet nozzles.
- Three ECC baffles (cross-flow allowed)
- Eight alignment drifts with vertical holes
- Downcomer extension

Simplified geometry:

- Elliptical perforated plate – modelled as porous medium with direction dependent internal resistance.
- Planar perforated plate – modelled as porous medium
- Lower core support plate – modelled as porous medium
- Core – modelled with porous media model

Omitted (i.e. not modelled) geometry:

- The inlet nozzles of two ECC pipes and the measuring pipe situated at the level of the RPV inlet nozzles.
- Lower guide tubes – omitted
- Small structures, protrusions and chamfers (except RPV inlet nozzles).

Inertial resistance coefficients for porous media model:

- Elliptical perforated bottom: 140 1/m.
- Lower support plate: 160 1/m.
- Core: 72 1/m.

B.4.1.2.5 Grid generation
Hybrid mesh with 1036252 (88%) hexahedral, 125590 (11%) tetrahedral and 10776 (1%) pyramid elements, i.e. total of 1172618 cells was used for AEKI calculations.

Grid quality: average skewness 0.14.

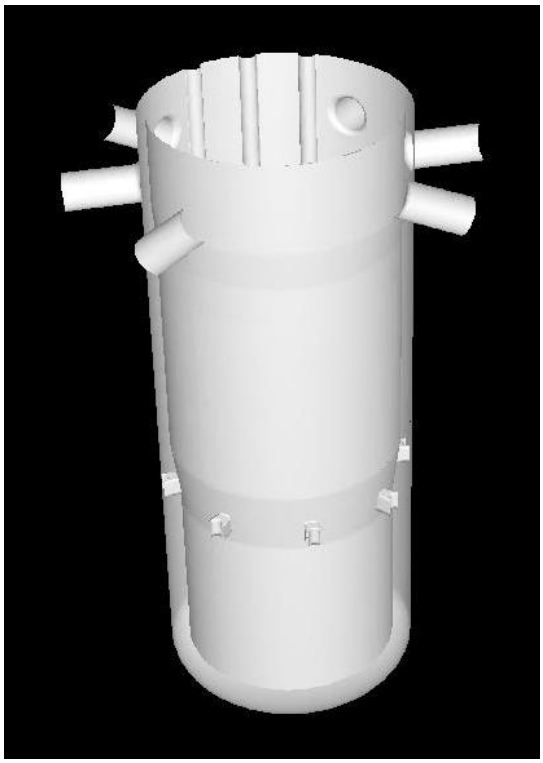

Fig. 4.1-4 AEKI model of VVER 440 V-213 reactor

B.4.1.2.6 Boundary Conditions
Following boundary positions were defined in the test calculations:

- Inlet boundary positions were located at the inlet nozzles of all 6 loops so that geometry of inlet nozzles was included.
- Outlet boundary position was located at the core outlet.

Boundary conditions for the inlets were:

- Mass flow inlet – the same value (1460 kg/s) in all 6 loops;
- Species concentration was defined as 1 in one loop and 0 in other 5 loops;
- Turbulence intensity at the inlet was 5%.

Boundary condition for the outlet was:

- Pressure outlet.

B.4.1.3 Paks NPP mixing tests calculated by TU Budapest

CFD code CFX5 on two PCs with Dual Xeon processors (2,4 GHz, 2*2 GB RAM) under Linux operation system was used in these analyses by Technical University Budapest.

B.4.1.3.1 Computational modelling

CFD code CFX5.5.1 was used by TU in analyses of Paks mixing tests.

Basic characteristics of CFX modelling capabilities are presented in Section 3.1.1, and fully described in references [CFX4, CFX5]. Therefore only specific options selected in TU calculations of Paks mixing tests are presented in this section.

B.4.1.3.2 Turbulence modelling

In presented calculations Standard k-ε model was used with "Scalable" option for the turbulent wall function.

"No Slip" option was selected for wall influence on the flow and "Smooth Wall" was selected for the wall roughness. The flow is non-buoyant. Therefore, no buoyancy terms in the turbulence models were applied.

B.4.1.3.3 Numerical diffusion, nodalization and time step size

Discretisation schemes

In calculations presented in this section, Second order ("High resolution") advection scheme was used by TU Budapest.

Time step

As the Paks mixing tests were calculated as steady-state problems, no time step was defined in the calculations.

B.4.1.3.4 Geometrical Simplifications, Local Details

Comprehensive computer model of VVER 440 reactor vessel was used for TU calculations. The model consisted of 1.838.991 cells and 490 388 nodes. It included inlet nozzles from all 6 loops up to 0.6 m from the reactor vessel. Three baffles of the coolant of the hydro-accumulators and eight alignment drifts in the downcomer were modelled accurately as well. The model outlet was located at the core inlet.

Simplified geometry:

- Baffles of the hydroaccumulators modelled with 3 semi-circular baffles, each 1.9 m long with 2 cm gap between the baffles and the inner wall of the downcomer (cross-flow allowed).

- Elliptical perforated plate – modelled with momentum sources. The components of momentum source were determined from steady state test calculations performed with a model of the perforated plate, with 250 holes with a diameter of about 8 cm (instead of the real geometry with 1344 holes with a diameter of 4 cm).
- Reactor lower plenum modelled with momentum sources. The horizontal components of the momentum source were set to act as a force in the opposite direction to the horizontal coolant velocity components in order to eliminate horizontal coolant flow in the guide tube chamber. The vertical component of the momentum source was set to zero.
- Core – momentum sources or omitted.

Omitted (i.e. not modelled) geometry:

- The inlet nozzles of two ECC pipes and the measuring pipe situated at the level of the RPV inlet nozzles.
- Lower guide tubes – omitted
- Small structures, protrusions and chamfers (except RPV inlet nozzles).
- The core

Fig. 4.1-5 Pressure vessel model used for the steady state calculations

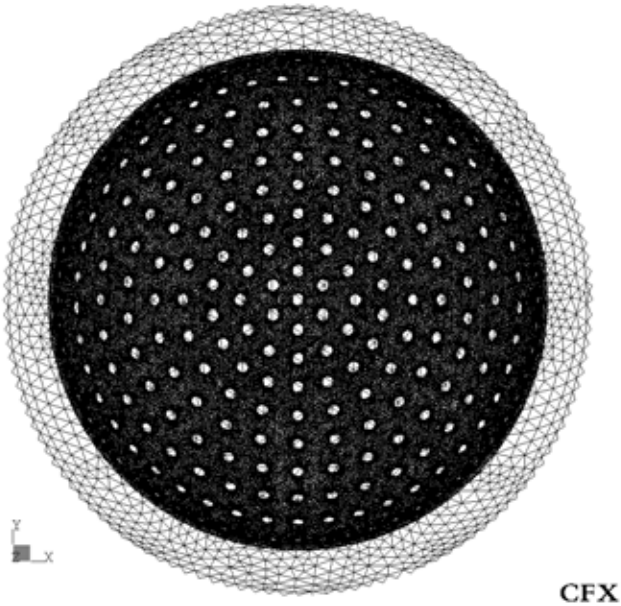

Fig. 4.1-6 Mesh of the simplified model of the elliptical perforated plate

B.4.1.3.5 Grid generation

Three different grids have been built for TU calculations:

- **Grid 1**: 1 559 363 cells (unstructured tetrahedral mesh with prism layers at the walls, including 1 149 439 tetrahedrons, 403 023 prisms and 6 901 pyramids)

- **Grid 2**: 2 780 395 cells (unstructured tetrahedral mesh with prism layers at the walls, including 2 263 963 tetrahedrons, 509 525 prisms and 6 907 pyramids)
- **Grid 3**: 1 838 991 cells (unstructured tetrahedral mesh with prism layers at the walls, including 1 417 823 tetrahedrons, 418 977 prisms and 2 191 pyramids)

Grid 1 is a coarse unstructured mesh, containing the detailed model of the downcomer (including the inlet nozzles, the hydro-accumulator baffles and the alignment drifts), and the lower plenum with the momentum source model of the elliptical perforated plate, without the modelling of the lower guide tubes.

Grid 2 covers the same geometry as Grid1 but with a finer mesh. The performed test calculations showed that there are differences between the calculated flow fields with the two grids, that means that the simulation with Grid1 is not grid-independent.

Grid 3 covers the same geometry as Grid1, but it also includes the momentum source model of the lower guide tubes (in order to avoid back-flow at the core inlet). The resolution of the mesh of the Grid 3 is between the mesh of Grid 1 and Grid 2 models.

No mesh adaption was used.

B.4.1.3.6 Boundary Conditions
Following boundary positions were defined in the test calculations:

- Inlet boundary positions were located at the inlet nozzles of all 6 loops so that geometry of inlet nozzles was included.
- Outlet boundary position was located at the core inlet.

Boundary conditions for the inlets were:

- Mass flow inlet – the same value (1500 kg/s) in all 6 loops;

The mixing factors were demonstrated with six scalar mixing components. The concentration of the mixing scalars was set to 1 kg/m^3 at one of the inlet nozzles, and to 0 kg/m^3 at the other five inlet nozzles. So the calculated values of the mixing scalars at the core inlet give back the mixing factors directly.

Turbulence intensity at the inlet was 5%.

Selected medium: “General Fluid” with following properties:
Density = 7.68E2 kg m^{-3}
Dynamic Viscosity = 1.E^{-4} kg m^{-1} s^{-1}
Specific Heat Capacity = 5 115 J kg^{-1} K^{-1}
Thermal Conductivity = 0.596 W m^{-1} K^{-1}
Thermal Expansivity = 2.1x10^{-3} K^{-1}
Boundary condition for the outlet was: Pressure outlet.

B.4.1.4 Results of calculations of Paks mixing tests

Summary of basic assumptions and used in the calculations of Paks mixing tests performed by AEKI, TU Budapest and VUJE is presented in Table 4.1.2.

Tab. 4.1.2 Summary of basic assumptions of Paks mixing tests calculations

	AEKI	**TU Budapest**	**VUJE**
CFD code used	FLUENT 6.1.22	CFX 5.5.1	FLUENT 6.1.18
Mesh	1 172 618	1 838 991	1 609 231
Elliptical perforated plate	Porous medium	Porous medium	Structure with 227 holes
Guide tubes	No	No	Yes (with perforations)
Discretisation scheme	1st order	2nd order	2nd order
Mixing model	Species transport (Mixing scalar)	Mixing scalar	Temperature
Turbulence model	RSM		k-ε
Wall function	Standard	Scalable	Standard

Results of calculations of all partners analysing Paks mixing tests are presented in the form of temperature fields for different temperature at the inlet from loop 3. The results are expressed in terms of mixing scalars at the core inlet and compared with experimental data. For assessment of deviations between calculated results and measurements, maps of errors are presented as well. The results are presented in Figs. 4.1-7 and 4.1-8.

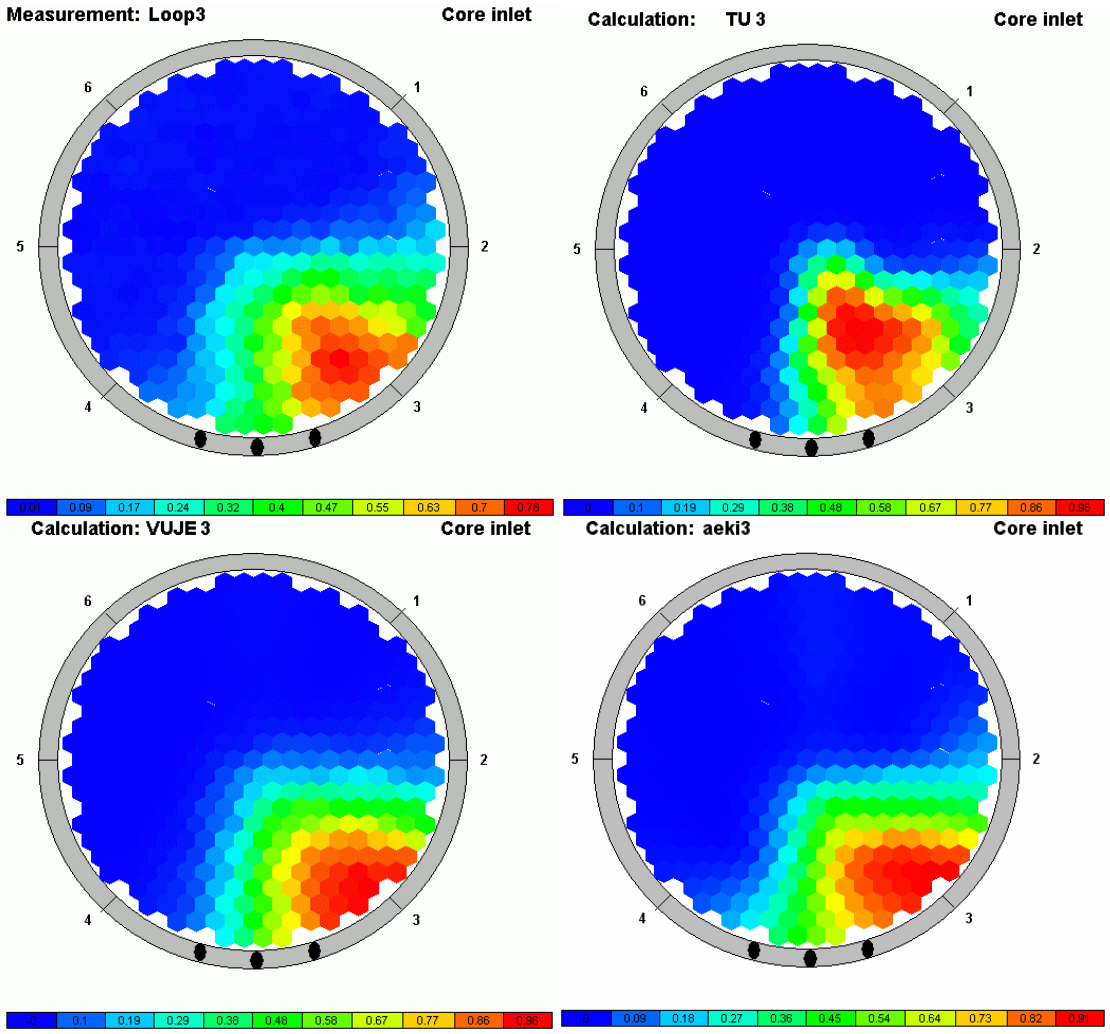

Fig. 4.1-7 Comparison of calculated core inlet temperatures with measured data for loop No.3

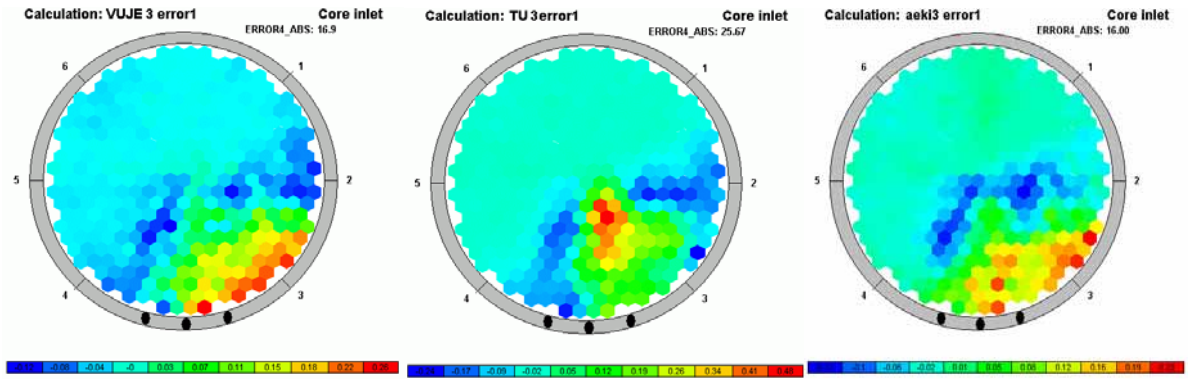

Fig. 4.1-8 Comparison of calculated core inlet temperatures with measured data for loop No.3

B.4.1.5 Summary and Conclusions from VVER mixing tests calculations

Observations and recommendations concerning CFD modelling:

Numerical convergence:

- Good numerical convergence was achieved with basic solver and solver settings based on residuals of continuity and momentum equations (using first order upwind discretization scheme and k-e or RSM turbulence model).
- Some variation of the flow field was observed under the ECC baffles in the downcomer, possibly due to some non-stationarity of flow field

Geometry modelling:

- Modelling of detailed internal geometry (e.g. flow buffles) may have a noticeable influence on results;
- ECC water baffles guide the main flow and generate turbulence effects in the downcomer;
- The alignment drifts have only local effect.
- Accurate model of the perforated elliptical bottom (modelling the elliptical perforated bottom as solid structure rather than using of porous medium) provides more realistic flow pattern and improves the accuracy of the calculation.
- Too much simplifications or too coarse grids can cause unphysical phenomena (e.g. mixing) which are a consequence of numerics.

Boundary conditions:

- Using pressure outlet boundary condition gives better numerical convergence than outflow boundary.

Grid and discretization methods:

- Boundary layer at the walls of downcomer should be less then 3mm, to keep y+ parameter less then 1000.
- High order methods decrease the stability of the solution.

Turbulence modelling:

- From the tested turbulence models the standard k-e with non-equilibrium wall function and RSM with standard wall function models give similar results and best agreement with experimental data. RSM model with non-equilibrium wall function and k-ω SST model overestimate the turbulent effects.

Observations concerning simulated primary circuit flow case:

- The flows from cold legs 1, 2, 5 and 6 mix only little in the downcomer and maintain own sectors. But flows from cold legs (3,4) located near to the ECC baffles are significantly mixed.

- Obtained results proved the applicability of CFD codes for reactor calculations, however there are still areas requiring further investigation;
- More accurate geometry modelling of perforated elliptical bottom and structures below the core is required;
- The models should include the upper plenum and the outlet nozzles.

B.4.2 CFD simulation of the flow field of VVER-440 reactor pressure vessel downcomer by Fortum

B.4.2.1 Introduction

Coolant flow and mixing in the downcomer and in the lower plenum of PWR affects to the coolant distribution at the core inlet, that is directly linked to the core power distribution. Also the mixing of different cold leg flows before the core is important to know in case of asymmetric flow conditions, that are possible for example due to the pump operation uncertainties during power operation or due to the total pump failure of some accident scenarios.

The most used approach to study the pressure vessel flow field is experimental studies using scale models. However the increasing capacity of Computational Fluid Dynamics (CFD) has made it an alternative analysis method, and more and more CFD analyses of power operation and different accident scenarios of PWRs have been made (e.g. [Te02]).

One of the objectives of Flomix-R project was to study and develop CFD methods for PWR primary circuit flow distribution analysis. In this work the commercial multi-purpose CFD code Fluent is used to simulate the flow field in the cold legs, downcomer and lower plenum of VVER-440 NPP during power operation flow conditions. Simulated results are then compared to available real plant data, and conclusions are made about the applicability of CFD methods.

The flow field in the downcomer during normal power operation is in principle straightforward to simulate with modern CFD codes. By following exactly the recommendations and guidelines of CFD use (e.g. [BPG], [ECO]) the one-phase turbulent forced flow in 3D geometry should be possible to be solved accurately enough for many applications. However in many simulations the recommendations can not be fully followed, mostly due to the limited computation resources. In this work the scope of CFD simulation is limited to downcomer and lower plenum having an idea to have enough computation resources to model that as recommended in guidelines. However this goal was not fully achieved.

B.4.2.2 Description of simulations

During the normal power operation the total flow rate in primary circuit of Loviisa VVER-440 is about 9000 kg/s. Having a water temperature of about 265 C the Reynolds numbers in the cold legs and downcomer are about 10^7.

The power operation of VVER-440 reactor was simulated with two different cold leg flow rates and two different geometries. In simulation case 1 a small asymmetry in the cold leg flow rates was set, in case 2 the boundary conditions were the same as in case 1 but the ECC water guides were removed from the model and in case 3 the cold leg flow rates were

symmetric and ECC water guides were included to the model. The case-dependent boundary conditions are presented in figures 4.2-7, 4.2-11 and 4.2-15.

For qualitative comparison the experimental data of cold leg flow mixing factors at the core inlet of VVER-440 reactors in Loviisa [Tsim] and Paks [Elt02] were used.

B.4.2.3 CFD model description

The geometry of Loviisa VVER-440 reactor modelled in detail included the cold leg starting after the reactor coolant pump and ending to the perforated elliptic bottom plate in the lower plenum as presented in figure 4.2-1. In addition the bottom plate and the volume below the core were modelled using simplified geometry.

The Loviisa VVER-440 reactor has six primary loops having the cold and hot leg nozzles at different levels. The downcomer gap is about 156 mm wide, the outer diameter of downcomer is about 3542 mm and the height of the downcomer is about 10 m. There is no thermal shield in the downcomer, but some other structures: eight alignment drifts and three vertical ECC water guides. The eight alignment drifts are located about 4.7 m below the cold leg level so that there is always 45 degree angle between drifts and one drift is always just below every cold leg nozzle. The three vertical ECC flow guides are located in the upper part of the downcomer between two cold leg nozzles, and obstruct the circumferential flow almost completely between these two nozzles. The modelling of these structures is found to be important also in some previous CFD studies [Bor02], [Gan97]. The alignment drifts and flow guides are visible in geometry figures 4.2-2 and 4.2-3.

The elliptic perforated bottom plate is modelled with simple fluid volume having a pressure loss coefficient relative to square of velocity magnitude, and volume just below the core is modelled without internal structures. Due to these simplifications the model is used only for downcomer flow studies, not for example to determine the core inlet mixing factors of cold leg flows.

B.4.2.3.1 Computation mesh

The computation mesh was made using GAMBIT pre-processor, which is part of commercial Fluent CFD software [Flu]. The design basis of mesh was to follow the recommendations of guidelines as much as possible. Also the idea was to have mesh structure that can be systematically upgraded later for new and more powerful computers. Having a steady state simulation the limiting factor for mesh size was the main memory of computation workstation, which was about 3.5 GB in time of meshing.

Following the design basis above, the final mesh had block structure and total of 3029616 hexahedral mesh cells. The detailed local mesh characteristics are presented in table 4.2-1, and the block structure and computation mesh are illustrated in figures 4.2-4 - 4.2-6.

Tab. 4.2-1 Mesh distribution in the CFD model

		radial	circumferential	axial
cold leg		14 20 mm, 0.3 mm	48 30 mm	64 100 mm
downcomer	**up**	36 4 mm, 0.3-0.4 mm	272 40 mm	132 60mm
	down	46 6 mm, 0.4-0.5 mm		
total		3029616		

In the table above the mesh distribution of one cold leg and the downcomer are presented. The width of the downcomer is 156 mm in the upper part and about 270 mm in the lower part of the pressure vessel. In each cell of the table are presented the number of nodes, the average size of one node interval and real node interval near the wall for radial, circumferential and axial directions.

B.4.2.3.2 Physical models

The turbulent viscosity of Reynolds-averaged Navier-Stokes equations was solved using Fluent's realizable k-ε turbulence model [Shi95]. That is a modified version of standard k-ε model, and should be better for example in case of flow with separation and circulation [Flu03].

The mixing of different cold leg flows was studied using different mixing scalar for each loop. The turbulence-dominated mixing was solved with default turbulent Schmidt number $Sc_t = 0.7$.

B.4.2.3.3 Boundary conditions

The boundary condition at wall for momentum was set using FLUENT's non-equilibrium wall functions. These are recommended to be used in cases with flow separation and reattachment. The main difference to the widely used standard wall functions [Lau74] is that the pressure gradients has own effect to function and the computation of turbulence kinetic energy at the wall cells is more sophisticated [Flu03].

The inlet boundary conditions for cold leg flows were set using constant velocity boundary condition and pre-defined turbulent viscosity $Tu_{in} = 1$ %. The case-dependent boundary flow rates are given in figures 4.2-7, 4.2-11 and 4.2-15.

The outlet boundary condition was defined with constant static reference pressure $P_{sta,out} = 0.0$ Pa. There was not backflow from the outlet.

B.4.2.3.4 Numerical methods

The equations were solved using FLUENT's segregated multigrid solver with QUICK spatial discretization and default solver values. QUICK is the most sophisticated discretization method available in Fluent, and was used for the minimization of numerical diffusion.

The basic SIMPLE algorithm was used for pressure-velocity coupling.

B.4.2.4 Results

B.4.2.4.1 Numerical convergence and models

Three target variables were used to monitor the numerical convergence of simulation: static pressure at the inlet of cold leg 1, local axial velocity in one arbitrary selected point in the downcomer and the total mass error specified as a sum of magnitude of mass errors of all mesh cells. Based on these target variables a good convergence was achieved with the default under-relaxation factors and about 3000 iterations, although the velocity field had tendency to "shift" even whit quite small residuals. This can indicate local time-dependent behaviour for example at the backflow area below the ECC water guides. The behaviour of target variables during simulation is presented in figures 4.2-21 - 4.2-23. The numerical convergence was quite similar in all three cases.

The appropriate mesh density at walls was examined using y^+ values. The proper mesh with logarithmic wall functions gives y^+ values of about 30-130 at the walls. y^+ values of about 1000 and over start to produce also qualitatively unphysical wall boundary behaviour. With mesh and flow rates used here the y^+ values at the core side of the downcomer wall were about 200-1000 and at the pressure vessel side about 100-700. Values this high indicate inaccuracies with boundary profiles, but should still mostly give qualitative reasonable results. However in following versions of mesh y^+ should be got to right level.

No mesh density studies were made because the computation resources limited the mesh size to the used about 3 million cells.

B.4.2.4.2 Flow field

The velocity field in the cold legs is not fully symmetric at the junction of downcomer and cold leg. The bends of the cold legs causes the velocity maximum near the outer wall as presented in figure 4.2-19.

The downcomer flow is not directly downward in any of the simulated cases. Flow tends to turn symmetrically to one direction and partly flow back upward through the bottom of the vessel so that below the ECC water guides there is area of swirl with low and locally upward velocity. This effect can be seen also in case 2 without ECC baffles, indicating that besides the baffles the cold leg velocity profile can also change the downcomer flow field to this direction. Velocity field at the downcomer in case 3 is presented in figure 4.2-20.

The axial velocity profiles 1 m below the cold legs and at the downcomer outlet level -7.58 m below the cold legs are presented in figures 4.2-8, 4.2-12 and 4.2-16. With the ECC water guides and symmetric flow rates in case 3 flow is quite symmetric except the area below the baffles. In the upper part of the downcomer flow tends to have maximum values between the cold leg nozzles. In the outlet of downcomer the axial velocity of main flow is about 6 m/s downward, while there is one clear backflow area having about equal velocity magnitude but opposite direction. The eight alignment drifts seem to flatten out the axial velocity field before the downcomer outlet.

With slightly asymmetric cold leg flow rates of case 1 flow is not fully symmetric in downcomer. At the downcomer outlet the flow from cold legs is twisted about 5-15 degree clockwise compared to symmetric case 3. This effect can be seen in the concentration figures 4.2-10, 4.2-14 and 4.2-18. Also the backflow below the baffles is uneven when compared to about symmetric backflow of case 3.

B.4.2.4.3 Mixing

The flow of different cold legs tends to maintain own sectors in the downcomer and mixes only slightly with flow from other cold legs. In CFD simulations the maximum concentrations of individual cold leg flow in the outlet of downcomer is around 95-100% as presented in figures 4.2-10, 4.2-14 and 4.2-18. The most effective mixing is between cold legs 3 and 4 because of the backflow, however also there are large areas effectively without mixing.

B.4.2.4.4 Comparison to real plant measurements

CFD results can be qualitatively compared to real plant measurements of cold leg mixing factors at the core inlet of references [Tsim] and [Elt02]. The mixing factors are weight-factor-type coefficients that can be used to determine the proportion of enthalpy of the different cold leg loops at the inlet of every fuel assembly. Based on references the maximum values of mixing factors at the core inlet are about 0.75 - 0.87, that indicates that mixing is not nearly perfect.

With symmetric flow rates [Elt02] the cold leg flow mixing factors at the core inlet are quite symmetric. The same symmetry can be seen in the downcomer flow of the CFD case 3 with symmetric flow rates. With slightly asymmetric cold leg flow rates [Tsim] there is clear twisting of the cold leg flows, even about 30-40 degrees. The direction is clockwise as in the CFD simulation of case 1 with same asymmetric flow rate, however the effect is clearly stronger in real plant measurements.

B.4.2.5 Summary and conclusions

The starting point of CFD simulation was to simulate the flow field and mixing in the downcomer of VVER-440 PWR at power operation using commercial CFD code, and by that to get an idea how the CFD methods are suited for this kind of study. In addition the CFD simulation would give more detailed information about the downcomer flow.

The CFD simulations were made with symmetric or slightly asymmetric cold leg flow rates and with or without the geometry of ECC water guides. The available guidelines of CFD modelling were followed as exactly as possible, but for example detailed mesh density studies were not made due to the computer resource limitations.

Based on the results of CFD calculations and to comparisons to experimental data from real plants the following conclusions concerning CFD modelling are made:

Geometry modelling:

- The cold leg bends affect to the nozzle area flow field. This indicates that the cold leg geometry should be included to the CFD model geometry.
- The ECC water guides and alignment drifts affect to the flow field and should be included to the geometry.
- Large part of the mixing of cold leg flows before the core inlet seem to happen in the bottom of the vessel and below the core. This indicates that attention must be paid to modelling of bottom structures like the perforated bottom plate if the core inlet flow is determined.

Mesh:

- The appropriate mesh size is quite hard but possible to attain with today's workstations: the 3 million cells used here was not enough based on wall y^+ values but about 4 million cells should be enough. However this must be checked with sensitivity studies.
- The detailed modelling of bottom structures is most probably essential for getting the cold leg mixing factors at the core inlet calculated accurately. In case of VVER-440 the detailed modelling of elliptic bottom plate with about 1300 small holes and the structures below the core can be estimated to be possible to make with about 4 million extra mesh cells. Before the fluent simulations with models having total of about 8 million cells the simplified modelling must be used. That requires separate validation of bottom plate modelling.

Mesh size estimations above are based on the used approach with hexahedral cells and to the suggestions of guidelines. Most probably useful results can be achieved in many cases with smaller number or using different type of cells.

Numerical methods and physical models:

- No turbulence model testing was made in this work. The forced flow simulation as in case of the downcomer flow should be possible to model with turbulence models available in modern commercial CFD codes with accuracy good enough for many applications. However the effect of turbulence modelling should be tested for example with sensitivity studies.
- The simulation converged quite well with QUICK discretization method. No sensitivity studies concerning discretization methods were made, however it is clear that the most accurate method available in used code should always be used.

Validation of CFD model:

- Before the comparison of calculated and measured data the numerical convergence (mesh, discretization) should be confirmed; the flow field twisting in case 1 was more similar to real plant data with still inadequate convergence.

As a summary the CFD methods seem to be a useful tool for PWR downcomer simulations. With recent computer capacity it is already possible to model steady-state downcomer flow as suggested in guidelines, and in addition there is experimental and measured data for validation available. After the numerical convergence can be confirmed the biggest problem will be the physical modelling and especially turbulence modelling, but the turbulence models of commercial codes should be suitable for this kind of forced flow situations during power operation.

Based on the CFD simulations some qualitative conclusions concerning flow field and mixing in the downcomer of VVER-440 PWR are made:

- The flows from different cold legs maintain own sectors in the downcomer and mixes only slightly before the bottom of the pressure vessel.
- The downcomer flow is not directly downward but turns a little due to the combined effect of the cold leg bends and the downcomer structures like ECC water guide.

There is also stagnant velocity area below the guides and in some case upward flow via the bottom of the vessel.

- Asymmetric cold leg flow rates can considerably turn the downcomer flow.

The CFD model used here will be updated in the future by adding more computation cells and modelling the bottom plate in detail. Also the structures below the core will be included to the geometry of model to make the more quantitative comparison to the real plant measurements possible.

Figures:

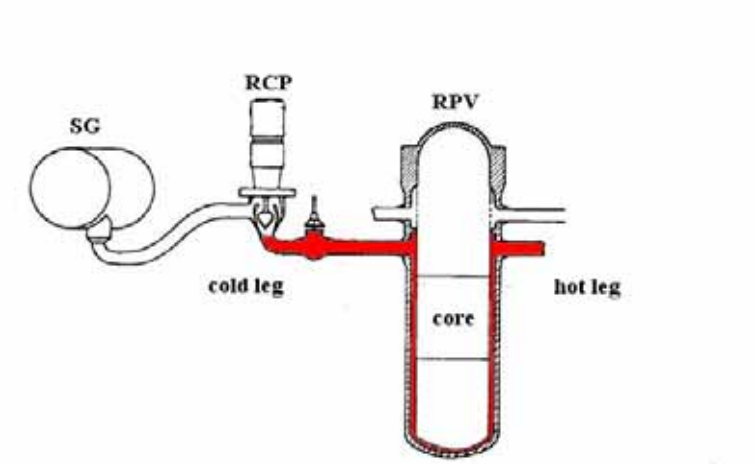

Fig. 4.2-1 Loviisa VVER-440 circuit geometry, modelled volume marked with red colour

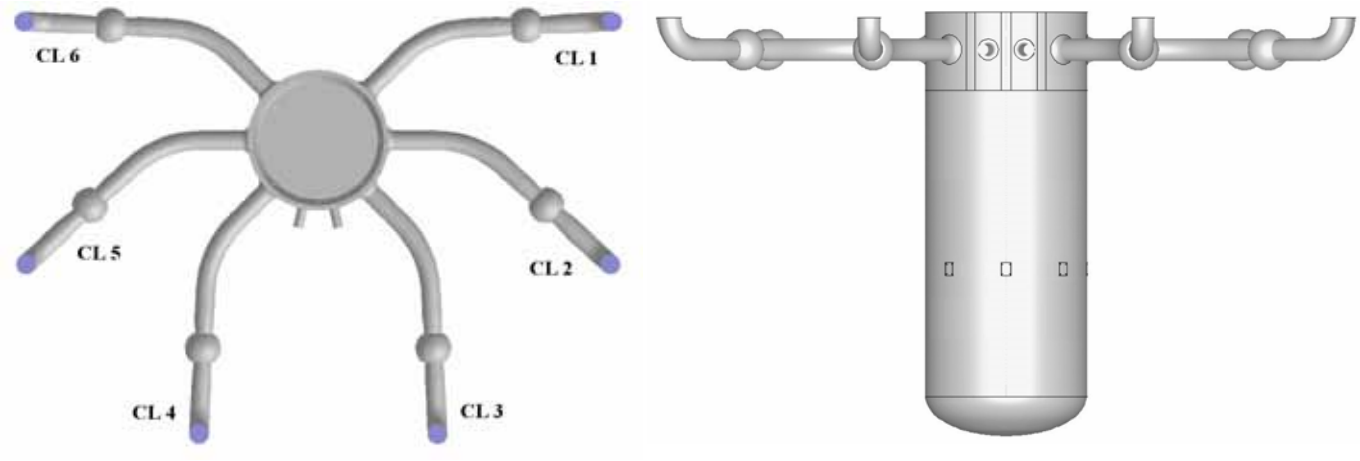

Fig. 4.2-2 Geometry of CFD model, outside of PV, and numbering of cold legs

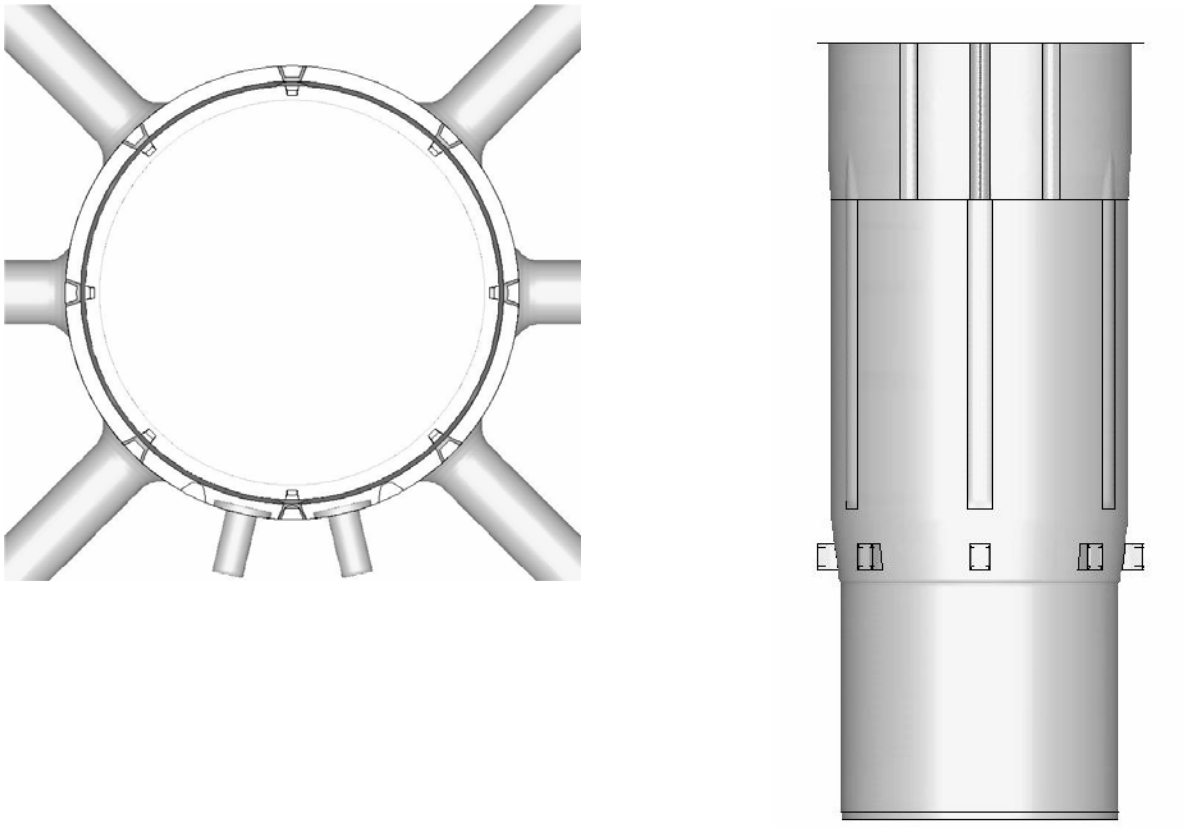

Fig. 4.2-3 Geometry of CFD model, inner structures

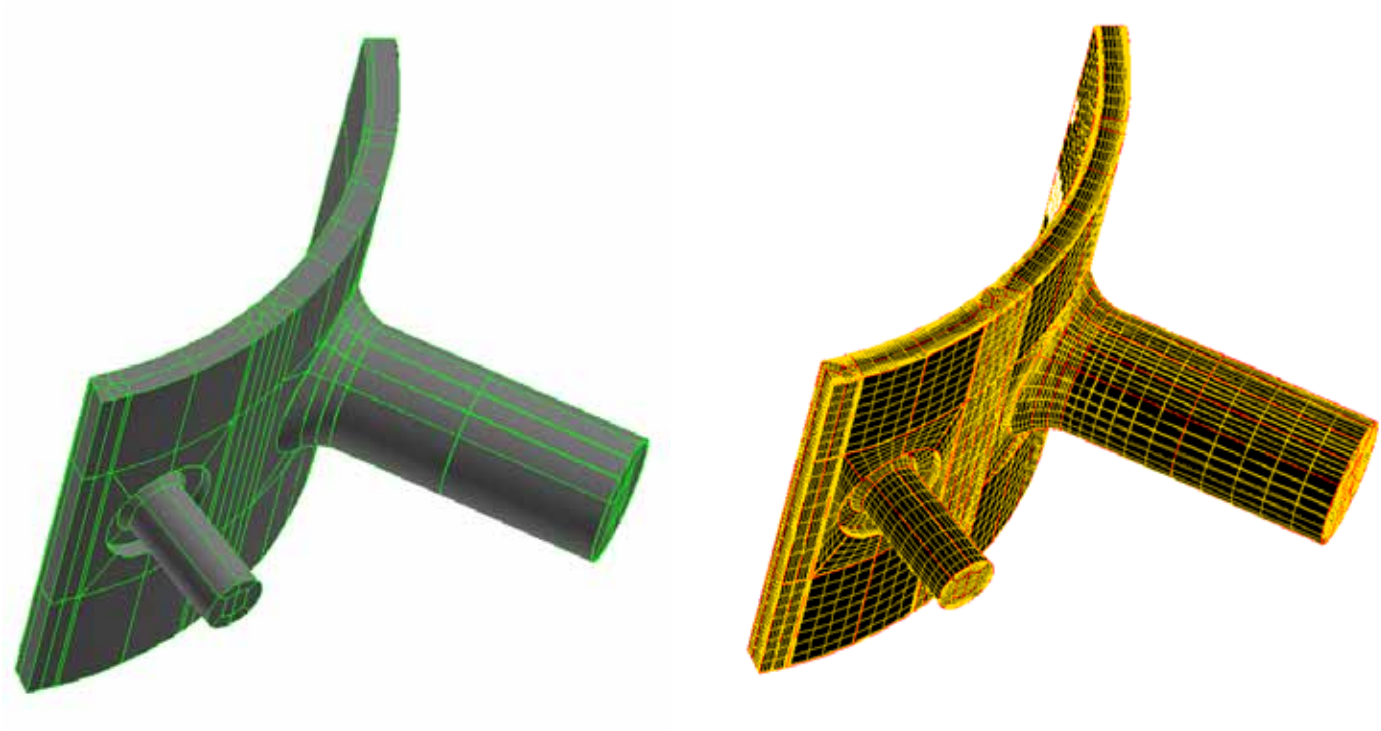

Fig. 4.2-4 Block structure (left) and mesh (right) in the upper part of the downcomer (CL 6 and ECC water junctions)

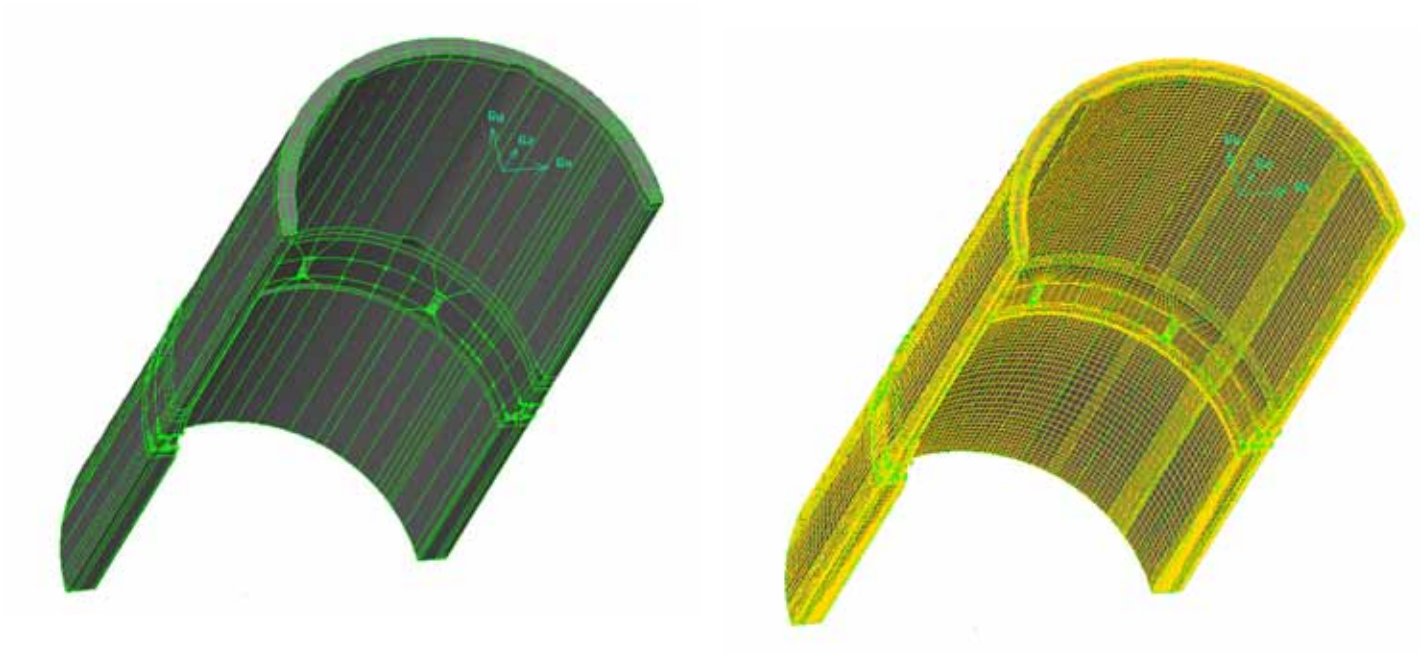

Fig. 4.2-5 Block structure (left) and mesh (right) in the downcomer

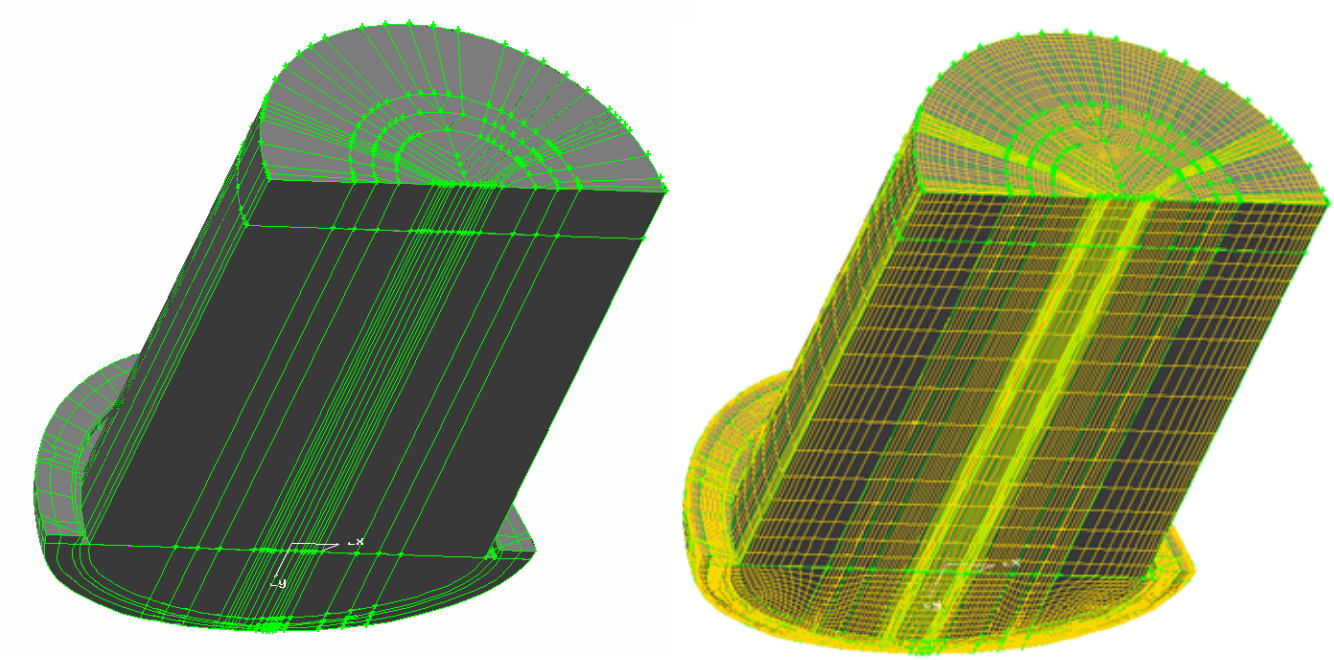

Fig. 4.2-6 Block structure (left) and mesh (right) in the lower plenum and the lower part of the core

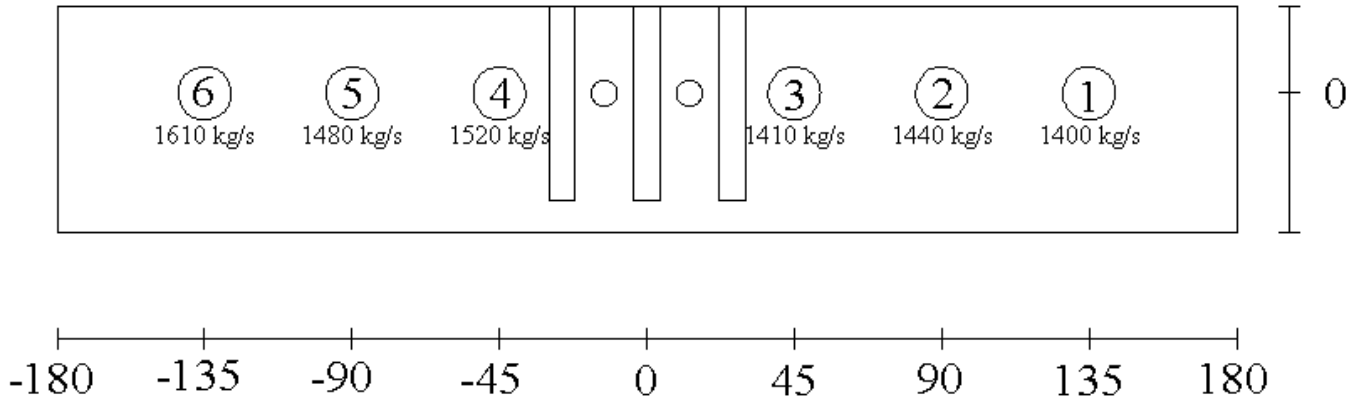

Fig. 4.2-7 Coordinate system for velocity and concentration graphs, case 1

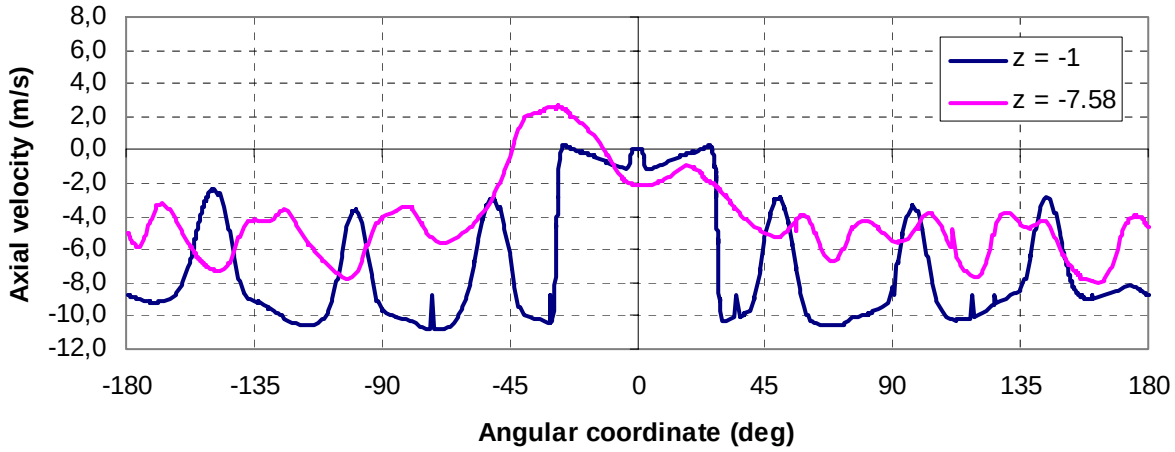

Fig. 4.2-8 Axial velocity in the downcomer, case 1

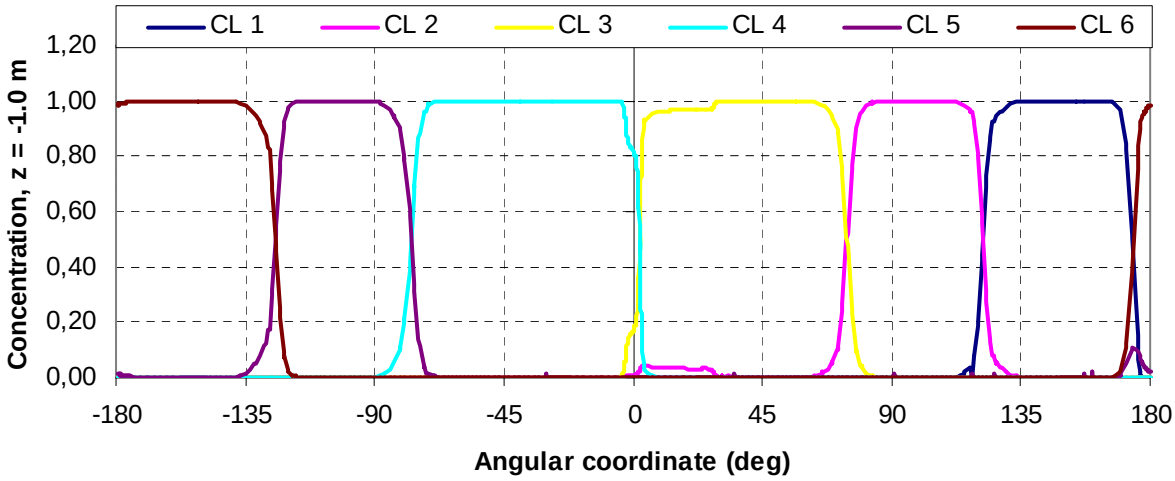

Fig. 4.2-9 Concentrations of cold leg flows at level -1 m below cold legs, case 1

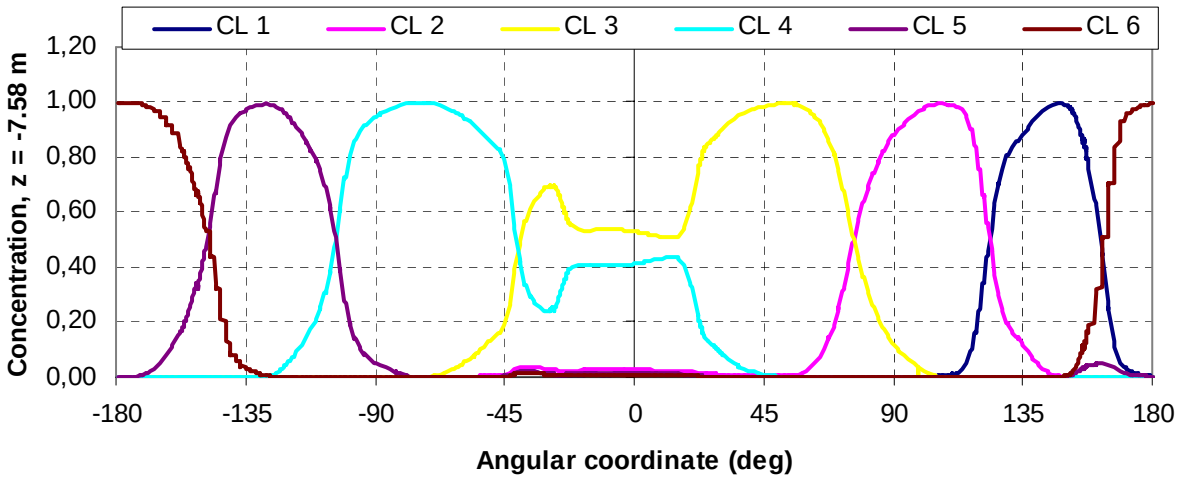

Fig. 4.2-10 Concentration of cold leg flows at level -7.58 m below cold legs, case 1

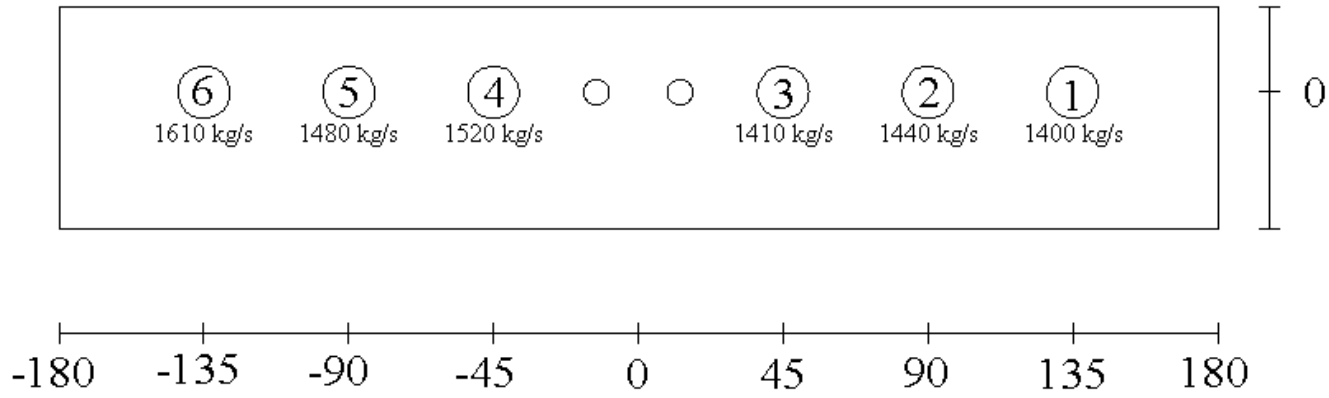

Fig. 4.2-11 Coordinate system for velocity and concentration graphs, case 2

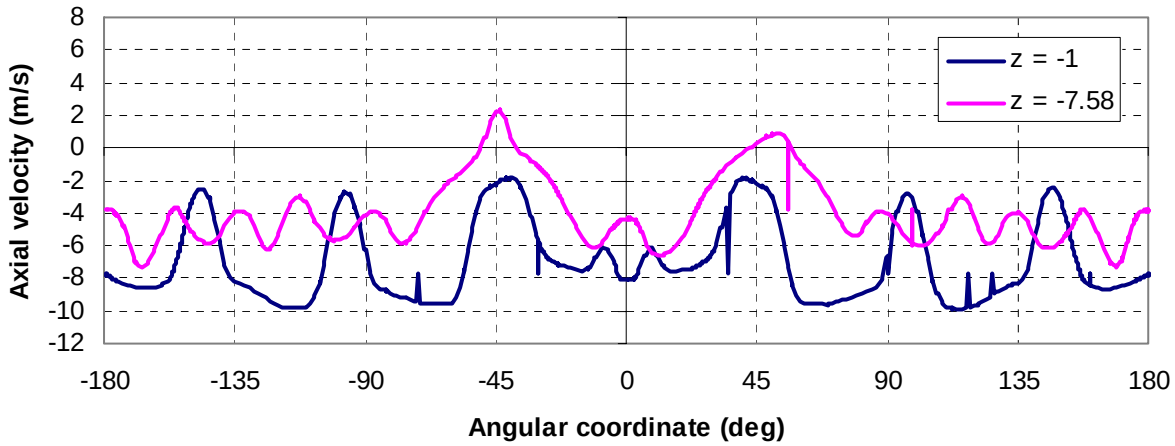

Fig. 4.2-12 Axial velocity in the downcomer, case 2

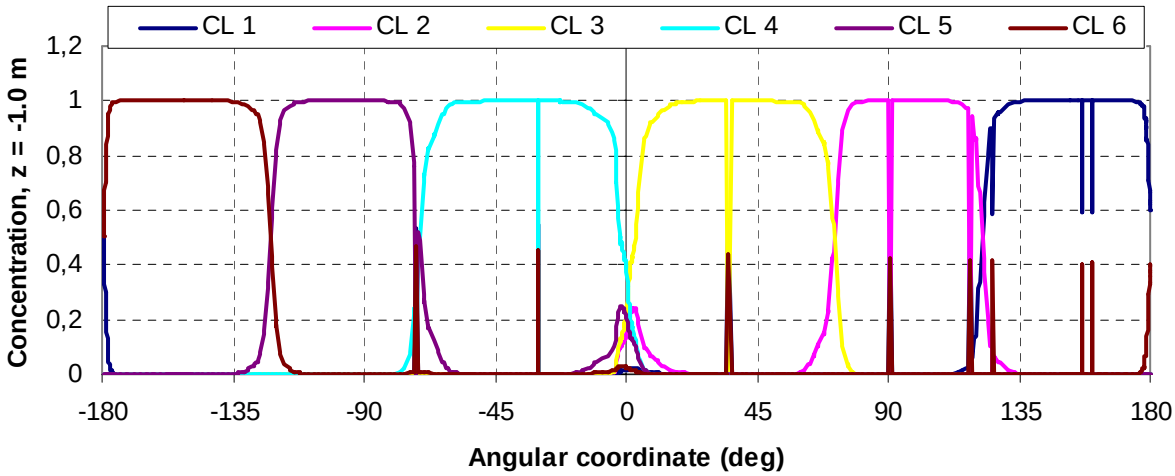

Fig. 4.2-13 Concentration of cold leg flows at level -1 m below cold legs, case 2

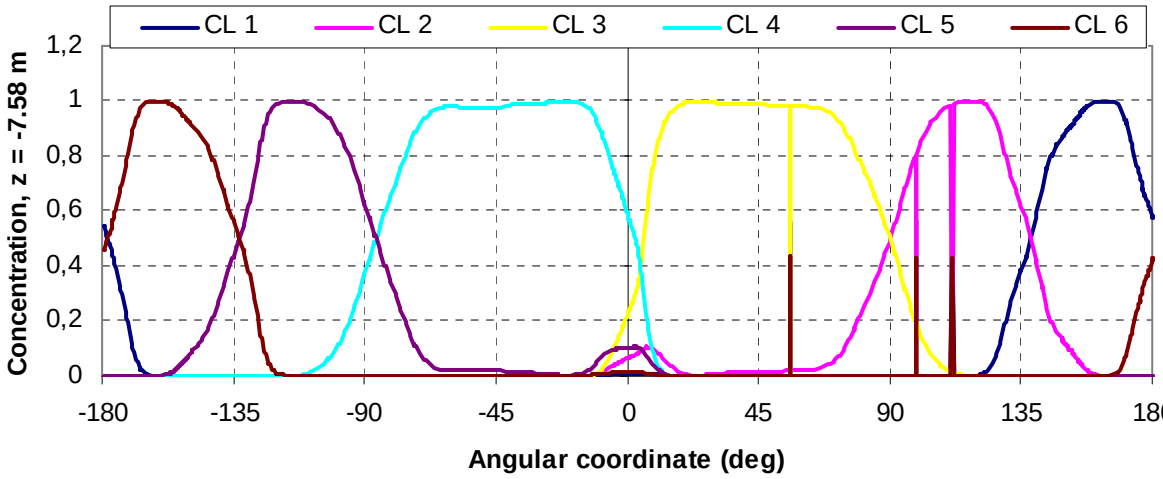

Fig. 4.2-14 Concentration of cold leg flows at level -7.58 m below cold legs, case 2

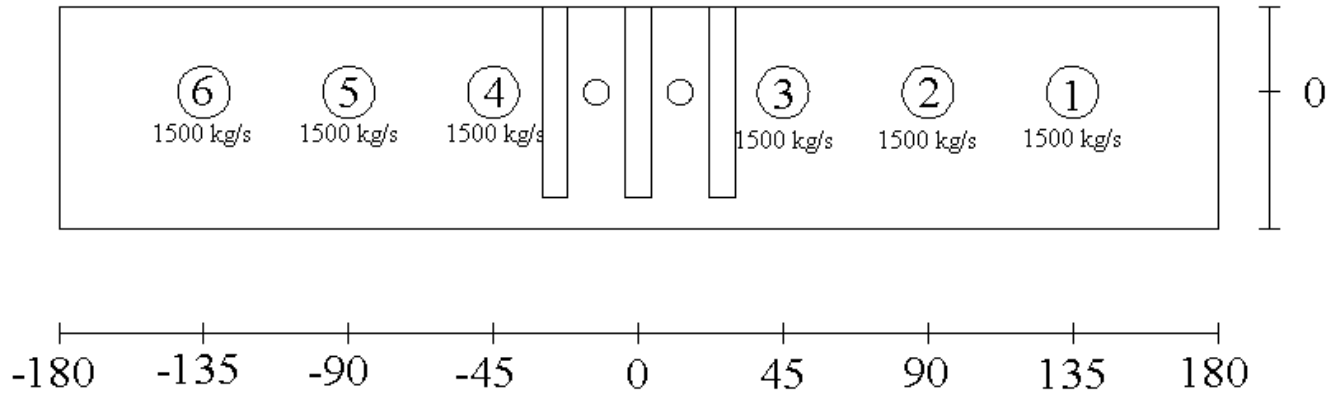

Fig. 4.2-15 Coordinate system for velocity and concentration graphs, case 3

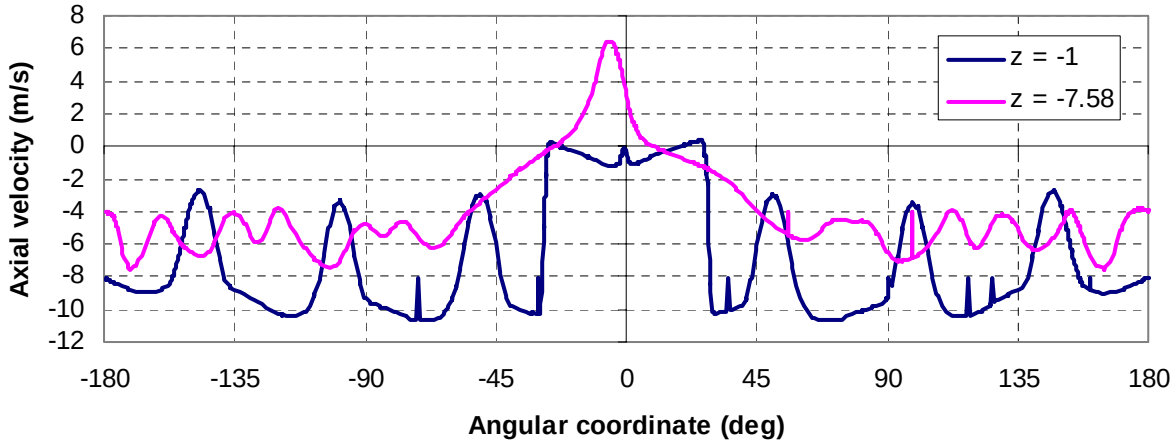

Fig. 4.2-16 Axial velocity in the downcomer, case 3

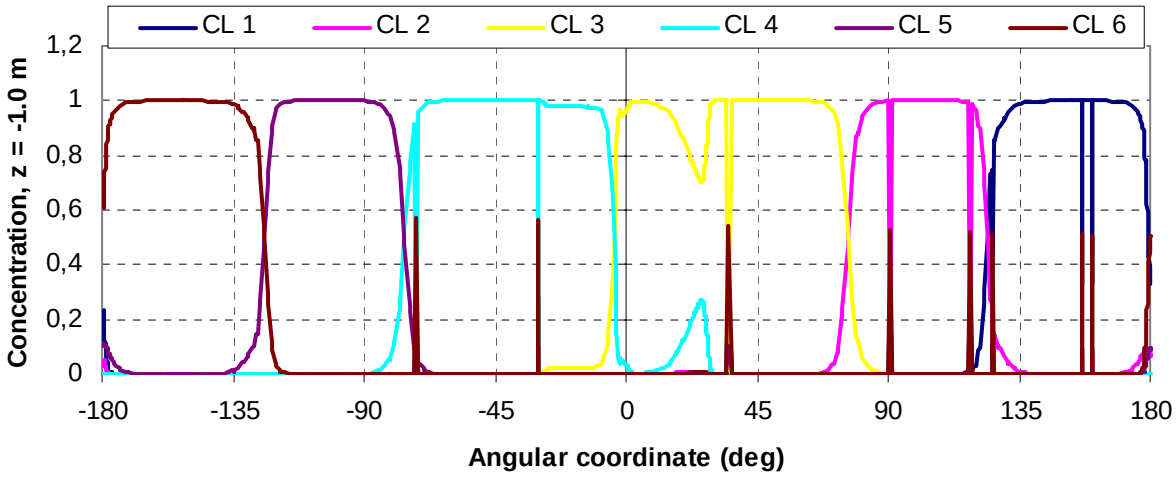

Fig. 4.2-17 Concentration of cold leg flows at level -1 m below cold legs, case 3

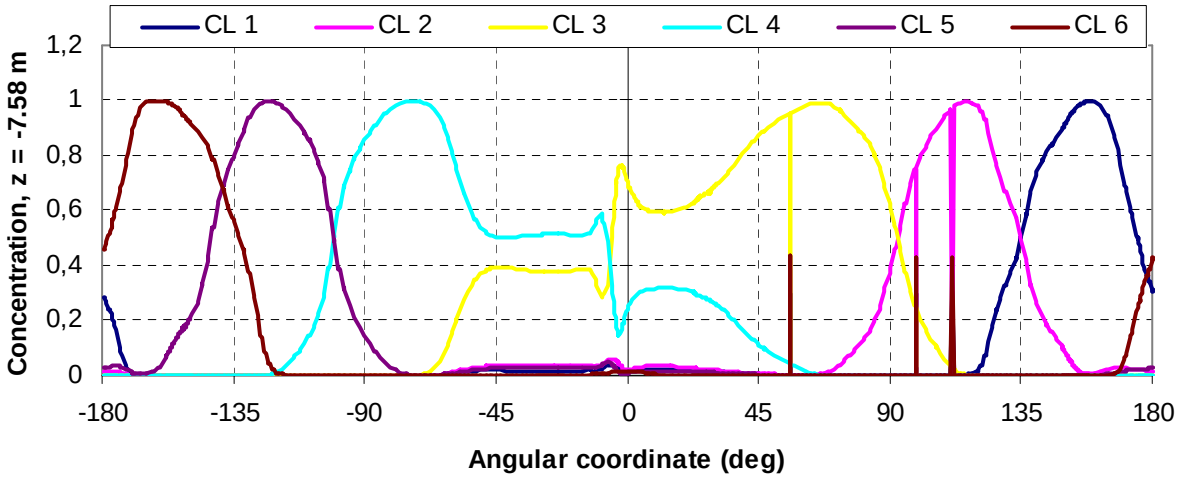

Fig. 4.2-18 Concentration of cold leg flows at level -7.58 m below cold legs, case 3

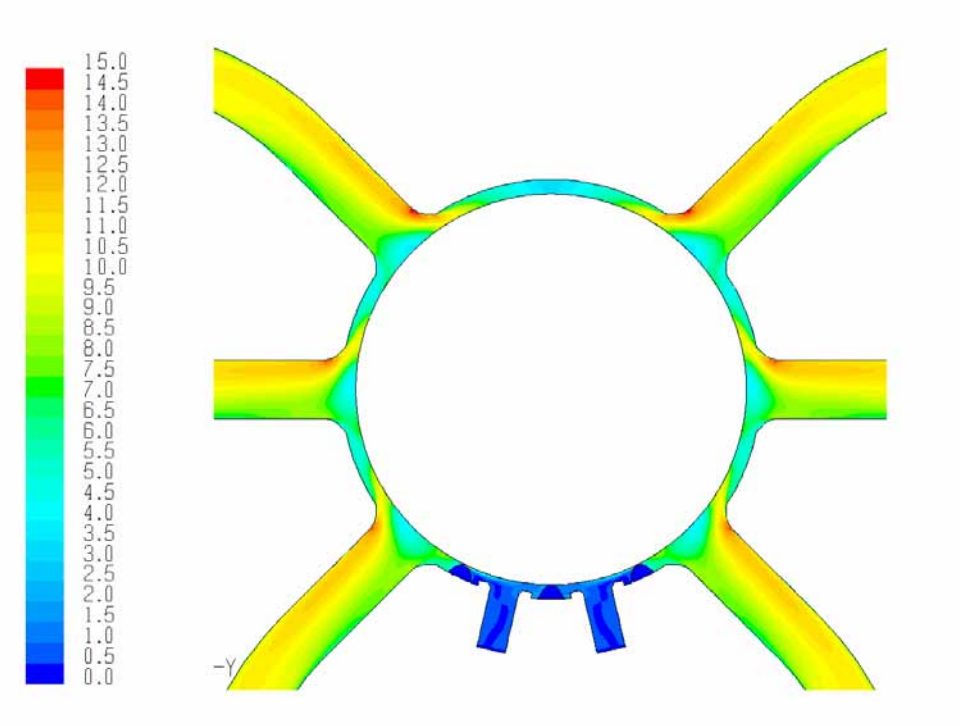

Fig. 4.2-19 Velocity magnitude (m/s) at the cold leg level z= 0.0 m, case 3.

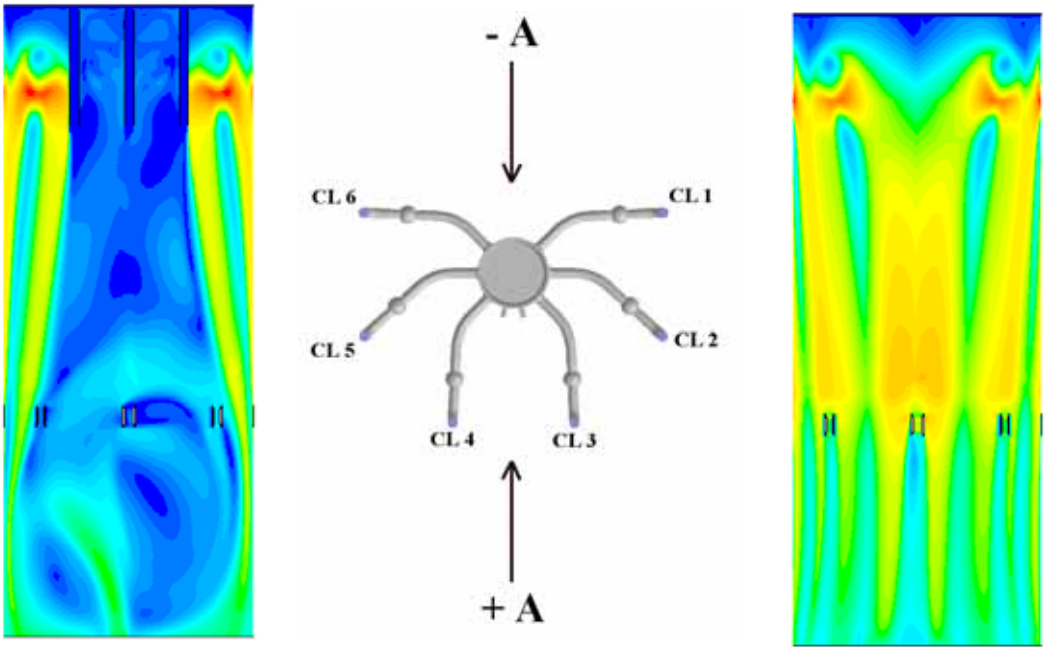

Fig. 4.2-20 Velocity magnitudes (m/s) in the downcomer, case 3 (view +A left, -A right)

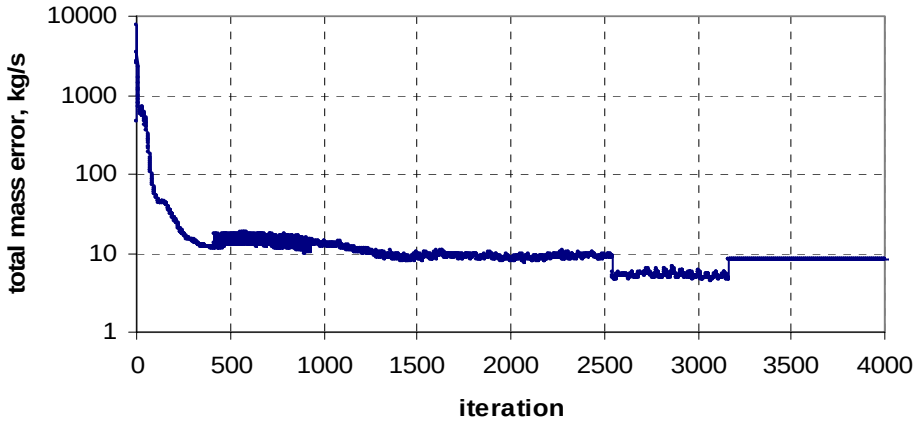

Fig. 4.2-21 Summed up total mass error

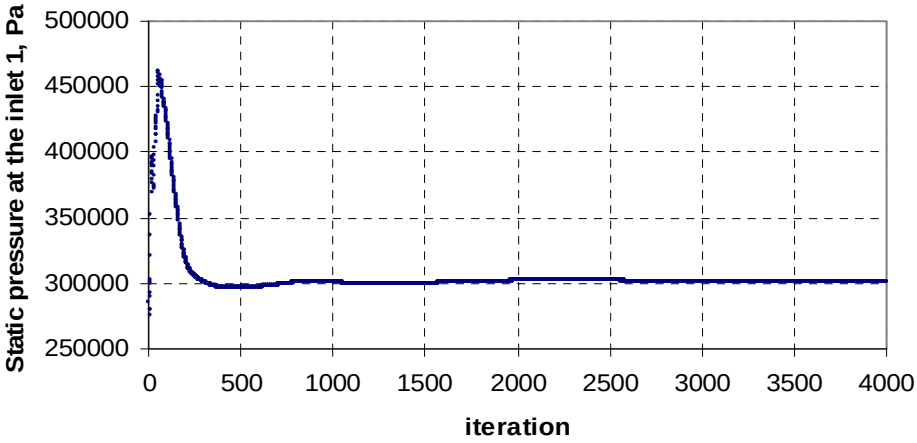

Fig. 4.2-22 Average static pressure in the inlet CL 1

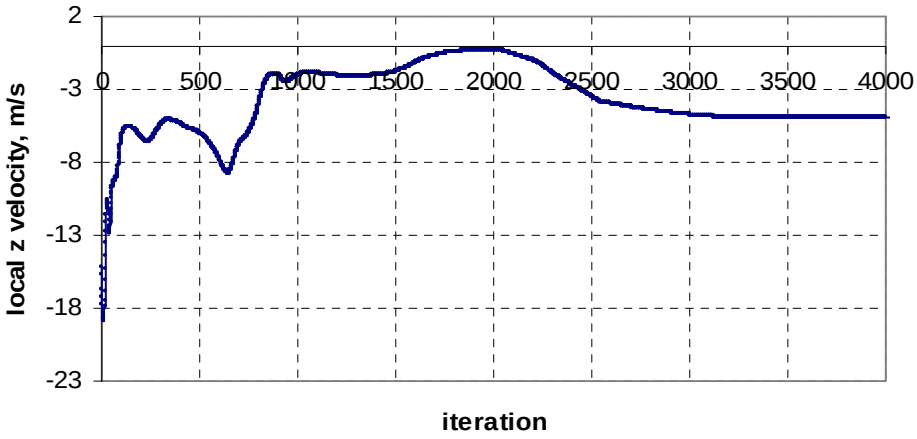

Fig. 4.2-23 Local point velocity in the downcomer

C Summary and conclusions

The flow distribution in the primary circuit of the pressurized water reactor was studied with experiments and Computational Fluid Dynamics (CFD) simulations. The main focus was on the flow field and mixing in the downcomer of the pressure vessel: how the different factors like the orientation of operating loops, the total loop flow rate and the asymmetry of the loop flow rates affect the outcome. In addition to the flow field studies the overall applicability of CFD methods for primary circuit thermal-hydraulic analysis was evaluated based on the CFD simulations of the mixing experiments of the ROCOM (Rossendorf Coolant Mixing Model) test facility and the mixing experiments of the Paks NPP.

The experimental part of the work in work package 3 included series of steady state mixing experiments with the ROCOM test facility and the publication of results of Paks VVER-440 NPP thermal mixing experiments. The ROCOM test facility models a 4-loop KONVOI type reactor. In the steady-state mixing experiments the velocity field in the downcomer was measured using laser Doppler anemometry and the concentration of the tracer solution fed from one loop was measured at the downcomer and at the core inlet plane. The varied parameters were the number and orientation of the operating loops, the total flow rate and the (asymmetric) flow rate of individual loops. The main observations concerning the flow field, mixing and the effect of varied parameters were:

- With all four loops operating the velocity profile at the outlet level of the downcomer is highly non-uniform with velocity maxima in the middle of the two neighbouring inlet nozzles.
- With one loop operating the flow from the operating loop splits to two and flows around to the barrel to the opposite side, where it reunites and flows downwards. There is a clear recirculation area below the inlet nozzle.
- With two operating loops with varied locations it was seen that two loops just at or close to the opposite sides of the downcomer induced maximum downward flow velocities between the operating loops and recirculation below the operating loops.
- With two operating loops 45˚ from each other the flow field is not symmetric but the velocity maximum is below the one of the operating loops and the minimum with recirculation is about below the other operating loop. So the flow field is like a combination of a one-loop case and a four-loop case.
- In case of two operating loops the sector of one tracer at the core inlet plane is about 50 % indicating only slight mixing when the second loop position is one of the two locations at the other side of the facility. The tracer sector is larger when the two operating loops are only 45˚ from each other, indicating more effective mixing. Also the maximum tracer concentration at the core inlet plane is about 10% lower than with longer distance between loops.
- The asymmetric flow rates in two loops induce the increase/decrease of the width of the tracer sector in the downcomer so that the change happens only at the border between the two sectors of the modified flow rates. The maximum tracer concentration at the downcomer stays in the same location as with the symmetric flow rates.
- With a growing asymmetry the second maximum tracer concentration arises at the core inlet. That is induced by the changes in the downcomer flow field.

The Paks NPP thermal mixing experiments took place during commissioning tests of replaced steam generator safety valves in 1987-1989. It was assumed that in the reactor vessels of Paks

VVER-440 NPP equipped with six loops the mixing of the coolant is not ideal. For the realistic determination of the active core inlet temperature field for the transients and accidents associated with different level temperature asymmetry a set of mixing factors were determined. Based on data from the online core monitoring system and a separate mathematical model the mixing factors for loop flows at the core inlet were determined.

The results indicate that the distribution of the mixing factors is symmetric and the maximum values of the mixing factors are around 0.75 meaning that 75 % of the enthalpy flowing through an assembly comes from the closest loop. It also means that under certain processes the effect of the cooling asymmetry might be dominantly noticed in the nuclear behaviour of the core.

It was also notable that distribution of the mixing factor in the lower plenum is in full agreement with the engineering view. The distributions on the longitudinal axis of the core – due to geometrical layout – are symmetrical, and no swirls could be identified.

In the numerical simulation part of the work package 3 the detailed measurements of ROCOM tests were used for the validation of CFD methods for primary circuit studies. The selected steady state mixing experiments were simulated with CFD codes CFX-4 and CFX-5 by FZR and with FLUENT by VUJE and AEKI.

The velocity field in the downcomer and the mixing of the scalar were compared between CFD simulations and experiments with the following observations:

- The velocity field in the downcomer is qualitatively similar in simulation and experiment.
- There is a good agreement between the measured and simulated core inlet mixing scalar concentration. The averaged global mixing scalar concentration at the core inlet is quite similar, and the difference in the maximum disturbance at the core inlet is small.

Concerning the CFD modelling the following conclusions were made:

- Finer grids tend to give better results indicating that fully grid-independent results are not yet achieved.
- Modelling of perforated sheets (such as the drum in the downcomer) as real structure rather than porous medium improves the quality of results. However, also with the porous body approach for the modelling of lower plenum structures, reasonable results were achieved when the core inlet scalar concentrations were compared.
- The porous medium as a substitute for a perforated sheet can be, in some extent, made more reasonable by proper definition of direction-dependent resistance of the porous medium.

The CFD simulations of full scale PWR included the simulation of Paks VVER-440 mixing experiment by AEKI, VUJE and TU Budapest and the simulation of Loviisa VVER-440 downcomer flow field by Fortum. In the simulations of Paks experiments the experimental and simulated concentration field at the core inlet were compared and conclusions made concerning the results overall and the VVER-440 specific geometry modelling aspects like how to model the perforated elliptic bottom plate and what is the effect of the cold leg bends to the flow field entering to the downcomer. With Loviisa simulations the qualitative

comparison was made against the original commissioning experiments but the emphasis was on the CFD method validation and testing.

The main conclusions concerning the flow field and mixing in the downcomer of VVER-440 reactor based on the CFD simulations are summarized below:

- The flows from different loops mix only slightly in the downcomer and maintain their own sectors quite distinctly. However in some simulations the flow from two loops next to the ECC baffles (three axially located structures in the upper part of the downcomer) mixes together more effectively.
- The ECC baffles have an effect on the flow field: below the baffles there is an area of nearly stationary or recirculating flow.
- Asymmetric flow rates combined with the guiding effect of the ECC baffles seems to turn the downcomer flow a little and therefore induce a "twisted" loop flow concentration field at the core inlet.
- The most effective mixing of the loop flows before the core barrel seems to occur in the bottom of the pressure vessel, not in the nozzle area or in the downcomer.
- The alignment drifts have only a local effect on the flow field.

These simulations-based observations were to the extent possible confirmed with comparison to real plant measurements.

Concerning the CFD modelling of VVER-440 pressure vessel flow field the following observations were made:

- Modelling of the detailed internal geometry (e.g. flow buffles) may have a noticeable influence on results; the detailed geometry should be included in the CFD model.
- An accurate model of the perforated elliptical bottom (modelling the elliptical perforated bottom as solid structure rather than using of porous medium) provides more realistic flow pattern and improves the accuracy of the calculation.
- The bends of the cold legs affect the flow field in the nozzle area but also in the downcomer and lower plenum: there is a tendency of backflow at one side of the downcomer while at the other side there are higher flow velocities. This indicates that the cold leg geometry should be included to the CFD model geometry.
- From the tested turbulence models in FLUENT the standard k-ε with FLUENT's so-called non-equilibrium wall function and the Reynold's Stress Model (RSM) with standard wall functions gave similar results and the best agreement with experimental data. The RSM model with non-equilibrium wall function and the k-ω SST model overestimated the turbulent effects.
- A large part of the mixing of cold leg flows before the core inlet seems to happen in the bottom of the vessel and below the core. This indicates that attention must be paid to modelling of bottom structures like the perforated bottom plate.

It must be noted that most of the conclusions and observations concerning the CFD modelling of VVER-440 flow field can be quite directly applied also to other PWR types. However the possible effect of geometric differences like the width of the downcomer gap, the loop orientation and number and the geometric details in the downcomer must be kept in mind.

The combining of various experimental results and CFD simulation results to common conclusions is not straightforward because of the different geometries and flow states. The

western-type reactor modelled for example by the ROCOM test facility typically has a larger downcomer gap than in the VVER 440 type reactors, the number and the orientation of the loops is different and there is also differences with structures in the downcomer and in the bottom of the pressure vessel. However the main observations are similar in different experiments and CFD simulations: with all loops operating with equal flow rates the loop flows maintain their own sectors in the downcomer with only slight mixing and the velocity maxima are in the middle of two neighbouring inlet nozzles. The non-operating loops and/or different obstacles that block the flow like ECC baffles in the VVER-440 concept affect the flow field and may cause recirculation areas in the downcomer.

The overall conclusion concerning the CFD modelling of the flow field and mixing in the PWR primary circuit could be that the current computation capacity and physical models also in commercial codes is beginning to be sufficient for simulations giving reliable and useful results for many real primary circuit applications. However the misuse of CFD methods is easy, and the general as well as the nuclear power specific modelling guidelines should be followed when the CFD simulations are made.

References

[Be96] Bernard, J.P., Haapalehto, T., Review of Turbulence Modelling for Numerical Simulation of Nuclear Reactor Thermal-Hydraulics, Research Report, Lappeenranta University of Technology, 1996.

[Bor02] Boros, I., et al., Numerical Analysis of Coolant Mixing in the RPV of VVER-440 Type Reactors with the Code CFX-5.5.1, IAEA/OECD Technical meeting on the use of computational fluid dynamics (CFD) for safety analysis of reactor system including containment, Pisa, 11-15 November 2002.

[BPG] ERCOFTAC Best Practice Guidelines, see http://imhefwww.epfl.ch/lmf/ERCOFTAC/

[CFX4] CFX-4.4 Flow Solver User Guide, AEA Technology, 2001.

[CFX5] CFX-5.6 User Documentation, ANSYS-CFX, 2003.

[ECO] Menter, F., CFD Best Practice Guidelines for CFD Code Validation for Reactor Safety Applications, ECORA FIKS-CT-2001-00154, 2002

[Elt02] Elter, J., Experiment Summary Report, Experimental Investigation of Thermal Mixing Phenomena in a six loop VVER Type Reactor, Paks Nuclear Power Plant Ltd, Safety Assessment Group, Flomix-R project February 2002.

[Flu] Fluent Inc., see http://www.fluent.com/

[Flu03] Fluent 6.1 User's guide, Fluent Inc., 2003.

[Gan97] Gango, P., Numerical Boron Mixing Studies for Loviisa Nuclear Power Plant, Nuclear Engineering and Design 177, 239-254, 1997.

[Kle04] Klepac, J., Remis, J., Progress Report on VUJE Contribution to the WP3, FLOMIX-R-D17, VUJE, Slovakia, 2004.

[Kli03] Kliem, S., Rohde, U., Höhne, T., Data Sets on Steady State Mixing Experiments at ROCOM Facility, EU/FP5 FLOMIX-R report, FLOMIX-R-D07, FZ Rossendorf, Germany, 2003.

[Lau74] Launder, B. E., et al., the Numerical Computation of Turbulent Flows, Computer Methods in Applied Mechanics and Engineering, 3, 269-289, 1974.

[Pr03] H.-M. Prasser, G. Grunwald, T. Höhne, S. Kliem, U. Rohde, F.-P. Weiss, Coolant Mixing in a Pressurized Water Reactor: Deboration Transients, Steam-Line Breaks, and Emergency Core Cooling Injection, Nuclear Technology 143 (1), p.37, 2003.

[Roh02] Rohde, U., Kliem, S., Toppila, T., Hemström, B., et al., Identification of Mixing and Flow Distribution Key Phenomena, EU/FP5 FLOMIX-R report, FLOMIX-R-D02, FZ Rossendorf, Germany, 2002.

[Roh04] Rohde, U., et al., Description of the Slug Mixing Experiments at the Different Test Facilities, EU/FP5 FLOMIX-R report, FLOMIX-R-D09, FZ Rossendorf, Germany, 2004.

[Shi95] Shih, T.-H., et al., A New-Eddy-Viscosity Model for High Reynolds Number Turbulent Flows-Model Development and Validation. Computers Fluids, 24(3), 227-238, 1995.

[Te02] IAEA/OECD Technical Meeting on the Use of Computational Fluid Dynamics (CFD) for Safety Analysis of Reactor System Including Containment, Pisa, 11-15 November 2002.

[Tsim] Tsimbalov, S., et al., Coolant temperature Distribution at VVER-440 Core Inlet. Atomnaya Energiya 52 (5), 304-308.

[Ul83] Ulrych, G., Weber, E., Neuere Ergebnisse zur Kühlmittelströmung in Druckwasserreaktoren, Atomkernenergie-Kerntechnik 42 4, 217-223.

Appendices

1. J. Elter: EXPERIMENT SUMMARY REPORT, Experimental Investigation of Thermal Mixing Phenomena in a Six Loop VVER Type Reactor. PAKS NUCLEAR POWER PLANT LTD, report.

APPENDIX 1

Experiment summary report
József Elter, PAKS NUCLEAR POWER PLANT LTD.

EXPERIMENT SUMMARY REPORT

Experimental Investigation of Thermal Mixing Phenomena in a Six Loop VVER Type Reactor

Abstract

Certain conditions in a pressurised water reactor with six coolant loops may cause the flow rate and the temperature from one of the cold legs to differ significantly from those in the other loops.

Thermal mixing tests at the Paks NPP indicated that total mixing did not occur in the downcomer and in the lower plenum, thus temperature distribution at the core inlet becomes non-uniform. The assumption of perfect mixing may lead to an erroneous prediction the inlet temperature field.

The paper presents a simple experimental method used an operational reactor for the measurement of temperature field at the core entrance and based on these tests the determination of the mixing factors.

In order to create a significant asymmetry between the temperatures of the cooling loops, the measurements were performed on power, undertaking serious problems arising during the test evaluation.

The different steam generator pressure has been used as a source of the asymmetry, which has been reached by successively closing the valves on the steam lines.

With linear regression analyses the mixing factors for the inlet points of those assemblies in the outlet of which the thermometers are located have been determined.

1. Introduction

There is no inlet temperature measurement in the Paks VVER 440 type. For this reason the inlet temperatures might be derived from the signals of thermometers located in the cold legs of the loops.

When the loops are of nearly the same temperature then the average temperatures of the cold legs of the six loops could be used as the uniform inlet temperature. However in case of certain accident situation significant loop temperature asymmetry might occur and the averaged inlet temperatures will not be of the desired accuracy.

It means that in certain accident situations (i.e. steam line break) resulting asymmetry, the inlet temperatures usually are defined by two different extreme approaches. It is either stipulated that the thermal mixing between the loops is ideal, or that the coolant flowing in the different loops forming kind of a channels and do not mix at all.

From the point of view of a realistic approach neither of those methods is acceptable and consequently the temperature distribution beneath the core is usually given by mixing factors determined by experiments.

The inlet temperature of a given (i) assembly might be produced by linear combination of the temperatures (T_k) of the six loops:

$$t_i = \sum_{k=1}^{6} a_k^i \cdot T_k \,. \qquad (1)$$

Where a_k^i are the six mixing factors characteristic for the given (i) assembly, corresponding to the six cooling loops, depending on the flow rates. Those figures are actually some kind of weight-factors that indicate the proportion of the enthalpy of the different loops at the inlet of the given assembly.

2. Principle of derivation of the mixing factors from measurements

The online core monitoring system is the most practical measuring instrument for performing measurements on an operating reactor. The accuracy of the measurements was assessed and it revealed that those instruments were adequate and accurate enough for the execution of the measurements. The data collection program integrated to the reactor's in-core monitoring system was used for data recording. Using this system it was possible to record in an easy-to-process form a given number measurement cycles the following measured data:

- assembly outlet temperatures, measured by 210 thermocouples, located in the assembly heads;
- the loop temperatures measured by 2 thermocouples and 1 resistance thermometer located in the cold and hot legs of the cooling loops;
- signals of the ionisation chambers measuring the reactors nuclear power;
- the loop flow-rate value, that can be calculated on the basis of pressure drop measured on the main cooling pumps and the pump characteristics.

The best way to determine of the mixing factors is to create many different, and significantly asymmetrical temperature fields.

There were earlier as well measurements aimed for determination of the mixing factors for VVER-440 reactors (Tsimbalov and Kraiko 1982, Jirous 1989), however in those cases much simpler and consequently less accurate method was used. Those were executed on zero power, since in such cases the temperatures measured by the thermometers at the assembly outlet could be identified by the assembly inlet temperatures without any needs for corrections.

The basic weakness of such measurements was that due to technological reasons there was no possibility to create significant asymmetry between the loops and consequently the inaccuracy of determination of the mixing factors was expressive.

In order to achieve more reliable results our measurements were carried out on power, undertaking by this the problems occurring in the evaluation.

We were successful to carry out one series of measurements on each unit of Paks NPP. The measurements were performed on power (10-15%) during the operational process phase when the replaced new steam-generator safety valves were tested for the proper opening value.

The power of a selected (i) assembly can be calculated in the following way on the basis of thermo-technical data:

$$N_i = g_i \cdot \left(i_i^{out} - i_i^{in}\right), \tag{2}$$

where N_i and g_i are the assembly power and flow-rate through the assembly, while i_i^{out} and i_i^{in} are the coolant enthalpies at assembly outlet and inlet correspondingly.

Since the temperature differences between the assembly outlet and inlet are not significant (3-4 ^oC), the thermal capacity of the coolant (c_p) can be taken as a constant and independent from the temperature:

$$N_i = g_i c_p \cdot \left(t_i^{out} - t_i\right), \tag{3}$$

where t_i^{out} and t_i are the temperatures at the outlet and inlet of the assembly.
Using equation (1):

$$N_i = g_i c_p \cdot \left(t_i^{out} - \sum_{k=1}^{6} a_k^i \cdot T_k \right) \tag{4}$$

Having reorganised and taking into account that $\Delta t_i = N_i / g_i c_p$ is resulted from:

$$t_i^{out} - \Delta t_i = \sum_{k=1}^{6} a_k^i \cdot T_k . \tag{5}$$

On the basis of equation (5) it is obvious to determine mixing factors a_k^i by regression. Different loop temperature asymmetries are to be adjusted and the power, flow-rate, outlet temperature of the selected (i) assembly along with loop inlet temperature are to be measured. Following, having adequate enough independent measurements a special linear regression method should be used (Seber 1977). The different batches of six numbers a_k^i achievable as a result of the individual fitting process for the assemblies will be more precise by increasing the number of the different asymmetrical conditions created on the reactor system and by setting more significant temperature differences on the cold legs of the loops.

Two more additional conditions should be used the in process of determination the mixing factors:

$$\sum_{k=1}^{6} a_k^i = 1 \text{ and } \forall a_k^i \geq 0 \tag{6}$$

The assembly power and flow-rate cannot be directly measured by the in-core monitoring system, consequently they have to be determined on the basis of the measured power of the reactor and measured earlier – yet under symmetric conditions – assembly power distribution.

3. The executed measurements

The measurements took place during commissioning tests of newly replaced steam generator safety valves (1987-1989).

During the tests – which was carried out independently from the measurements of the mixing factors, according to a standard procedure – the steam consumption from the investigated steam generator was ceased by closing the gate valves on the steam-lines and by slow increase of the reactor power the safety valves were forced to open (see Fig. 1). In such cases the pressure in the secondary side of the investigated steam generator might be as high as 55-59 bar, while in the other opened or only partially closed steam generators this value was 45-47 bar. This resulted that in the moment just prior to the opening of the safety valve the cold leg temperature of the investigated steam generator was about 8-9 ^{o}C higher than that of the others. This is rather significant temperature difference, having on mind that the assembly heat-up in such cases is only 3-4 ^{o}C. In opposition to 2 ^{o}C temperature difference achieved by other referred measurements (Tsimbalov and Kraiko 1982, Jirous 1989), in our case the effect of the asymmetry was significantly reflected in the outlet temperatures measured in the assembly heads. The measurement errors influence in the accuracy of the final result is much less in case of so significant asymmetry.

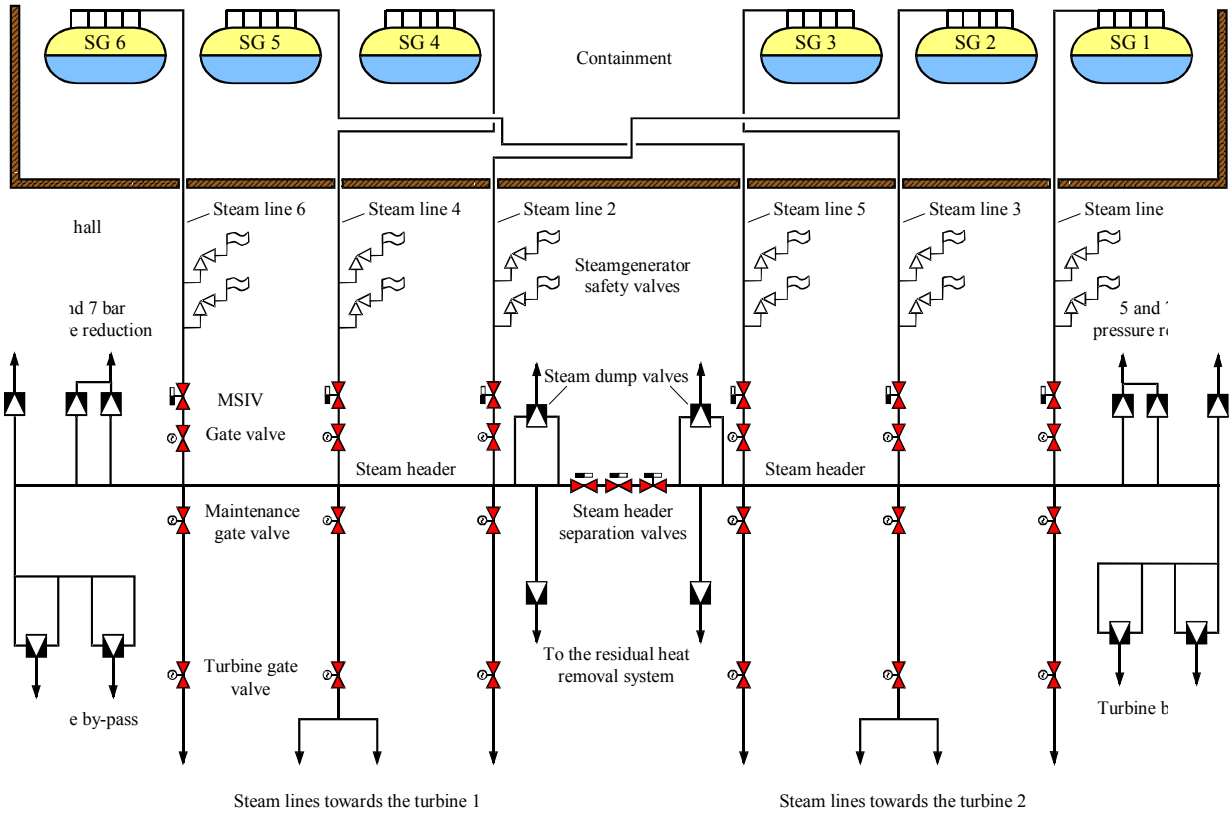

Figure 1. Scheme of the secondary side steam system

All together 12 valves had to be tested, since there are 2 safety valves on each steam generator and consequently at least 12 different collected data sets might be used for the purpose of evaluation. “Fortunately”, the fine tuning of the new valves sometimes required repetitive tests, consequently the number of collected data sets were even higher.

A given measurement series starts with the isolation of the steam generator and lasts following an approximately 15-20 minutes heating up phase until opening of the safety valve. During this period of time all the measurable values for equation (5) might be recorded in every 16^{th} seconds with the data-recording system. The recorded so 60-80 conditions could have used later during the evaluation.

4. Method of assembly power determination

When evaluating the measurement results the greatest problem was that a method had to be developed for determination of the heat-up value in the measured assemblies.

As a simple approach, one might postulate that the power peaking factor (k^i) of the assemblies would not change during the measurements and its value would be the same that could have determined at the beginning of the measurement series (yet under symmetric conditions). The peaking factor might be defined as quotient of the heat-up of the given assembly (Δt_i) and the average heat-up of the assemblies (Δt). So, in such case the assembly power necessary for the linear fitting should not be determined on the basis of assembly heat-ups corresponding to the asymmetric conditions.

Instead, data are to be recorded during a symmetrical, so called reference distribution, where from the measured heat-ups the power peaking factors could be derived. Under conditions corresponding to different valve tests each Δt_i value could be produced by multiplication of the average heat up of the corresponding k^i. The independence of the peaking factors from the actual asymmetrical temperature distribution during the measurements obviously could not be achieved due to rather strong local neutron-physical feed-back, in certain cases the peaking factors would change significantly.

According to the perturbation theory it could be proved that under steady power conditions the assembly heat-ups react with good accuracy linearly to the changes of the inlet temperatures.

With help of a series of 3D core physical calculations performed beforehand and independently from the measurements we could also recognise and prove the linear relationship between the power of individual assemblies and that of the reactor in case of constant inlet temperature.

Based on the above, the following correlation for assembly heat-up under an individual asymmetry condition was suggested:

$$\Delta t_i = \Delta t^{ref} \frac{P}{P^{ref}} \cdot k^{i,ref} + \alpha_i \cdot \left(P - P^{ref}\right) + \beta_i \cdot \left(t_i - t_i^{ref}\right), \qquad (6)$$

where Δt^{ref}, P^{ref}, and $k^{i,ref}$ are correspondingly the assembly heat-up, the reactor power and the peaking factor calculated from assembly heat-up for every assembly, during the reference conditions. Such an approach assumes that the heat-up of the given assembly will be primarily determined by its own power and inlet temperature. The effect of the neighbouring assemblies was neglected, since the thermal connection between the neighbouring assemblies was assumed weak, the changes in the power and inlet temperature would influence nearly in the same way the neighbours of the given assembly as well. The estimated relative uncertainty of the assembly heat-up defined with this method is about 4-5 % that would result about 1% additional absolute uncertainty of the mixing factors.

The two parameters characteristic for the back fitting α_i and β_i, might be determined during evaluation of the measurement series by iteration.

Since we usually had more than 12 different independent asymmetrical data sets the eight unknown values (α_i, β_i and the six a^i_k) would readily be determined by a linear regression technique.

5. The measurement results

Measurement results could be obtained only for such assemblies of which there is an operating thermometer at the assembly outlet. The number of these assemblies was usually 210, while there were 349 assemblies in the core. For such positions where there were no thermometers we suggest to use the mean value of the mixing factors of the neighbouring assemblies.

The results gained on the four different units of Paks NPP indicated that the mixing conditions are very similar to each other. Naturally this fact is not at all surprising since the level of the mixing is primarily influenced by the reactor geometry what is identical on all the units. A detailed, statistical error analysis revealed that the differences in the measurement results cannot be assumed significant (see Fig. 2).

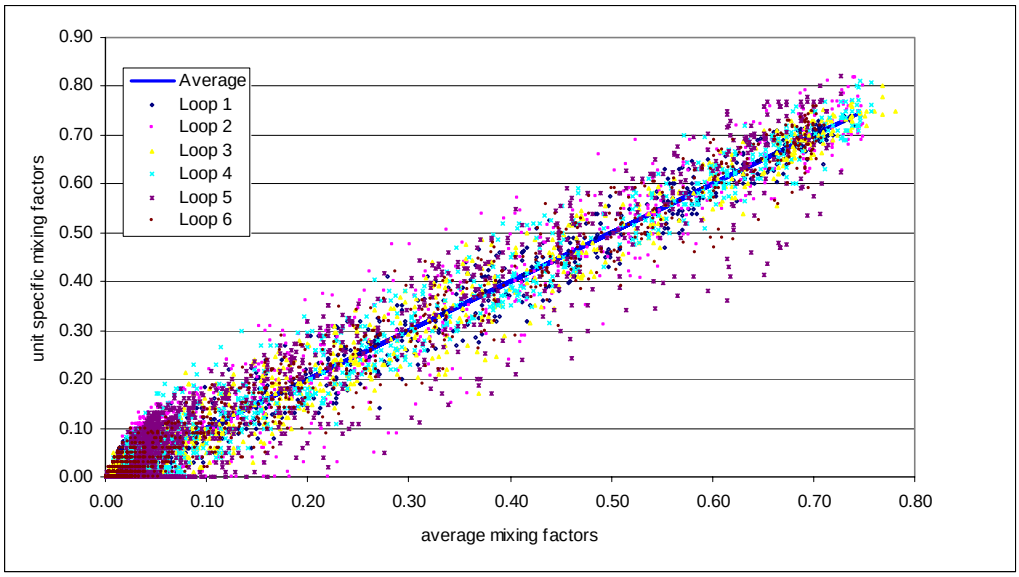

Figure 2 Differences of the unit specific values from the average mixing factors

For this reason it is more useful and actually more accurate to use the average of the mixing factors gained from measurements performed on all four units. This is shown on Fig. 3 and the actual values of the average mixing factors are collected in the Table 1.

It can be seen from the figure and the table that the maximum values of the mixing factors are around 0.75. It means that 75 % of the enthalpy flowing through an assembly comes from the closest loop. It is also notable that distribution of the mixing factor in the lower plenum is in full accordance with engineering view. The distributions on the longitudinal axis of the core – due to geometrical layout – are symmetrical, and no swirls could be identified.

The error caused by the linear regression has been determined for all the assemblies. The histogram of the calculated uncertainties is shown on the Fig. 4. It can be noticed that the bulk of the determined mixing factors (independently of their actual values) have 2-3 % absolute

uncertainty caused by the linear fitting process. There is 1% additional uncertainty caused by the method used for assembly power determination.

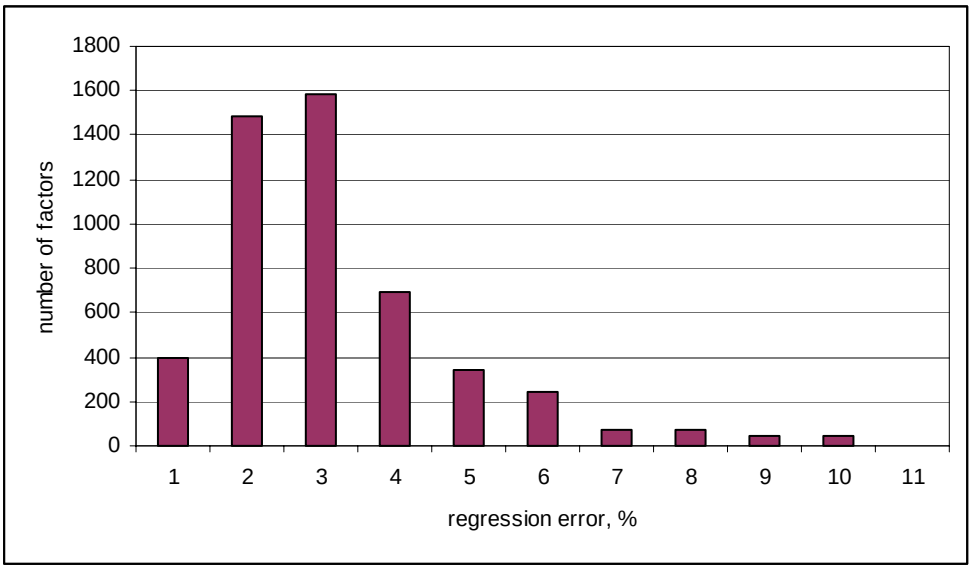

Figure 4. Histogram of the uncertainty of the mixing factors

Summary

In the reactor vessels of Paks NPP equipped with six loops the mixing of the coolant is not ideal. For the realistic determination of the active core inlet temperature field for the transients and accidents associated with different level temperature asymmetry a set of mixing factors have been suggested.

Those mixing factors were determined by measurements executed during standard operational tests carried out on operating reactors without disturbing the normal operation of the units. The procedure of the measurements and evaluation was demonstrated. A separate mathematical method made it possible to evaluate the information gained from reactors operating on relatively high power.

The results indicate that the distribution of the mixing factors is fully corresponding to the view and it is symmetrical. Its highest value around 75%, however each loop evidently determines the temperature of the closest to it sector. It also means that under certain processes the effect of the cooling asymmetry might be dominantly noticed in the nuclear behaviour of the core. This fact can be realistically modelled by mixing factors determined during the measurements.

References

Jirous F., 1989, Teplotni a rychlostni pole na vstupu do aktivni zony VVER-440 (in Czech). *Jaderna energie* **35**, 390-396.

Seber G.A., 1977, Linear regression analysis. John Wiley and sons, London. 48-96.

Tsimbalov C.A., Kraiko A.V., 1982, Temperature field at the core inlet of the VVER-440 reactor (in Russian). *Atomic Energie* **52/5**, 304-308.

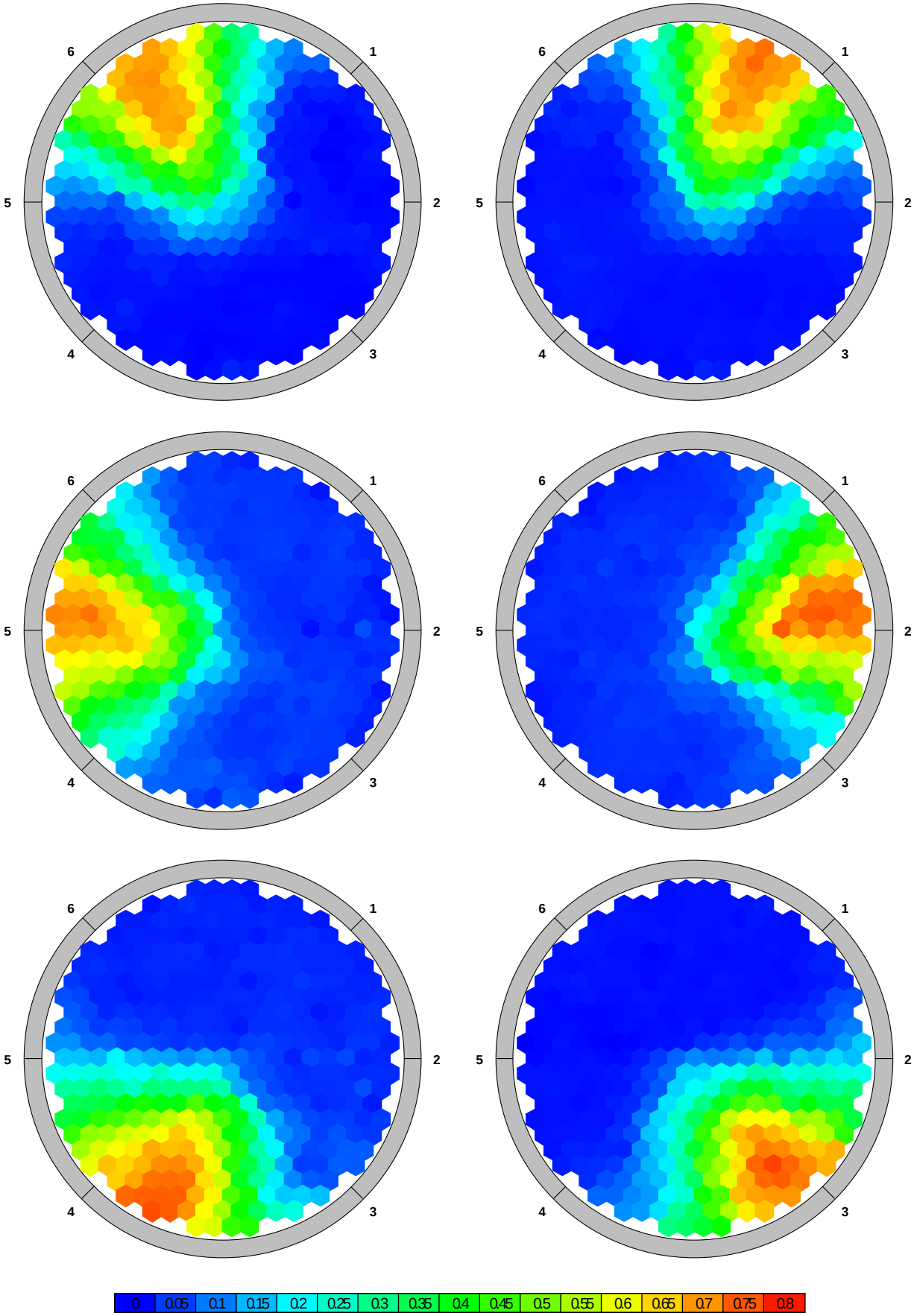

Figure 3. Distribution of the mixing factors

Assembly	Loop1	Loop2	Loop3	Loop4	Loop5	Loop6
1	0.30	0.02	0.02	0.01	0.03	0.61
2	0.42	0.03	0.03	0.01	0.03	0.48
3	0.57	0.04	0.03	0.01	0.02	0.34
4	0.64	0.04	0.03	0.00	0.01	0.28
5	0.15	0.02	0.03	0.00	0.11	0.70
6	0.21	0.02	0.02	0.01	0.06	0.67
7	0.27	0.02	0.02	0.02	0.03	0.63
8	0.38	0.03	0.02	0.01	0.03	0.52
9	0.49	0.03	0.03	0.01	0.02	0.41
10	0.57	0.04	0.03	0.02	0.03	0.32
11	0.67	0.04	0.03	0.01	0.03	0.22
12	0.71	0.06	0.03	0.01	0.03	0.16
13	0.74	0.07	0.03	0.01	0.03	0.11
14	0.09	0.01	0.03	0.01	0.18	0.68
15	0.12	0.02	0.03	0.01	0.12	0.70
16	0.16	0.02	0.03	0.02	0.06	0.70
17	0.23	0.03	0.03	0.01	0.05	0.65
18	0.31	0.03	0.02	0.01	0.04	0.59
19	0.44	0.03	0.03	0.02	0.04	0.46
20	0.55	0.03	0.03	0.01	0.03	0.34
21	0.64	0.04	0.03	0.01	0.03	0.25
22	0.71	0.05	0.02	0.02	0.03	0.17
23	0.75	0.07	0.03	0.01	0.03	0.11
24	0.71	0.14	0.03	0.01	0.02	0.09
25	0.70	0.18	0.02	0.00	0.00	0.09
26	0.07	0.01	0.03	0.01	0.21	0.68
27	0.07	0.02	0.03	0.01	0.16	0.71
28	0.10	0.03	0.03	0.01	0.13	0.71
29	0.19	0.03	0.03	0.01	0.07	0.67
30	0.28	0.03	0.03	0.01	0.04	0.61
31	0.34	0.03	0.03	0.01	0.03	0.55
32	0.52	0.03	0.03	0.01	0.03	0.38
33	0.63	0.04	0.02	0.01	0.02	0.27
34	0.70	0.03	0.03	0.01	0.03	0.20
35	0.72	0.07	0.03	0.01	0.03	0.14
36	0.71	0.16	0.02	0.02	0.03	0.06
37	0.70	0.18	0.02	0.02	0.02	0.05
38	0.66	0.24	0.02	0.01	0.02	0.05
39	0.03	0.03	0.03	0.02	0.36	0.54
40	0.04	0.02	0.03	0.01	0.28	0.61
41	0.06	0.02	0.03	0.01	0.18	0.70
42	0.06	0.03	0.02	0.01	0.17	0.70

Assembly	Loop1	Loop2	Loop3	Loop4	Loop5	Loop6
43	0.10	0.03	0.02	0.02	0.13	0.70
44	0.19	0.04	0.02	0.02	0.04	0.69
45	0.28	0.03	0.02	0.02	0.03	0.62
46	0.39	0.03	0.03	0.01	0.04	0.51
47	0.59	0.04	0.02	0.01	0.03	0.30
48	0.66	0.04	0.02	0.02	0.03	0.23
49	0.70	0.05	0.02	0.02	0.03	0.17
50	0.71	0.15	0.02	0.02	0.03	0.06
51	0.67	0.23	0.03	0.02	0.03	0.03
52	0.65	0.25	0.02	0.02	0.02	0.03
53	0.57	0.33	0.03	0.02	0.03	0.03
54	0.46	0.44	0.04	0.01	0.02	0.02
55	0.04	0.02	0.03	0.02	0.37	0.53
56	0.03	0.03	0.02	0.02	0.35	0.54
57	0.03	0.03	0.03	0.02	0.34	0.55
58	0.04	0.03	0.03	0.01	0.22	0.67
59	0.04	0.04	0.03	0.02	0.17	0.71
60	0.12	0.04	0.02	0.02	0.11	0.69
61	0.19	0.03	0.02	0.02	0.05	0.68
62	0.30	0.04	0.02	0.01	0.04	0.58
63	0.50	0.04	0.02	0.01	0.03	0.39
64	0.63	0.05	0.02	0.02	0.03	0.24
65	0.72	0.06	0.02	0.02	0.03	0.14
66	0.69	0.16	0.02	0.02	0.03	0.07
67	0.64	0.25	0.02	0.02	0.03	0.03
68	0.59	0.33	0.02	0.02	0.03	0.02
69	0.50	0.41	0.03	0.02	0.03	0.02
70	0.47	0.42	0.04	0.02	0.04	0.02
71	0.44	0.47	0.04	0.01	0.02	0.03
72	0.03	0.02	0.03	0.03	0.45	0.44
73	0.03	0.03	0.03	0.02	0.42	0.47
74	0.04	0.03	0.03	0.01	0.37	0.51
75	0.04	0.03	0.03	0.01	0.30	0.60
76	0.04	0.03	0.03	0.01	0.26	0.63
77	0.06	0.03	0.03	0.02	0.17	0.69
78	0.12	0.04	0.02	0.01	0.10	0.70
79	0.25	0.04	0.03	0.01	0.07	0.61
80	0.39	0.05	0.02	0.01	0.03	0.49
81	0.56	0.05	0.02	0.02	0.02	0.32
82	0.68	0.07	0.03	0.01	0.03	0.18
83	0.68	0.13	0.03	0.02	0.03	0.11
84	0.67	0.22	0.02	0.02	0.04	0.03
85	0.59	0.32	0.02	0.03	0.02	0.03

Assembly	Loop1	Loop2	Loop3	Loop4	Loop5	Loop6
86	0.51	0.40	0.02	0.02	0.03	0.02
87	0.42	0.48	0.03	0.02	0.04	0.01
88	0.38	0.54	0.03	0.01	0.02	0.02
89	0.36	0.54	0.04	0.01	0.02	0.03
90	0.02	0.02	0.02	0.05	0.62	0.28
91	0.02	0.02	0.02	0.04	0.56	0.33
92	0.03	0.03	0.03	0.01	0.46	0.44
93	0.04	0.03	0.03	0.01	0.44	0.46
94	0.02	0.04	0.02	0.01	0.34	0.57
95	0.05	0.03	0.02	0.01	0.24	0.64
96	0.08	0.02	0.03	0.01	0.17	0.68
97	0.15	0.03	0.03	0.01	0.13	0.65
98	0.34	0.03	0.02	0.01	0.07	0.51
99	0.47	0.06	0.02	0.02	0.05	0.38
100	0.60	0.07	0.03	0.02	0.03	0.26
101	0.61	0.15	0.03	0.02	0.03	0.17
102	0.58	0.31	0.02	0.02	0.03	0.03
103	0.58	0.33	0.02	0.02	0.03	0.02
104	0.51	0.40	0.03	0.02	0.03	0.02
105	0.42	0.49	0.03	0.02	0.03	0.01
106	0.36	0.54	0.04	0.02	0.03	0.01
107	0.24	0.63	0.07	0.01	0.03	0.01
108	0.22	0.65	0.08	0.02	0.02	0.02
109	0.02	0.03	0.02	0.06	0.64	0.23
110	0.02	0.03	0.02	0.04	0.64	0.25
111	0.02	0.04	0.02	0.02	0.58	0.33
112	0.02	0.03	0.02	0.03	0.51	0.39
113	0.02	0.03	0.02	0.02	0.43	0.47
114	0.05	0.03	0.02	0.02	0.31	0.56
115	0.11	0.04	0.03	0.01	0.21	0.61
116	0.24	0.04	0.02	0.02	0.16	0.52
117	0.38	0.06	0.02	0.02	0.09	0.43
118	0.48	0.09	0.02	0.01	0.05	0.34
119	0.54	0.18	0.02	0.02	0.03	0.20
120	0.56	0.31	0.03	0.02	0.03	0.06
121	0.52	0.38	0.02	0.03	0.02	0.03
122	0.43	0.47	0.04	0.02	0.02	0.02
123	0.32	0.60	0.04	0.00	0.03	0.01
124	0.21	0.69	0.05	0.01	0.03	0.01
125	0.18	0.69	0.07	0.02	0.02	0.02
126	0.16	0.70	0.09	0.03	0.00	0.02
127	0.02	0.03	0.02	0.08	0.68	0.18
128	0.02	0.03	0.02	0.06	0.68	0.19

Assembly	Loop1	Loop2	Loop3	Loop4	Loop5	Loop6
129	0.02	0.03	0.02	0.03	0.66	0.23
130	0.02	0.03	0.02	0.04	0.62	0.27
131	0.02	0.03	0.02	0.04	0.55	0.34
132	0.03	0.04	0.02	0.02	0.44	0.44
133	0.05	0.04	0.02	0.03	0.43	0.43
134	0.10	0.05	0.02	0.02	0.32	0.50
135	0.24	0.06	0.02	0.02	0.19	0.48
136	0.37	0.12	0.03	0.02	0.10	0.37
137	0.46	0.16	0.03	0.01	0.04	0.29
138	0.47	0.26	0.04	0.02	0.04	0.17
139	0.45	0.43	0.04	0.02	0.02	0.04
140	0.38	0.51	0.04	0.02	0.02	0.02
141	0.28	0.59	0.06	0.02	0.03	0.02
142	0.19	0.69	0.06	0.01	0.03	0.01
143	0.16	0.73	0.06	0.02	0.02	0.01
144	0.12	0.73	0.10	0.02	0.01	0.02
145	0.10	0.73	0.12	0.02	0.01	0.02
146	0.01	0.03	0.01	0.10	0.70	0.14
147	0.02	0.03	0.02	0.10	0.70	0.13
148	0.02	0.03	0.03	0.07	0.71	0.14
149	0.02	0.03	0.02	0.07	0.68	0.19
150	0.02	0.03	0.02	0.04	0.62	0.27
151	0.02	0.03	0.01	0.05	0.62	0.28
152	0.03	0.03	0.02	0.04	0.51	0.38
153	0.06	0.03	0.02	0.03	0.48	0.38
154	0.11	0.05	0.03	0.04	0.33	0.44
155	0.25	0.10	0.03	0.03	0.20	0.39
156	0.40	0.20	0.05	0.02	0.07	0.26
157	0.40	0.30	0.05	0.04	0.04	0.17
158	0.34	0.41	0.07	0.04	0.03	0.11
159	0.33	0.51	0.06	0.03	0.02	0.05
160	0.23	0.61	0.09	0.03	0.02	0.03
161	0.13	0.71	0.09	0.02	0.02	0.02
162	0.12	0.74	0.09	0.01	0.03	0.01
163	0.10	0.75	0.10	0.03	0.01	0.02
164	0.07	0.73	0.14	0.03	0.02	0.02
165	0.08	0.71	0.18	0.01	0.00	0.01
166	0.02	0.03	0.02	0.15	0.69	0.10
167	0.02	0.03	0.02	0.14	0.68	0.10
168	0.02	0.02	0.02	0.14	0.69	0.10
169	0.02	0.03	0.03	0.19	0.66	0.07
170	0.02	0.03	0.02	0.14	0.63	0.16
171	0.02	0.03	0.02	0.12	0.61	0.20

Assembly	Loop1	Loop2	Loop3	Loop4	Loop5	Loop6
172	0.05	0.04	0.04	0.12	0.50	0.26
173	0.09	0.04	0.06	0.10	0.40	0.32
174	0.10	0.06	0.09	0.12	0.31	0.31
175	0.26	0.20	0.12	0.11	0.11	0.20
176	0.30	0.28	0.11	0.07	0.06	0.17
177	0.28	0.41	0.12	0.05	0.03	0.11
178	0.24	0.50	0.14	0.03	0.03	0.06
179	0.15	0.62	0.17	0.01	0.03	0.01
180	0.07	0.74	0.12	0.04	0.00	0.03
181	0.07	0.69	0.17	0.03	0.02	0.02
182	0.04	0.72	0.16	0.04	0.01	0.02
183	0.05	0.69	0.19	0.01	0.05	0.01
184	0.07	0.71	0.17	0.02	0.02	0.01
185	0.03	0.03	0.03	0.20	0.65	0.06
186	0.03	0.03	0.03	0.20	0.65	0.06
187	0.03	0.03	0.03	0.22	0.64	0.06
188	0.03	0.03	0.03	0.23	0.64	0.05
189	0.02	0.03	0.03	0.19	0.65	0.07
190	0.03	0.03	0.03	0.19	0.63	0.09
191	0.03	0.03	0.04	0.24	0.54	0.12
192	0.06	0.04	0.07	0.20	0.45	0.19
193	0.08	0.06	0.10	0.20	0.35	0.21
194	0.12	0.09	0.19	0.22	0.21	0.18
195	0.17	0.25	0.19	0.13	0.11	0.15
196	0.17	0.37	0.23	0.06	0.05	0.12
197	0.16	0.44	0.24	0.05	0.04	0.07
198	0.10	0.52	0.29	0.03	0.03	0.04
199	0.07	0.57	0.28	0.02	0.03	0.03
200	0.04	0.64	0.24	0.03	0.03	0.02
201	0.04	0.63	0.26	0.03	0.02	0.02
202	0.04	0.65	0.26	0.02	0.02	0.02
203	0.04	0.66	0.24	0.02	0.03	0.02
204	0.04	0.65	0.24	0.02	0.03	0.02
205	0.03	0.03	0.03	0.27	0.60	0.05
206	0.03	0.02	0.03	0.27	0.60	0.04
207	0.03	0.02	0.03	0.30	0.58	0.04
208	0.02	0.04	0.02	0.28	0.60	0.04
209	0.03	0.03	0.03	0.24	0.60	0.07
210	0.03	0.04	0.03	0.30	0.53	0.07
211	0.03	0.03	0.05	0.29	0.49	0.10
212	0.06	0.06	0.08	0.29	0.36	0.15
213	0.07	0.09	0.18	0.29	0.22	0.13
214	0.09	0.14	0.22	0.26	0.16	0.12

Assembly	Loop1	Loop2	Loop3	Loop4	Loop5	Loop6
215	0.13	0.28	0.26	0.13	0.10	0.11
216	0.12	0.35	0.34	0.07	0.06	0.06
217	0.07	0.41	0.39	0.04	0.05	0.04
218	0.03	0.49	0.39	0.03	0.02	0.03
219	0.04	0.54	0.34	0.02	0.03	0.03
220	0.04	0.57	0.31	0.02	0.03	0.03
221	0.03	0.54	0.34	0.03	0.03	0.03
222	0.03	0.57	0.31	0.05	0.01	0.03
223	0.03	0.58	0.33	0.02	0.02	0.02
224	0.02	0.02	0.03	0.33	0.57	0.03
225	0.03	0.02	0.03	0.34	0.55	0.03
226	0.03	0.03	0.02	0.35	0.55	0.02
227	0.03	0.03	0.03	0.39	0.50	0.03
228	0.03	0.04	0.04	0.41	0.44	0.05
229	0.02	0.04	0.05	0.39	0.45	0.05
230	0.03	0.04	0.09	0.39	0.36	0.08
231	0.03	0.06	0.20	0.45	0.18	0.07
232	0.04	0.09	0.25	0.39	0.15	0.08
233	0.05	0.09	0.32	0.37	0.11	0.06
234	0.07	0.21	0.40	0.23	0.05	0.04
235	0.06	0.32	0.47	0.07	0.05	0.03
236	0.03	0.34	0.51	0.06	0.05	0.02
237	0.03	0.39	0.48	0.04	0.03	0.03
238	0.03	0.52	0.37	0.02	0.03	0.03
239	0.03	0.47	0.42	0.02	0.03	0.02
240	0.03	0.52	0.37	0.03	0.02	0.03
241	0.03	0.53	0.38	0.01	0.03	0.02
242	0.02	0.01	0.02	0.35	0.56	0.04
243	0.03	0.02	0.03	0.37	0.53	0.03
244	0.03	0.02	0.03	0.43	0.46	0.03
245	0.03	0.02	0.03	0.45	0.45	0.02
246	0.03	0.04	0.03	0.48	0.39	0.03
247	0.02	0.03	0.04	0.51	0.36	0.03
248	0.02	0.04	0.11	0.55	0.26	0.03
249	0.02	0.04	0.18	0.58	0.15	0.02
250	0.02	0.06	0.26	0.54	0.08	0.03
251	0.03	0.07	0.35	0.46	0.07	0.03
252	0.02	0.07	0.46	0.38	0.05	0.02
253	0.02	0.09	0.58	0.25	0.03	0.02
254	0.02	0.18	0.63	0.12	0.03	0.02
255	0.02	0.22	0.63	0.07	0.04	0.02
256	0.02	0.26	0.62	0.05	0.04	0.01
257	0.02	0.35	0.54	0.04	0.04	0.01

Assembly	Loop1	Loop2	Loop3	Loop4	Loop5	Loop6
258	0.02	0.35	0.55	0.04	0.03	0.01
259	0.03	0.43	0.48	0.02	0.02	0.02
260	0.03	0.54	0.37	0.03	0.00	0.03
261	0.02	0.01	0.03	0.44	0.47	0.03
262	0.03	0.02	0.03	0.51	0.38	0.02
263	0.03	0.03	0.03	0.52	0.37	0.02
264	0.03	0.03	0.03	0.56	0.33	0.02
265	0.02	0.03	0.05	0.58	0.30	0.02
266	0.02	0.04	0.07	0.60	0.24	0.03
267	0.02	0.04	0.17	0.65	0.11	0.02
268	0.02	0.04	0.21	0.61	0.10	0.02
269	0.02	0.06	0.30	0.53	0.07	0.02
270	0.02	0.06	0.46	0.40	0.04	0.02
271	0.02	0.06	0.55	0.33	0.03	0.01
272	0.02	0.08	0.68	0.18	0.02	0.01
273	0.02	0.12	0.71	0.10	0.04	0.01
274	0.02	0.18	0.69	0.08	0.03	0.01
275	0.02	0.23	0.66	0.04	0.04	0.01
276	0.02	0.28	0.61	0.05	0.03	0.01
277	0.02	0.34	0.56	0.04	0.03	0.01
278	0.02	0.46	0.46	0.03	0.01	0.02
279	0.02	0.02	0.03	0.53	0.38	0.03
280	0.03	0.02	0.04	0.57	0.32	0.02
281	0.03	0.03	0.04	0.60	0.29	0.02
282	0.03	0.03	0.04	0.62	0.26	0.02
283	0.02	0.04	0.04	0.67	0.21	0.02
284	0.02	0.04	0.13	0.65	0.14	0.02
285	0.02	0.04	0.18	0.66	0.08	0.02
286	0.02	0.03	0.27	0.60	0.05	0.02
287	0.02	0.04	0.39	0.51	0.04	0.01
288	0.02	0.04	0.48	0.42	0.02	0.01
289	0.01	0.05	0.61	0.27	0.03	0.02
290	0.02	0.07	0.68	0.19	0.03	0.02
291	0.02	0.12	0.73	0.08	0.03	0.02
292	0.02	0.16	0.72	0.04	0.04	0.01
293	0.02	0.19	0.69	0.05	0.03	0.01
294	0.02	0.21	0.67	0.06	0.02	0.01
295	0.02	0.21	0.69	0.06	0.01	0.01
296	0.03	0.02	0.04	0.59	0.31	0.02
297	0.03	0.03	0.05	0.65	0.23	0.02
298	0.03	0.03	0.05	0.64	0.22	0.03
299	0.02	0.04	0.06	0.66	0.20	0.02
300	0.02	0.04	0.10	0.70	0.13	0.02

Assembly	Loop1	Loop2	Loop3	Loop4	Loop5	Loop6
301	0.02	0.03	0.16	0.70	0.07	0.02
302	0.02	0.04	0.20	0.67	0.06	0.02
303	0.02	0.03	0.30	0.59	0.04	0.02
304	0.02	0.03	0.49	0.43	0.03	0.01
305	0.02	0.04	0.55	0.35	0.03	0.01
306	0.02	0.04	0.65	0.25	0.02	0.01
307	0.01	0.06	0.75	0.13	0.03	0.02
308	0.02	0.11	0.78	0.04	0.04	0.02
309	0.02	0.15	0.75	0.04	0.03	0.01
310	0.02	0.15	0.72	0.06	0.03	0.01
311	0.02	0.21	0.69	0.06	0.01	0.01
312	0.03	0.03	0.05	0.64	0.23	0.03
313	0.02	0.03	0.07	0.67	0.17	0.02
314	0.02	0.04	0.09	0.72	0.13	0.01
315	0.02	0.03	0.14	0.72	0.08	0.01
316	0.02	0.03	0.17	0.71	0.05	0.01
317	0.02	0.03	0.26	0.63	0.05	0.01
318	0.02	0.03	0.35	0.56	0.03	0.02
319	0.02	0.04	0.52	0.38	0.03	0.02
320	0.02	0.04	0.61	0.28	0.03	0.02
321	0.02	0.06	0.70	0.18	0.03	0.02
322	0.02	0.08	0.75	0.10	0.04	0.02
323	0.02	0.11	0.76	0.06	0.03	0.02
324	0.02	0.15	0.73	0.05	0.03	0.01
325	0.02	0.03	0.10	0.72	0.12	0.02
326	0.02	0.04	0.10	0.73	0.11	0.02
327	0.02	0.03	0.12	0.73	0.08	0.02
328	0.02	0.04	0.14	0.73	0.06	0.02
329	0.02	0.03	0.21	0.66	0.06	0.01
330	0.02	0.04	0.26	0.61	0.06	0.01
331	0.02	0.03	0.44	0.45	0.04	0.01
332	0.02	0.04	0.48	0.41	0.04	0.01
333	0.02	0.06	0.68	0.19	0.03	0.02
334	0.02	0.07	0.70	0.15	0.04	0.02
335	0.02	0.07	0.71	0.16	0.03	0.01
336	0.02	0.08	0.71	0.14	0.03	0.02
337	0.01	0.03	0.13	0.74	0.07	0.02
338	0.02	0.03	0.14	0.73	0.06	0.02
339	0.02	0.03	0.19	0.69	0.06	0.01
340	0.02	0.02	0.30	0.60	0.06	0.01
341	0.02	0.04	0.35	0.53	0.05	0.02
342	0.02	0.04	0.47	0.40	0.05	0.01
343	0.02	0.05	0.56	0.32	0.03	0.01

Assembly	Loop1	Loop2	Loop3	Loop4	Loop5	Loop6
344	0.02	0.06	0.64	0.25	0.02	0.01
345	0.02	0.06	0.68	0.22	0.01	0.01
346	0.02	0.02	0.32	0.59	0.04	0.01
347	0.02	0.03	0.34	0.57	0.02	0.02
348	0.04	0.04	0.39	0.44	0.06	0.03
349	0.03	0.04	0.43	0.42	0.05	0.03

Table 1. Average mixing factors of the assemblies

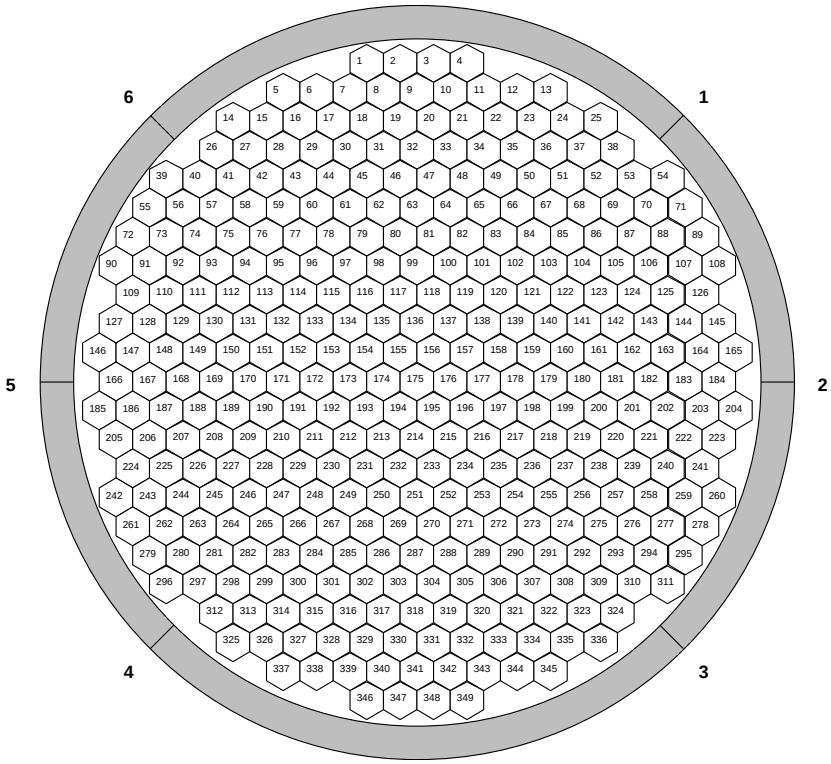

Figure 4. Numbering of the assemblies